Graduate School of Engineering
Hokkaido University

Experimental Investigation and Analytical Modeling of Masonry Wall for In-Plane Shear Strength after Strengthening by Various FRPs

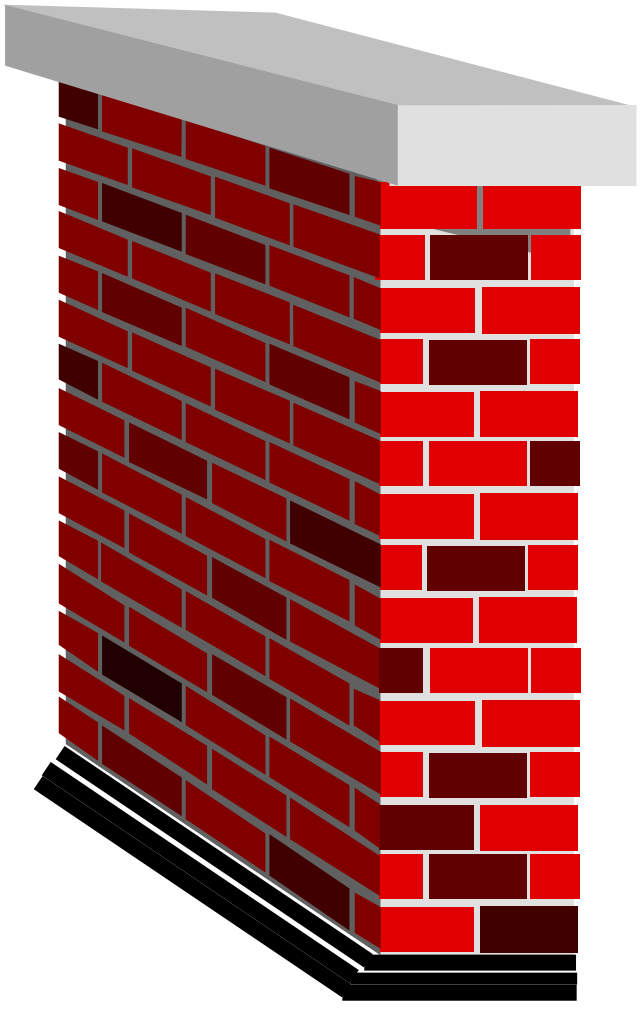

北海道大学
HOKKAIDO UNIVERSITY

ATAUR RAHMAN

September, 2016

Experimental Investigation and Analytical Modeling of Masonry Wall for In-Plane Shear Strength after Strengthening by Various FRPs

種々の FRP で補強された組積壁構造の面内せん断耐力に関する実験的研究と解析モデル

By

ATAUR RAHMAN

A dissertation in civil engineering submitted as a fulfillment of the requirement for the degree of Doctor of Philosophy

Graduate School of Engineering
Hokkaido University

September, 2016

Acknowledgements

The research work presented in this dissertation has been completed successfully under the kind supervision of Professor Dr. Tamon Ueda, from Division of Engineering and Policy for Sustainable Environment at Faculty of Engineering, Hokkaido University of Japan.

I wish to express my sincere thanks and gratitude to Professor Ueda for his invaluable guidance, constructive criticism, and encouragement during the whole period of my study. I specially acknowledge his support to carryover this research work at KUET after the end of my staying here in Japan. I am also thankful to Associate Prof. Y. Sato and Assistant Professor H. Furuuchi for their assistance at the beginning of experimental work at Hokkaido University and later on at KUET.

I would also like to thank Mr. T. Kimura who helped me a lot during the whole experimental program. During my stay in Japan, my colleagues and friends at this graduate school had supported me a lot, which is deeply remembered. Special thanks go to Dr. Sabry, Dr. David, Dr. Zakaria, Dr. Aun, Dr. Dillon, Dr. Khuram, Mr. Maeda, Ms. Maria for their kind assistance and support.

Back at KUET, the undergraduate students as well as the lab assistants helped me a lot to perform some of the unfinished experimental works. Sincere thanks should be extended to them as well.

This PhD program was initially funded by the Ministry of Education of Japan (MEXT) Government Scholarship and later on supported by JSPS RONPAKU fellowship from Japan and CSR grant from KUET, Bangladesh, which are gratefully acknowledged.

I am also thankful to Nittetsu-Sumikin Materials Co. Ltd. Japan and Maeda Kosen Ltd. Japan, for their support in providing necessary materials for CFRP and PET-FRP, respectively that have been used in this experiment.

I also acknowledge the support and encouragement that I received from Dr. Werawan and Ms. Natalya, who are the two most dynamic program coordinators for the e3 English Program here in Hokkaido University.

Taking this opportunity, I would like to thank my parents and my wife, Shermin Sultana for their great loves, supports, and endurance during the all three years I was in Japan and following few years in Bangladesh. Lots of love for my three beloved kids who were at the center of my inspiration and perseverance, during all these difficult years.

Originality Statement

‘I hereby declare that this submission is my own work and to the best of my knowledge it contains no materials previously published or written by another person, or substantial proportions of material which have been accepted for the award of any other degree or diploma at Hokkaido University or any other educational institution, except where due acknowledgement is made in the thesis. Any contribution made to the research by others, with whom I have worked at Hokkaido University or elsewhere, is explicitly acknowledged in the thesis. I also declare that the intellectual content of this thesis is the product of my own work, except to the extent that assistance from others in model design and conception or in style, presentation and linguistic expression is acknowledged.’

Signed …….....

Date …….....

LIST OF PUBLICATIONS

Peer Reviewed Journal

Rahman. M. A., Ueda T., 2016. "In-Plane Shear Performance of Masonry Walls after Strengthening by Two Different FRPs" *ASCE Journal of Composites for Construction. p.1-14.*

Rahman. M. A., Ueda T., 2016. "In-Plane Shear Strength of Masonry Wall Strengthening by Two Distinct FRPs" *JSCE journal of Structural Engineering A, Vol. 62A.*

Rahman. M. A., Ueda T., 2014. "Experimental Investigation and Numerical Modeling of Peak Shear Stress of Brick Masonry Mortar Joint Under Compression" *ASCE Journal of Materials in Civil Engineering. Vol. 26(9), p.1-13.*

International Conference

Rahman. M. A., Ueda T., 2015. "In-Plane Shear Strength of Masonry Wall Strengthening by Two Distinct FRPs" *IABSE-JSCE joint conference, Aug., 2015, Dhaka.*

Rahman M. A., Ueda T., 2013. "Performance Evaluation of Masonry Shear Walls Strengthening by Two Different FRPs" *Proceedings of the 13 International East-Asia Pacific Conference on Structural Engineering & Construction (EASEC-13), 11 ~ 13 Sep, 2013, Hokkaido University, Sapporo, Japan, Paper No. 462.*

Rahman. M. A., Ueda T., 2011. "Numerical Simulation of FRP Retrofitted Laterally Loaded Masonry" *11 North American Masonry Conference, June 5-8, 2011, NAMC, MN US.*

Rahman. M. A., Ueda T., 2011. "Numerical Modeling for Response of Brick Masonry Bed-Joint Under Shear and Compression" *9th Australasian Masonry Conference Queenstown, New Zealand 15 – 18 February 2011.*

Rahman. M. A., Ueda T., 2009. "Numerical Simulation of FRP Retrofitted Masonry Wall by 3D Finite Element Analysis" *IABSE, Bangkok, 2009.*

Rahman. M. A., Ueda T., 2008. "3D Finite Element Analysis of Unreinforced Masonry Wall Using Simplified Interface Model" *AMCM 2008, Lodz, Poland, June 9, 2008.*

Abstract

Recent earthquakes in Nepal, Pakistan, Afghanistan, and elsewhere in the world caused an extensive damage to human lives and properties and left over a large inventory of unreinforced masonry (URM) buildings that are still in service. Some of them are as old as 700 years and have great historical significance and are included in UNESCO heritage buildings. The majority of those URM buildings which have been constructed with little or no attention to seismic considerations demonstrate the need for strengthening due to their poor seismic performance posed by their inherent brittleness and low tensile strength. In the event of an earthquake, apart from the existing gravity loads, horizontal racking loads are imposed on walls. Hence if the stress state within the wall exceeds masonry strength, brittle failure occurs, followed by possible collapse of the wall and the building. Therefore, URMs are vulnerable to earthquakes, and should be confined and/or reinforced whenever possible. Therefore, there is an urgent need to improve the performance of URM structures by retrofitting and strengthening them to resist potential earthquake damage.

This research work investigates the in-plane shear performance of externally strengthened masonry walls using two types of fiber reinforced polymer (FRP) sheets, they are: synthetic FRPs and FRPs with natural fibers. Among these two types, Carbon FRP (CFRP), Polyethylene Terephthalate-FRP (PET-FRP) and Nylon-FRP are the synthetic one and FRP made from Jute and Cotton fibers are the natural one. Although the conventional FRPs possess superior mechanical strength over natural FRPs, they have got some serious drawbacks such as high density, high cost and poor recycling and non-biodegradable properties. On the other hand, the strength of bio-fibers is not as great as conventional fibers, but their specific properties are comparable and compatible with conventional resins and masonry. Moreover, the durability of the natural fibers can be enhanced due to embedment of the fibers within the resin.

Among the three synthetic FRPs, PET-FRP has a low tensile strength but possess a higher fracturing strain (more than 10 %) than CFRP (about 1.5 %) which has drawn a significant attention as a unique alternative to CFRP or GFRP due to its pronounced ductile behavior and relatively low material cost. On the other hand, Nylon-FRP has a higher fracturing strain (about 15 %) but with low tensile strength than PET-FRP and CFRP. Regarding natural fibers, Jute possesses higher tensile strength (about 250 MPa) and fracturing strain (about 22%) than Cotton (about 175 MPa and 10%, respectively).

Fifteen masonry walls made from clay brick were tested for static lateral loading under constant compression, after bonding those FRP sheets onto their surfaces in three different configurations, namely cross-diagonal configuration, FRP in grid system and fully wrapped with FRP. Strengthening is considered on both sides of the wall to ensure uniformity and symmetrical stiffness of those walls. The ultimate shear strength and deformation at peak load were the two important observations. The mechanisms by which load was carried were observed, varying from the initial uncracked state to the final, fully cracked state. The propagation of potential flexural and diagonal cracks were noticed in each masonry wall and at the end several failure modes were observed. For FRP strengthened walls, damages and distresses on FRPs were marked and categorized as either FRP debonding or fracture. Based on the experimental results and observations, the following remarks were outlined:

(1) This experimental study demonstrates the ability of all of the FRPs such as CFRP, PET-FRP, Nylon-FRP, Jute-FRP and Cotton-FRP sheets to enhance the shear resistance to a great extent; more than twice the capacity of the URM wall in the case of diagonal bracing and about three times in the case of gird configuration and walls fully wrapped with FRPs. Among the synthetic FRPs, PET-FRP and Nylon-FRP have a better ductility performance than CFRP, as they show pronounced ductile behavior in pre-peak regime and softening behavior in post-peak regime. Ductility is a must needed criterion rather than strength for a structure to absorb substantial seismic energy and ensure structural integrity and margin of safety against collapse. Though the CFRP increases the shear capacity of a masonry wall, it substantially reduces the ductility of the wall, which may eventually cause an explosive type of masonry failure. On the other hand, Jute-FRP and Cotton-FRP also enhanced the shear capacity of masonry wall to almost thrice of that of URM wall and they also showed better ductile behavior than CFRP.

(2) The elastic stiffness of URM wall was largely modified by the use of FRPs, externally bonded over the surface of the walls but it was observed that stiffness value beyond some specific range does not increase the in-plane shear strength of masonry and it will only increase the cost of strengthening works.

(3) As masonry is quite fragile against lateral movement with a low lateral stiffness, diagonal bracing with PET-FRP sheet can be one of the options, if the cost of the material is not compromised. If seeking for a low-cost strengthening material, Nylon-FRP, Jute-FRP and Cotton-FRP could be one of the variable alternatives, where not only capacity is enhanced but, at the same time, the wall is made quite ductile, reversing a catastrophic mode of failure to a ductile one. Moreover, unlike synthetic FRP such as CFRP, PET-FRP and Nylon-FRP, Jute and Cotton

are bio-degradable materials, and they do not pose any threat to the ambient environment. For low cost strengthening work, Jute, Cotton or Nylon can be good alternatives to PET and Carbon.
(4) Another interesting point that is manifest from this experimental study is that the FRP strengthening of the masonry can have only marginal effect on the structural performance at the service load condition but contribute a lot at some accidental overloading such as earthquake, where the seismic demand is high.
(5) The in-plane shear strengths observed in this experimental study are almost equal to each other for the cases where the amount of FRP was greater than a certain limit. This information has assisted to some extent to develop an analytical model for FRP strengthened wall based on effective strain in FRP.

At the end, a simplified model for evaluating shear strength of FRP retrofitted masonry wall is proposed and validated with the experimental results of this research and results from other sources. This can be a good source of guideline in developing design standards for performance based design of strengthening masonry structures for in-plane shear strength. Although the numerical models proposed in this study were not extensively verified for full scale walls, yet they can be an efficient tool to implement in any general purpose FEA program for furthering the simulation works of FRP strengthened masonry walls in future.

Table of Contents

PART-1

Chapter 1

Introduction

Brick masonry is the process of constructing a building from individual bricks laid in a specific pattern and bound together, usually by mortar (Fig.1.1). A large number of historical buildings had been constructed using masonry. Some of them are as old as 4000 years. In the present, masonry is still widely being used in building industries due to its simplicity in construction, aesthetics, durability, low maintenance, versatility, sound absorption and above all low cost. The basic advantage of masonry construction is that it is possible to use the same element to perform a variety of functions simultaneously, such as, provide structure, subdivision of space, thermal and acoustic insulation as well as fire and weather protection. As a material, it is relatively cheap but durable and produces external wall finishes of very acceptable appearance. Masonry construction is flexible in terms of building layout and can be constructed without very large capital expenditure on the part of the builder (Hendry 2004).

The problems to adequately define the mechanical properties of masonry are related, amongst other reasons, to the possibility of finding the elements needed to build masonry almost everywhere. This situation makes it possible to build masonry in many different ways, methods and qualities. Because of this, the input parameters to define the mechanical properties of masonry are wide and its properties are many and various. According to many studies, around 50% of the world's population live in earthquake prone areas (Uzoegbo 2011) and the effects of earthquakes worldwide have claimed approximately 8 million lives over the last 2000 years (Jaiswal and Wald 2008). Moreover, around 40% of urban the population lives in houses made of masonry and this number increases in the developing countries. In Bangladesh, for instance, the percentage rises to about 70%. Additionally, unreinforced masonry is responsible for approximately 60% of human casualties due to structural damage caused by earthquakes all over the world (Mayorca and Meguro 2003).

Taking these facts into account, it is clear that more research and development about the mechanical properties and structural performance of masonry is needed, in order to improve its safety against seismic demands.

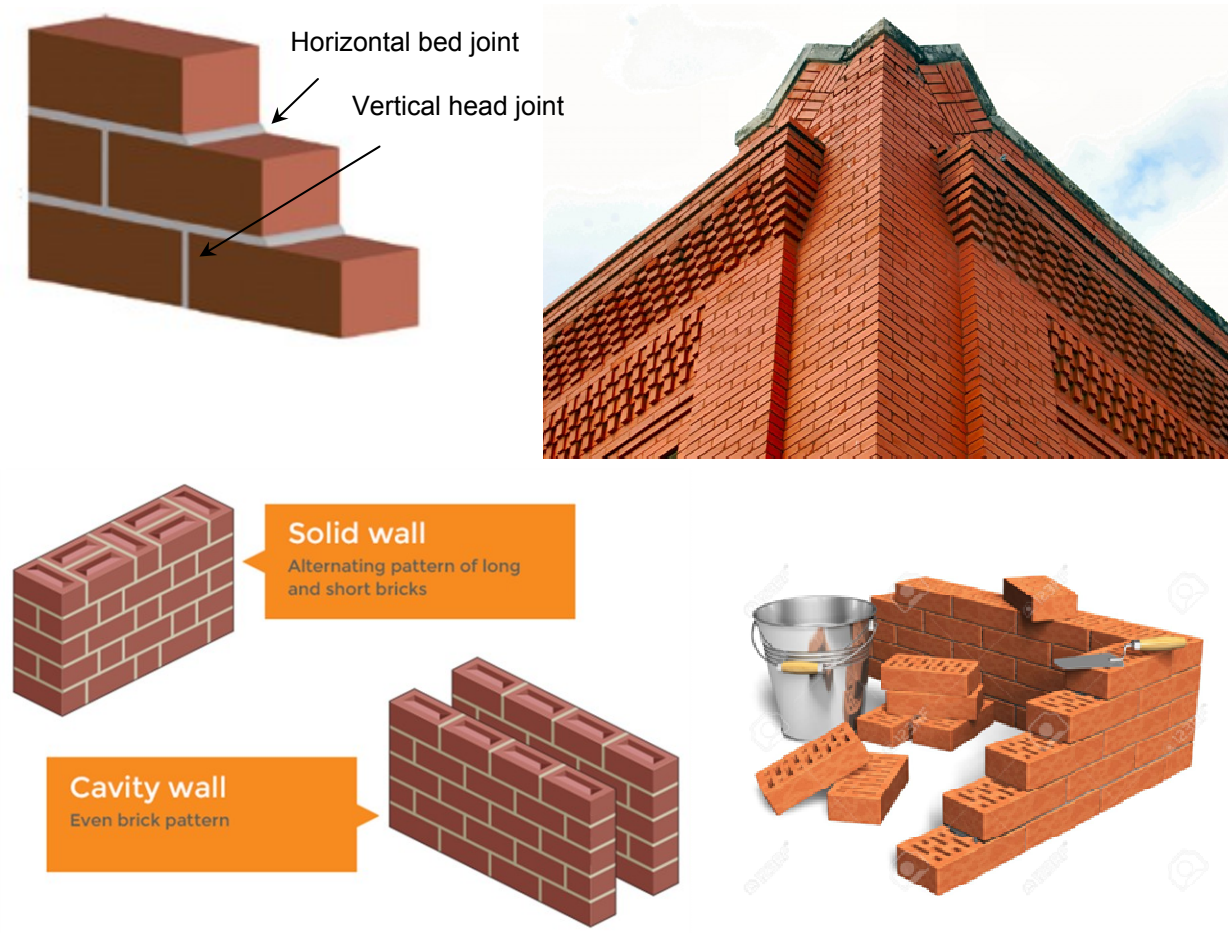

Fig.1.1. *Various types of masonry works (123RF.com)*

1.1 Research Background

Bricks were first fired around 3500 BC, in Mesopotamia, present-day Iraq, one of the high-risk seismic areas of the world. From Roman aqueducts and public buildings to the Great Wall of China, from the domes of Islamic architecture to the early railway arch bridges, from the first 19th century American tall buildings to the 20th century nuclear power plants, bricks have been used as structural material in all applications of building and civil engineering. The most commonplace use of bricks worldwide throughout time is in residential dwellings (Fig.1.2). The shape and size of bricks can vary considerably, and similarly the mortars used depend on local material availability, but the basic form of construction for houses has minor geographical variations and has changed relatively little over time. So far, all the major recent earthquakes have occurred away from major cities, and have affected relatively sparsely populated areas. This has limited the human casualty and the economic losses. However, earthquakes in Gujurat (India 2001), Bam (Iran 2003), and Kashimir (Pakistan and India 2005) have demonstrated that

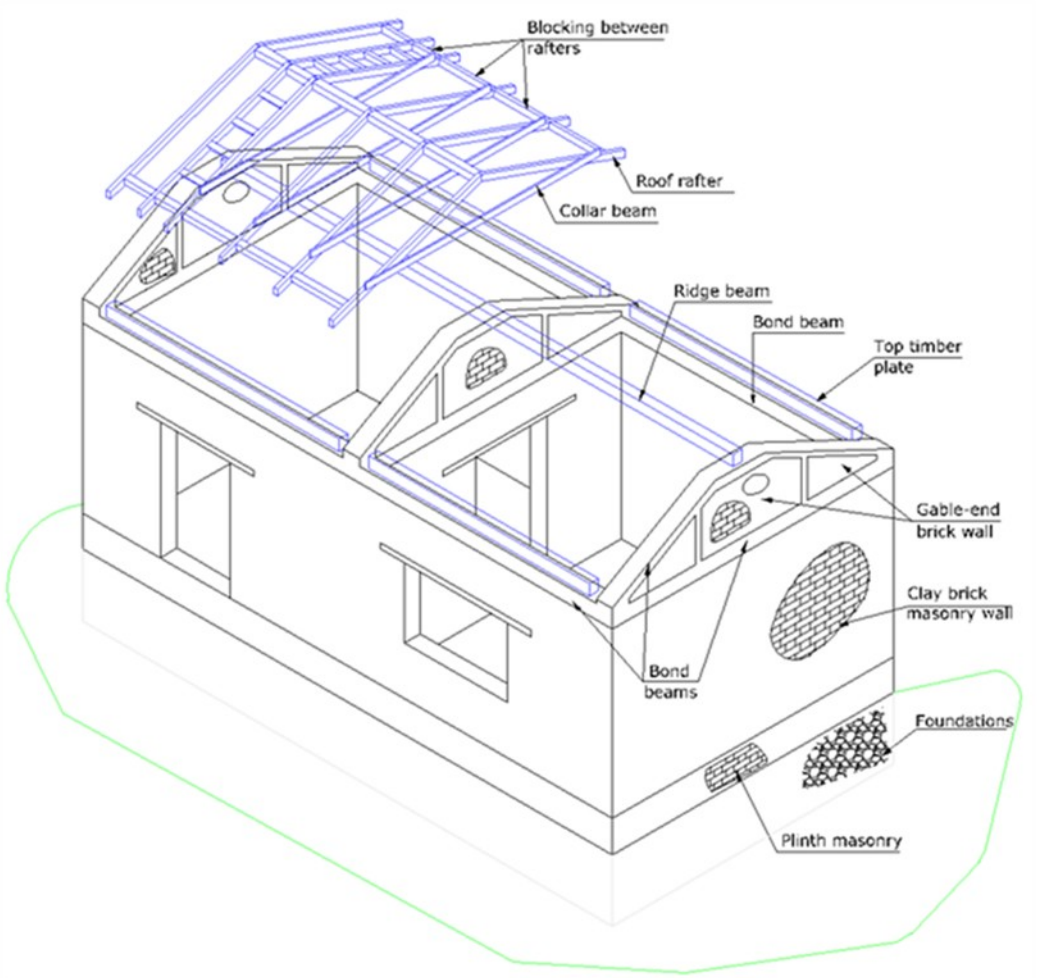

Fig. 1.2. *A typical masonry house (WHE, 2011)*

inappropriate construction technology may lead to high casualty levels even for moderate earthquakes. The worst death toll from an earthquake in the past century occurred in 1976 in China (T'ang Shan Province), where it is estimated that 240,000 people were killed. Most of the deaths were due to the collapse of brick masonry buildings. In more recent times, the earthquake in Nepal with a magnitude of 7.9 caused wanton destruction to masonry buildings where more than 10,000 people perished under the rubble of collapsed masonry walls. In 1897, an earthquake of magnitude 8.7 caused serious damage to buildings in the northeastern part of India including Bangladesh and over 1,500 people were killed (Ansary 2006).

In the event of an earthquake, apart from the existing gravity loads, horizontal racking loads are imposed on walls. However, the unreinforced masonry behaves as a brittle material. Hence if the stress state within the wall exceeds masonry strength, brittle failure occurs, followed by possible collapse of the wall and the building. Therefore unreinforced masonry walls are vulnerable to earthquakes, and should be confined and/or reinforced whenever possible. Recently, seismic codes place substantial constraints on unreinforced brick masonry construction in earthquake-prone areas, limiting the allowed number of stories, the minimum thickness of walls, and the

number and position of openings. As a result, construction of load-bearing unreinforced brick masonry structures has dwindled in these countries, and alternative forms of construction such as confined masonry or reinforced masonry, considered less vulnerable, have been developed instead. (Dina 2003).

At present, a lot of research has been made to characterize the non-linear structural behavior of reinforced concrete and steel buildings and, according to these advances, not only "single pushover analysis" has been developed, but also "multimodal pushover analysis" are also developed to define multimodal "pushover curve". These advances are widely described in reports and technical papers (Chopra and Goel 2002), (Kalkan and Kunnath 2006). Having defined this "pushover curve" and considering the seismic demand in the form of a "reduced earthquake spectra" (Wu and Hanson 1989), (Vidic et. al. 1994), (Ordaz and Pérez 1998), the "performance level" of the structure can be obtained, following the steps given in the different methods (SEAOC 1995 and FEMA 2000).

The "performance level" defines the base shear and top displacement reached by the structure during the action of the seismic demand. This point determines the structural situation of the building after the earthquake, and, therefore, a performance evaluation can be made according to some predefined parameters or limit states.

Unfortunately, for masonry there is still no clear model to describe the nonlinear behavior of this material, because of its complexity and wide variety of forms and, therefore, it is not easy to determine the "pushover curve" of a masonry structure. Some efforts have been made earlier in order to solve this situation (Gellert 2010 and Norda et. al. 2010), but the results are still not conclusive.

In order to contribute to this research field, in this thesis an analytical model is developed to predict the shear strength of unreinforced as well as reinforced masonry and the pushover curves are furnished for these two types of walls from the experimental results and after performance analysis of them.

1.2 Problem Statement

Masonry is one of the oldest and perhaps the most widely used construction methods around the world. Throughout history, masonry has been primarily employed as a compression member in construction of arches, domes and vaults spanning openings and bearing walls to support floors and roofs. Although masonry buildings have suffered more damage during past earthquakes than any other type of structures, they continue to be popular. Due to its relatively poor seismic performance, the use of masonry construction has been discouraged in seismically active zones in the United States for a long time. Despite this fact, numerous unreinforced masonry (URM)

structures are still in service not only in the United States, but all over the world (Casabonne 2000, USGS report 2008, and ACI SP-147). The majority of those URM buildings have been constructed with little or no attention to seismic considerations. This has resulted in a large inventory of buildings that lack ability to dissipate energy through inelastic deformation during seismic activity. Moreover, many aspects of masonry design and construction are still based on traditional construction practice rather than on some rationalized design requirements. One of the reasons behind this is the lack of good understanding in the complex fracture behavior of masonry. Therefore, there is an urgent need to improve the performance of URM structures by retrofitting and strengthening them to resist potential earthquake damage and to minimize loss of lives and properties.

Aside from existing code and design guidelines, there is also lack of good understanding in the complex fracture behavior of masonry. Recently discovery in the realm of material nonlinearity, like softening and dilatancy, being virtually absent in the masonry literature, play a crucial role in the nonlinear processes. Nonlinear finite element analyses will always be helpful for the validation of the design of complex masonry structures under complex loading conditions. Much research effort is still required for refining and improving the existing models to capture full spectrum of fracture in masonry. This study aims to put an endeavor in carrying on the numerical modeling of masonry structure one step forward.

1.3 Objectives and Scope

The specific objectives and scope of this research work can be summarized as follows:

- Strengthening of quasi-brittle masonry walls with various FRPs for in-plane shear loading that normally comes during an earthquake.
- Comparative study of different strengthening techniques among various synthetic and natural FRPs and search for a suitable strengthening method with such a FRP that fits best with the fragile nature of masonry and at the same time the strengthening work is cost effective.
- Define an analytical model for predicting shear strength of FRP retrofitted masonry walls and validate it with the experimental results.
- Propose a simplified numerical model that can be implemented into a general purpose Finite Element Program to carry on this research in the future direction.

1.4 Dissertation at a Glance

This dissertation has been divided into three parts; each includes two chapters, where the last chapter (Chapter 7) is self-standing and belongs to none of the parts. So, there are in total of 7 chapters. Fig. 1.3 presents the research flow and organization of this dissertation. A general overview each of these chapters is given in the following paragraphs.

PART 1

In Chapter 1 (Introduction), a general research background of masonry structures are stated followed by a section that gives the brief review of masonry structures, their performance in the past earthquakes and their seismic strengthening around the world. The statement of the problem, research objectives and scope are stated in the following sections.

Chapter 2 (Masonry Materials and Behavior) depicts the general aspects of masonry materials and their fundamental properties after surveying a good number of literatures on masonry structures. A short review of the types of masonry and modes of masonry failures are discussed. Various types of FRP materials their fundamental properties, and strengthening techniques of masonry structures using these FRPs in light of existing design codes is also discussed in the following sections.

PART 2

In chapter 3 (Interface Shear and Tensile Strength) the shear and tensile strengths at brick-mortar interface are discussed based on experimental findings.

In Chapter 4 (Numerical Modeling for Brick Interface), numerical models for interface shear and tension are proposed and validated at element level.

PART 3

Chapter 5 (In-Plane Shear Strength of Masonry Wall) gives the detail experimentation and test procedure of masonry walls under combined action of compression and shear loads. Unreinforced masonry (URM) walls as well as masonry walls reinforced with different types of FRPs are tested in this testing scheme. An exhaustive discussion of the test results are discussed in the following sections and sub-sections. At the end performance of URM and FRP reinforced masonry walls are shown.

In Chapter 6 (Analytical Modeling for Masonry Wall) the fundamentals and details of the proposed analytical models to predict the shear strengths of both unreinforced and FRP strengthened masonry walls are discussed. Models are verified at member level at the end, followed by some general conclusions.

Finally, in Chapter 7 (Conclusions and Recommendations) general conclusions are outlined encapsulating the whole experimental as well as analytical and numerical works. At the very end, some future recommendations are stated.

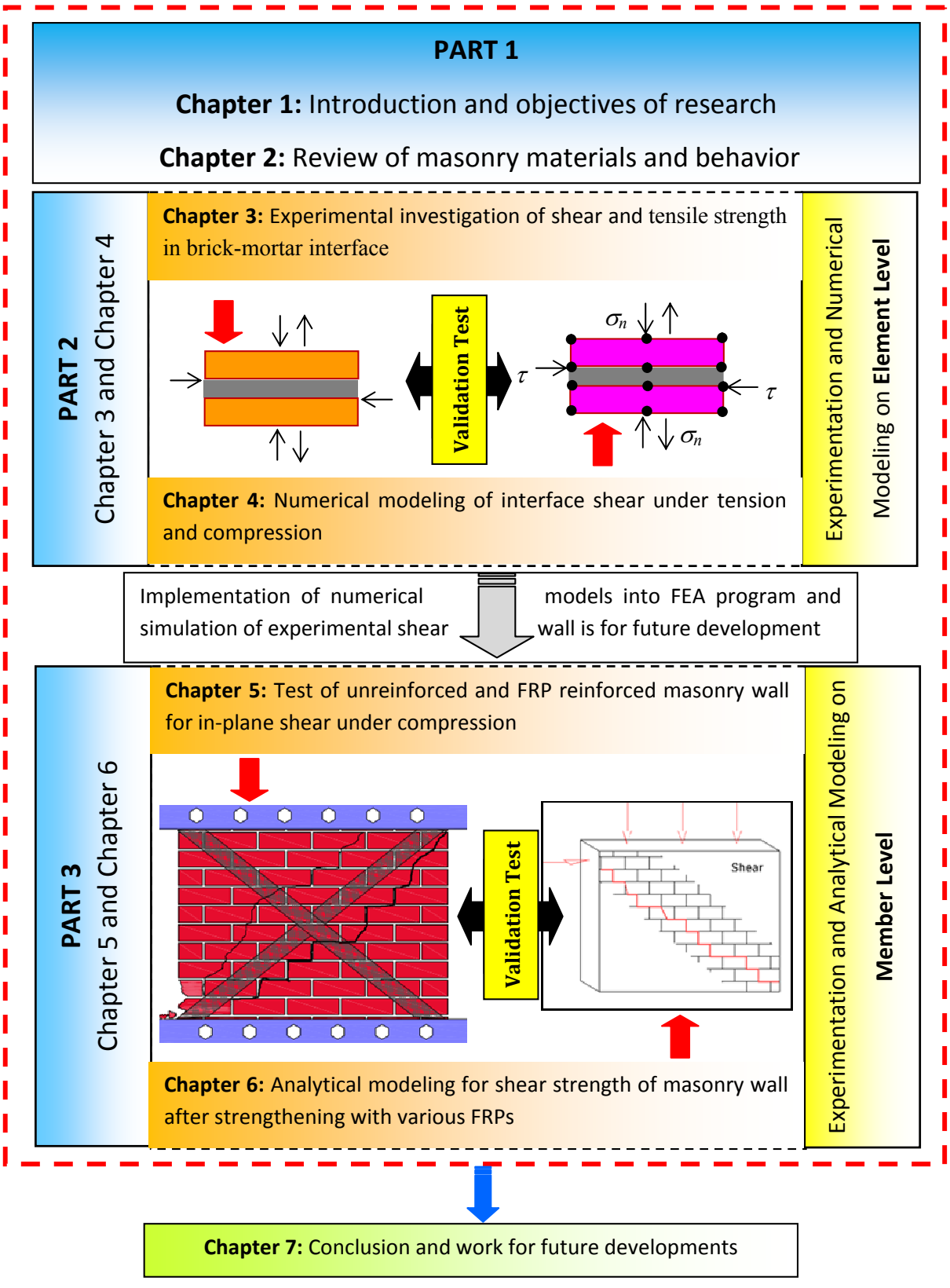

Fig. 1.3. *Flow of research and organization of dissertation*

References

123RF.com. (http://www.123rf.com/aboutus.php)

Ansary M. A. (2006). "Recent earthquake related activities in Bangladesh". ICUS NEWSLETTER, International Center for Urban Safety Engineering Institute of Industrial Science, The University of Tokyo, Vol.5(4).

Chopra, A. K., and Goel, R. K. (2002). "A modal pushover analysis procedure for estimating seismic demands for buildings". *Earthquake engineering and structural dynamics* , S. 561-582.

Dina. D. (2006). "Report on unreinforced brick masonry construction" *University of Bath, United Kingdom.*

FEMA 356. (2000). "Prestandard and commentary for the seismic rehabilitation of buildings." *Federal emergency management agency,* Washington, D.C.

Gellert, C. (2010). "Nichtlinearer Nachweis von unbewerten Mauerwerksbauten unter Erdbebeneinwirkung". *Aachen, Deutschland: Univ.*-Prof. Dr.-Ing. Konstantin Meskouris.

Hendry A.W., Sinha B. P., and Davies S. R. (2004). " Design of Masonry Structure". Taylor & Francis, London.

Jaiswal, K., and Wald, D. J. (2008). "Creating a global building inventory for earthquake loss assessment and risk management". *U.S.A.: U.S. Geological Survey*.

Kalkan, E., and Kunnath, S. (2006). "Adaptive modal combination procedure for nonlinear static analysis of buildings structures". *Journal of Structural Engineering,* S. 1721-1731.

Mayorca, P., and Meguro, K. (2003). "Proposal of a new economic retrofitting method for masonry structures". *JSCE Journal of Earthquake Engineering ,* S. 1-4.

Norda, H., Reindl, L., and Meskouris, K. (2010). "A nonlinear multimodal procedure for masonry buildings". 10th International Conference on Computational Structures Technology. Valencia, Spain: Civil-Comp Press.

Ordaz, M., and Pérez, E. (1998). "Estimation of Strength Reduction Factors for Elastoplastic Systems, New Approach." *Earthquake Engineering and Structural Dynamics.*

SEAOC (1995). "Performance Based Seismic Engineering." *Report prepared by Structural Engineers Association of California.*

Uzoegbo, H. C. (2011). "Seismic behaviour of single-story URM buildings with light weight steel roof". *International Journal of Advanced Technology in Civil Engineering,* S. 28-35.

Vidic, T., Fajfar, P., and Fischinger, M. (1994). "Consistent Inelastic Design Spectra: Strength and Displacement". *Earthquake Engineering and Structural Dynamics*

Wu, J., and Hanson, R. (1989). "Study of inelastic spectra with high damping". *Journal of Structural Engineering . ,* S. 1632-1642.

WHE (2011). "Unreinforced brick masonry construction" World Housing Encyclopedia, a joint project *by the Earthquake Engineering Research Institute (EERI) and the International Association for Earthquake Engineering (IAEE).*

Chapter 2

Review of Masonry Materials and Behavior

2.1 Introduction

The basic rules to be followed and various requirements to be satisfied for masonry construction are specified in the codes of practice for structural masonry construction. The information in this chapter is based on the ASTM, FEMA 2000, ACI 440, ACI 318, CNR_DT 200 R1 and European structural design codes (EC6 and EC8). Eurocode 6 specifies the rules and provisions for structural masonry. Additional provisions to be considered for masonry construction in earthquake regions are outlined in Eurocode 8. The discussion in this section aims at achieving safe unreinforced masonry houses constructed from burnt clay brick units.

2.2 Properties of Brick, Mortar and FRPs

2.2.1 Brick

The fundamentals of brick manufacturing have not changed over time. However, technological advancements have made contemporary brick plants substantially more efficient and have improved the overall quality of the products. A more complete knowledge of raw materials and their properties, better control of firing, improved kiln designs and more advanced mechanization have all contributed to advancing the brick industry (BIA 2006). Clay is one of the most abundant natural mineral materials on earth. For brick manufacturing, clay must possess some specific properties and characteristics. Such clays must have plasticity, which permits them to be shaped or molded when mixed with water; they must have sufficient wet and air-dried strength to maintain their shape after forming. Also, when subjected to appropriate temperatures, the clay particles must fuse together.

Clays occur in three principal forms, all of which have similar chemical compositions but different physical characteristics.

Surface Clays: Surface clays may be the upper crust of older deposits or of more recent sedimentary formations. As the name implies, they are found near the surface of the earth.

Shales: Shales are clays that have been subjected to high pressures until they have nearly hardened into slate.

Fire Clays: Fire clays are usually mined at deeper levels than other clays and have refractory qualities.

Surface and fire clays have a different physical structure from shales but are similar in chemical composition. All three types of clay are composed of silica and alumina with varying amounts of metallic oxides. Metallic oxides act as fluxes promoting fusion of the particles at lower temperatures. Metallic oxides (particularly those of iron, magnesium and calcium) influence the color of the fired brick. The manufacturer minimizes variations in chemical composition and physical properties by mixing clays from different sources and different locations in the pit. Chemical composition varies within the pit, and the differences are compensated for by varying manufacturing processes. As a result, brick from the same manufacturer will have slightly different properties in subsequent production runs. Further, brick from different manufacturers that have the same appearance may differ in other properties.

1) Manufacturing

Although the basic principles of manufacture are fairly uniform, individual manufacturing plants tailor their production to fit their particular raw materials and operation. Essentially, bricks are produced by mixing ground clay with water, forming the clay into the desired shape, and drying and firing. In ancient times, all molding was performed by hand. However, since the invention of brick-making machines during the latter part of the 19th century, the majority of brick produced in the United States have been machine made.

2) Phases of Manufacturing

The manufacturing process has six general phases: 1) mining and storage of raw materials, 2) preparing raw materials, 3) forming the brick, 4) drying, 5) firing and cooling and 6) de-hacking and storing finished products (Fig. 2.1).

3) Properties

All properties of brick are affected by raw material composition and the manufacturing process. Most manufacturers blend different clays to achieve the desired properties of the raw materials and of the fired brick. This improves the overall quality of the finished product. The quality control during the manufacturing process permits the manufacturer to limit variations due to processing and to produce a more uniform product. The most important properties of brick are: durability, color, texture, size variation, compressive strength and absorption.

4) Durability

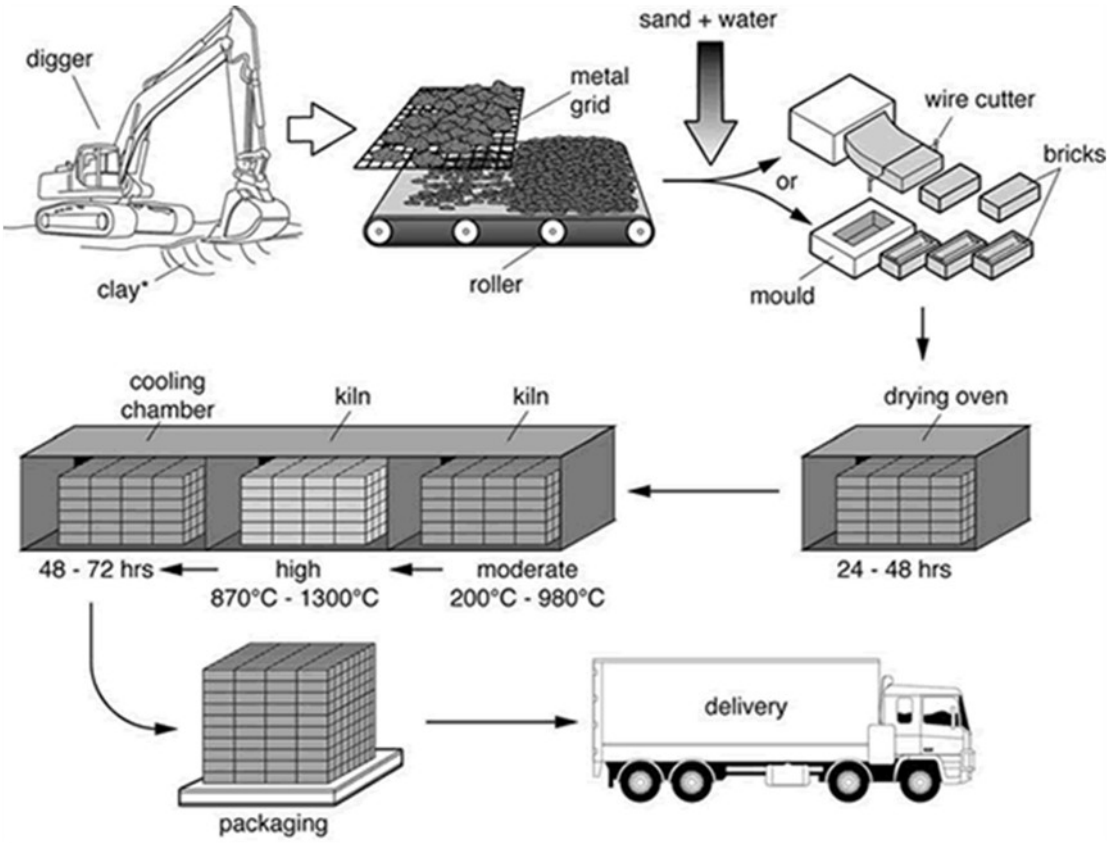

Fig.2.1. *Diagrammatic representation of manufacturing of brick (BIA, 2006)*

The durability of brick depends upon achieving incipient fusion and partial vitrification during firing. Because compressive strength and absorption values are also related to the firing temperatures, these properties, together with saturation coefficient, are currently taken as predictors of durability in brick specifications. However, because of differences in raw materials and manufacturing methods, a single set of values of compressive strength and absorption will not reliably indicate the degree of firing.

5) Color

The color of fired clay depends upon its chemical composition, the firing temperatures and the method of firing control. Of all the oxides commonly found in clays, iron probably has the greatest effect on color. Regardless of its natural color, clay containing iron in practically any form will exhibit a shade of red when exposed to an oxidizing fire because of the formation of ferrous oxide. When fired in a reducing atmosphere, the same clay will assume a dark (or black). Creating a reducing atmosphere in the kiln is known as flashing or reduction firing. Given the same raw material and manufacturing method, darker colors are associated with higher firing temperatures, lower absorption values and higher compressive strength values. However, for

products made from different raw materials, there is no direct relationship between strength and color or absorption and color.

6) Texture

Many brick have smooth or sand-finished textures produced by the dies or molds used in forming. A smooth texture, commonly referred to as a die skin, results from pressure exerted by the steel die as the clay passes through it in the extrusion process. Most extruded brick have the die skin removed and the surface further treated to produce other textures using devices that cut, scratch, roll, brush or otherwise roughen the surface as the clay column leaves the die (Fig. 2.1).

7) Size Variation

Because of the shrinkage of clay during both drying and firing, allowances are made in the forming process to achieve the desired size of the finished brick. Both drying shrinkage and firing shrinkage vary for different clays, usually falling within the following ranges:

• Drying shrinkage: 2 to 4 percent

• Firing shrinkage: 2.5 to 4 percent

Firing shrinkage increases with higher temperatures, which produce darker shades. When a wide range of colors is desired, some variation between the sizes of the dark and light units is inevitable. To obtain products of uniform size, manufacturers control factors contributing to shrinkage. Because of normal variations in raw materials and temperature variations within kilns, absolute uniformity is impossible. Consequently, specifications for brick allow size variations.

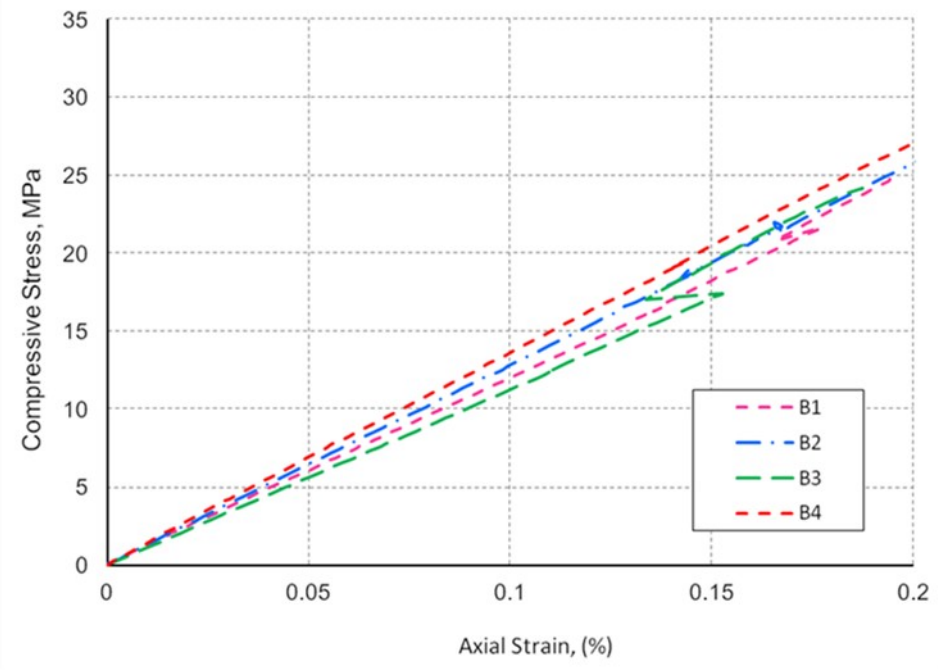

Fig. 2.2. *Compressive stress vs. strain for typical masonry bricks*

8) Compressive Strength and Absorption

Both compressive strength and absorption are affected by properties of the clay, method of manufacturing and degree of firing. For a given clay and method of manufacture, higher compressive strength values and lower absorption values are associated with higher firing temperatures. Although absorption and compressive strength can be controlled by manufacturing and firing methods, these properties depend largely upon the properties of the raw materials. Fig. 2.2 shows test results of typical compressive stress-strain relationship of fired clay bricks, performed by the author.

9) Classification of Bricks

Masonry units are classified into the following types: solid, perforated unit, hollow unit, cellular unit and horizontally perforated unit (Fig. 2.3). EC6 2005 gives specifications regarding the use of the following masonry units:

- Fired clay units
- Fired clay lightweight units
- Calcium silicate units
- Concrete block units
- Lightweight concrete block units
- Autoclaved aerated concrete units

Solid masonry units are either units without depression or units with depression (also known as Frog Mark) that are filled with mortar during construction, or units with up to 25% by volume of vertical holes. In ASTM standards, a solid brick is defined as a unit whose net cross- sectional area in every plane parallel to the bearing surface is 75 percent or more of its gross cross-sectional area measured in the same plane. Thus, a solid brick has a maximum coring or void area of 25 percent. A hollow brick is defined as a unit whose net cross-sectional area in every

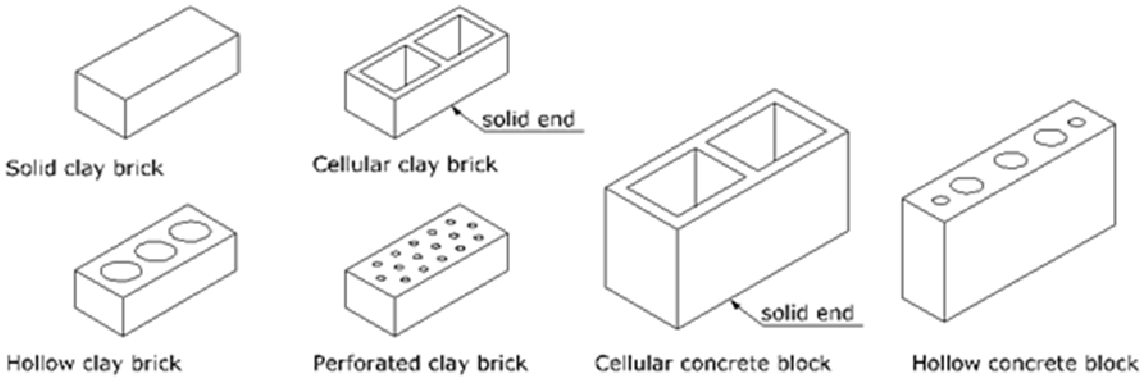

Fig. 2.3. *Type of masonry units (WHE, 2011)*

plane parallel to the bearing surface is less than 75 percent of its gross cross-sectional area measured in the same plane. A hollow brick has a minimum coring or void area greater than 25 percent, and a maximum of 60 percent. Brick are cored or frogged at the option of the manufacturer (BIA 2007).

2.2.2 Masonry Mortar

Mortar bonds individual brick together to function as a single element. In its hardened state, mortar must be durable and must help resist moisture penetration. Mortar also must have certain properties in its plastic state so that it is both economical and easy to place. Centuries ago, combinations of sand and lime were used as mortar. These combinations took months and even years to harden, as the lime slowly combined with carbon dioxide from the air to form calcium carbonate. Because it took so long for these mortars to harden and gain strength, it was necessary to use very thin joints. In many instances the joints were so thin that adjacent masonry units would bear on each other in direct contact. This type of construction required an excessive amount of labor to carefully fit and place each masonry unit. However, sand-lime mortars were adequate for the then massive construction and slow-paced construction procedures. The development of mortars that harden and gain strength rapidly made it possible to place masonry units quickly. Also, thicker joints provided cushions for dimensional variations in the masonry units. The stronger mortars were first obtained by "sweetening" the lime with a small amount of portland cement (PCA 2004). Later, the ratio of Portland cement was progressively increased until the process involved sweetening the cement with a small amount of lime.

In the later 19$_{th}$ century, the advancement of strong mortars with controlled setting characteristics was a major step forward for masonry construction. Another important step was the development of masonry cements in the 1930s (see detail in sec 2.2.3).

Today, most mortars are made with masonry cement due to the ease of use and consistent performance. These mortars are a combination of a masonry cement, clean and well-graded sand, and enough clean water to produce a plastic, workable mix. Masonry cements that meet the requirements of ASTM C 91 or Canadian Standards Association (CSA) standard A3002 ensure workable, sound, and durable mortar. In the 1990s, increased use of masonry in demanding structural applications and high seismic areas resulted in the development of a new product, mortar cement. Mortar cement is similar to masonry cement in that it is factory-prepared hydraulic cement primarily used to produce masonry mortar. However, ASTM C 1329, the Standard Specification for Mortar Cement, places lower maximum air content limits on mortar cement than permitted for masonry cements, and ASTM C 1329 is the only ASTM masonry

material specification that includes bond strength performance criteria. According to the specification used in EC 6, several types of mortar can be used for masonry walls:

- General purpose mortar, used in joints with thickness greater than 3mm and produced with dense aggregate.
- Thin layer mortar, which is designed for use in masonry with nominal thickness of joints 1-3mm.
- Lightweight mortar, which is made using perlite, expanded clay, expanded shale etc. Lightweight mortars typically have a dry hardened density lower than 1500kg/m^3.

Mortar for masonry is designed not only to join masonry units into an integral structure with predictable performance properties, but also to: (1) affect tight seals between units against the entry of air and moisture; (2) bond with steel joint reinforcement, metal ties, and anchor bolts, if any, so that they perform integrally with the masonry; (3) provide an architectural quality to exposed masonry structures through color contrasts or shadow lines from various joint-tooling procedures; and (4) compensate for size variations in the units by providing a bed to accommodate tolerances of units. Masonry mortar is composed of one or more cementitious materials; clean, well-graded masonry sand; and sufficient water to produce a plastic, workable mixture. Modern specifications call for proportions by volume ranging from one part of cementitious material to $2^1/_4$to $3^1/_2$ parts of damp, loose mortar sand. The choice of cementitious material—masonry cement, mortar cement, a portland cement and lime combination, or a portland cement and masonry cement or mortar cement combination—is largely a matter of economics and convenience. Any of these combinations will produce mortar with acceptable properties as long as applicable specifications are met and appropriate design procedures are followed.

Good mortar is necessary for good workmanship and proper structural performance of masonry construction. Since mortar must bond masonry units into strong, durable, weathertight walls, it must have the properties described below.

1) Workability

Probably the principal quality of plastic masonry mortar is workability, because of its influence on other important mortar properties in both the plastic and the hardened states. Workability is difficult to define because it is a combination of a number of interrelated properties. The properties considered as having the greatest influence on workability are consistency (flowability), water retentivity, setting time, weight, adhesion, and cohesion. An experienced mason judges the workability of mortar by the way it adheres to or slides from his trowel. Mortar

of good workability should spread easily on the masonry unit, cling to vertical surfaces, extrude readily from joints without dropping or smearing, and permit easy positioning of the unit without subsequent shifting due to its weight or the weight of successive courses. A mortar's consistency should be compatible with the units and weather conditions. For example, under hot summer conditions when using a high-absorption unit, a softer mortar having a higher water content is needed, compared to that used with a dense unit during cold winter construction.

2) Water Retentivity

Mortar having this property resists rapid loss of mixing water (prevents loss of plasticity) to the air on a dry day or to an absorptive masonry unit. Rapid loss of water causes the mortar to stiffen quickly, making it practically impossible to obtain weather-tight joints. A mortar that has good water retentivity remains soft and plastic long enough for the masonry units to be carefully aligned, leveled, plumbed, and adjusted to proper line without danger of breaking the intimate contact or bond between mortar and unit. When low absorption units such as split block are in contact with a mortar having too much water retentivity, they may float. Consequently, the water retentivity of a mortar should be within tolerable limits. Water adds workability to the mortar; entrained air or extremely fine aggregate or cementitious materials not only add workability or plasticity to the mortar, they also increase its water retentivity.

3) Consistent Rate of hardening

The rate of hardening of a mortar due to hydration (chemical reaction) is the speed at which it develops resistance to an applied load. Rapid hardening may interfere with the use of the mortar by the mason. Very slow hardening may impede the progress of work, because the mortar will extrude from the completed masonry. During winter construction, slow hardening may also subject mortar to early damage from frost. A well defined, consistent rate of hardening assists the mason in laying the masonry units and in tooling the joints at the same degree of hardness. Hardening is sometimes confused with a stiffening caused by rapid loss of water, as when low-water retention mortar is used with highly absorptive units. Also, in very hot, dry weather, mortar may tend to stiffen more rapidly than usual. In this case, the mason may find it advisable to lay shorter mortar beds and fewer units in advance of tooling.

4) Durability

The durability of masonry mortar is its ability to endure exposure conditions. Mortar joints can deteriorate from exposure to freeze-thaw cycles when saturated, from exposure to aggressive chemical environments, or from the use of unsound materials. Damage by frost action—either to mortar joints or to mortar bond— has not been a problem in most masonry wall construction

above grade. In order for frost damage to occur, the hardened mortar must first be water-saturated or nearly so. Although mortar is saturated when first placed, the mixing water is absorbed by units and chemically combined with cement compounds as the mortar hardens. The saturated condition does not readily return except when the masonry is in continuous contact with saturated soils, when downspouts leak, when there are heavy rains, or when horizontal ledges are formed. Under these conditions, the masonry unit and mortar may become saturated, which can lead to freeze-thaw deterioration if temperatures drop to freezing or below. High-compressive-strength mortars usually have good freeze-thaw durability. Because air-entrained mortar will withstand hundreds of freeze-thaw cycles, its use provides good protection against localized freeze-thaw damage. Masonry cement and mortar cement mortars have higher air contents than non-air-entrained portland cement and lime mortar and therefore have better freeze-thaw resistance. Sulfate attack provides an example where deterioration of mortar results from exposure to an aggressive chemical environment. Sulfate resistance is usually not a concern for masonry above ground; however, in some parts of the world, masonry can be exposed to sulfate from soil, ground water, or industrial processes. Sulfate-resistant masonry materials should be used when they are going to be in contact with soils containing more than 0.1% water-soluble sulfate (SO_4) or water solutions containing more than 150 ppm of sulfate. Without the use of sulfate-resistant masonry units and mortar or use of a protective treatment, sulfates would attack and deteriorate masonry. Masonry cement, sulfate-resistant portland cements (Types II or V) or hydraulic cements (Types MS or HS), or sulfate-resistant blended cements should be used in mortar exposed to sulfates. One study demonstrated that masonry cement is significantly more sulfate resistant than a Type II portland cement and lime mortar when tested in accordance with ASTM C 1012. Expansion in mortars due to unsound ingredients can cause serious disintegration of masonry. Soundness of a hydraulically cementitious material is measured by the autoclave expansion test (ASTM C 151). ASTM specifications for masonry cement (ASTM C 91), mortar cement (ASTM C 1329), and portland cement (ASTM C 150) limit acceptable changes in length of the test specimen to ensure that no serious expansion of the hardened mortar will occur in a wall. While a method for measuring soundness of hydrated lime has been developed, correlation of results to field performance has not yet been established. Thus, soundness is generally assured by limiting the unhydrated oxide content of the hydrated lime to a maximum of 8%. Absorption of mortar is a measure of how much water the hardened mortar will take in. Low absorption mortars will be less susceptible to saturation, freeze-thaw deterioration, and staining. Absoprtion is reduced by increasing cement content, using air-entrained mortars, and using water repellent admixtures.

5) Compressive Strength

The principal factors affecting the compressive strength of masonry structures are the compressive strength of the masonry unit, the proportions of ingredients comprising the mortar, the design of the structure, the workmanship, and the degree of curing. Although the compressive strength of masonry may be increased with a stronger mortar, the increase is not proportional to the compressive strength of the mortar. Tests have shown that compressive strengths of concrete masonry walls increase only by about 10% when mortar cube compressive strengths increase 130%. Composite wall compressive strengths increase by 25% when mortar cube compressive strength increases 160% (Fishburn 1961). Compressive strength of mortar is largely dependent on the type and quantity of cementitious material used in preparing the mortar. It increases with an increase in cement content and decreases with an increase in air entrainment, lime content, or water content. Portland cement requires a period in the presence of moisture to develop its full strength. To obtain optimum curing conditions, the mortar mixture should contain the maximum amount of water compatible with acceptable workability. Lean, oversanded mixtures should be avoided as they will have poor water retention characteristics. Freshly laid masonry should be protected from the sun and drying winds. With severe drying conditions, it may be necessary either to wet the exposed mortar joints with a fine water spray daily for about 3 days or to cover the masonry with a plastic sheet, or both.

6) Bond

The term bond refers to a specific property that can be subdivided into: (1) extent of bond, or degree of contact of the mortar with the masonry units; and (2) bond strength, or force required to separate the units. A chemical and a mechanical bond exist in each category. Good extent of bond (complete and intimate contact) is important to watertightness and tensile bond strength. Poor extent of bond at the mortar-to-unit interface may lead to moisture penetration through the unbonded areas. Good extent of bond is obtained with a workable and water-retentive mortar, good workmanship, full joints, and masonry units having a medium initial rate of absorption (suction). Bond strength is usually measured as tensile or flexural bond strength. In determining direct tensile bond strength, specimens representing unit and mortar are pulled apart. Test methods for measuring flexural (more properly termed “flexural-tensile”) bond strength place a more complex load on the mortar-to-unit interface, but can be applied to full-sized specimens. ASTM Method C 1072 utilizes a bond wrench apparatus and loading configuration to induce failure of prisms constructed from full-sized masonry units (see detail in Sec.3.4 in Chapter 3). While bond strength is an important property of masonry, current methods of test for determining bond strength are considered impractical as a basis for material specifications or

quality control at the jobsite, due to the high variability of results inherent in the testing methods. Many variables affect bond, including (1) mortar ingredients, such as type and amount of cementitious materials, water retained, and air content; (2) characteristics of the masonry units, such as surface texture, suction, and moisture content; (3) workmanship, such as pressure applied to the mortar bed during placing; and (4) curing conditions, such as temperature, relative humidity, and wind. The effects of some of these variables on bond will be briefly discussed in Chapter 3. All other factors being equal, mortar bond strength is related to mortar composition, especially the cement content. The bond strength of the mortar increases as the cement content increases (Fig. 3.17 and Fig.3.18 on Chapter 3). Bond strength tends to decrease as air contents increase. However, excellent bond strengths can be achieved using air-entrained mortars. An extensive study of over 20 different masonry cements representing a cross section of producers throughout the United States confirms that masonry cements yield excellent flexural bond strengths (Dubovoy and Ribar 1990). 75% of these masonry cement mortars tested with a brick unit having an IRA* (initial rate of absorption) of 9 yielded bond strengths in excess of 100 psi (690 kPa). None produced values lower than 65 psi (450 kPa). Bond strength is low on smooth, molded surfaces, such as glass or die skin surfaces of clay brick or tile. On the other hand, good bond is achieved on concrete block or on wire-cut or textured surfaces of clay brick. For high absorption clay brick, bond strengths can be increased by wetting the units prior to laying them. However, surfaces of wetted brick should not be saturated. Concrete masonry units should not be wetted before use.

There is a distinct relationship between mortar flow (water content) and bond strength. For all mortars, bond strength increases as water content increases, within reasonable limits. The optimum bond strength is obtained by using a mortar with the highest water content compatible with workability, even though mortar compressive strength may decrease (Isberner 1974 and Ritchie and Davison 1963). Workmanship is paramount in determining bond strength. The time lapse between the spreading of mortar and the placing of the masonry units should be kept to a minimum because the water content of the mortar will be reduced through suction of the masonry unit on which it is first placed. If too much time elapses before the upper unit is placed, the bond between the mortar and that unit will be reduced. The mason should not realign, tap, or in any way move units after initial placement, leveling, and alignment. Movement disrupts the bond between unit and mortar, after which the mortar will not reestablish good bond with the masonry units.

7) Volume Change

As available water in mortar is absorbed by the masonry units and lost through evaporation, some drying shrinkage occurs. Though generally not a problem in masonry construction, extreme drying shrinkage can result in development of cracks in the mortar. Since drying shrinkage is related to the amount of water lost by the mortar, factors that increase water content of a mortar tend to increase its drying shrinkage. For example, air-entrained mortars tend to have a lower water demand than non-air-entrained mortars at an equivalent flow and thus exhibit less drying shrinkage. However, this principle should not be misinterpreted to mean that water content of a mortar should be arbitrarily reduced. As previously noted, workability and bond are directly related to the flow of the mortar and should be given priority in determining the water content of field mixed mortar. The shrinkage of mortar can be tested in accordance with ASTM C 1148.

8) Appearance

Uniformity of color and shade of the mortar joints greatly affects the overall appearance of a masonry structure. Atmospheric conditions, admixtures, and initial rate of absorption (suction) of the masonry units are some of the factors affecting the color and shade of mortar joints. Others are uniformity of proportions of the mortar mix, water content, and time of tooling the mortar joints. Careful measurement of mortar materials and thorough mixing are important to maintain uniformity from batch to batch and from day to day. Control of this uniformity becomes more difficult with the number of ingredients to be combined at the mixer. Pigments, if used, will provide more uniform color if premixed with a stock of cement sufficient for the needs of the whole project. In many areas, colored masonry cements are available; they provide better control over color uniformity. Tooling of mortar joints at like degrees of setting is important to ensure a uniform mortar shade in the finished structure. If the joint is tooled when the mortar is relatively hard, a darker shade results than if the joints are tooled when the mortar is relatively soft. Some masons consider mortar joints ready for tooling after the mortar has stiffened but is still thumb-print hard, with the water sheen gone. Tooling white cement mortar with metal tools may darken the joint. A glass or plastic joint tool should be used.

9) Specifications

ASTM C 270, Standard Specification for Mortar for Unit Masonry, and CSA Standard A179, Mortar and Grout for Unit Masonry, are the main specification documents in North America. ASTM C 270 covers four types of mortars (Type M, S, N, or O) while CSA A179 defines two types of mortars (Type S and N). Current specifications for mortars for unreinforced and reinforced unit masonry are shown in Tables 2.1 and 2.2. Mortar types are to be identified by

either proportion or property specifications, but not by both. An interplay of property and proportion specifications is not intended or recognized by the specifications. The proportion specifications (Table 2.2) identify mortar type through various combinations of portland or blended cement with masonry cement, masonry cement singly, and combinations of portland or blended cement and lime. The proportion specifications govern when ASTM C 270 or CSA Standard A179 are referred to without noting which specification —proportion or property— should be used. Mortar type classification under the property specifications (Table 2.2) is dependent on the compressive strength of 2-in. (50-mm) cubes, water retention, and air content, using standard laboratory tests per ASTM C 270 or CSA A179.

General purpose mortar, used in joints with thickness greater than 3mm is produced with dense aggregate. Thin layer mortar, which is designed for use in masonry with nominal thickness of joints 1-3mm. Lightweight mortar, which is made using perlite, expanded clay, expanded shale etc. Lightweight mortars typically have a dry hardened density lower than 1500kg/m^3. In Table 2.2 below are shown typical composition of prescribed general purpose mortar mixes and expected mean compressive strength.

Table 2.1 *Recommended Guide for selection of mortar type (ASTM C270)*

Building Segment	**Type**
Exterior, above grade,	
load-bearing	N or S
non-load bearing	N
parapet wall	N or S
Exterior, at or below grade	S or M
Interior	
load-bearing	N or S
non-load bearing	N

Table 2.2 *Typical prescribed composition and strength of general purpose mortars*

Mortar type	Mean compressive strength	Approximate composition in parts of volume		
		Cement	Hydrated lime	Sand
M2	2.5 MPa	1	1.25-2.50	
M5	5 MPa	1	0.50-1.25	2.25-3 times
M10	10 MPa	1	0.25-0.50	cement and lime
M20	20 MPa	1	0-0.25	

Mortars to be used in masonry construction in earthquake regions should comply with EC 8 (2005). According to this standard for the construction of plain and confined masonry, the minimum compressive strength of mortar f_m is set to 5 MPa. Mechanical properties of mortar are determined by testing mortar prisms 40 × 40 × 160mm (EN1015-11). The compressive strength of the mortar is calculated after averaging the strength values of six specimens. The thickness of bed and head joints is recommended to be in the range 8-15mm and all head joints should be fully filled with mortar.

2.2.3 Mortar Cement

Mortar cement is specially formulated and manufactured to produce masonry mortar for use in brick, block, and stone masonry construction. Mortar cement mortars have similar attributes to masonry cement mortars, but they have lower air contents than masonry cements, and the mortar cement specification includes a minimum bond strength requirement. Mortar cement mortars are appropriate for use in structural applications that require masonry with high flexural bond strength.

1) Composition and Materials

Mortar cement consists of a mixture of Portland cement or blended hydraulic cement and plasticizing materials (such as limestone or hydrated lime), together with other materials introduced to enhance one or more properties such as setting time, workability, water retention and durability. These components are proportioned at the cement plant under controlled conditions to assure uniformity of performance (PCA 2002).

Mortar cements are produced in Type N, Type S, and Type M classifications for use in preparation of ASTM Specification C 270 Type N, S, or M mortar, respectively, without further addition of cements. Table 2.1 is a general guide for selection of mortar type. Other factors, such as type and absorption of masonry unit, climate and exposure, applicable building codes, and engineering requirements, should also be considered. Mortar cement mortars conform to the physical properties listed in Table 2.3. These property requirements assure consistent performance of the product with respect to bond strength, compressive strength, workability, and durability.

2) Bond Strength

The mortar cement specification is the only ASTM masonry material specification that includes bond strength performance criteria. The bond strength criteria were established to assure comparable bond strength performance of the mortar cement to non-air-entrained portland cement-lime combinations of equivalent mortar type designation1. The procedure utilized in

determining conformance of mortar cement to bond strength criteria seeks to eliminate, insofar as possible, the effects of workmanship, curing, and unit properties on measured bond strength. Therefore, standard mixing, specimen fabrication, curing, and testing procedures are outlined, including the use of standard testing units. It should be noted that there are many factors that affect the bond of mortar to unit in actual construction, including properties of the unit and mortar, ambient conditions, and the quality of workmanship involved.

Table 2.3 *Physical properties of mortar cement mortar (ASTM C270)*

Mortar Type	Compressive Strength Minimum, MPa (psi)	Water Retention Minimum (%)	Air Content Maximum, (%)
M	17.2 (2500)	75	12
S	12.4 (1800)	75	12
N	5.2 (750)	75	14
O	2.4 (350)	75	14

3) Compressive Strength

By simplifying mortar materials batching at the job site, the use of mortar cement assures consistent strengths between batches and and jobs. Mortar cement mortars mixed according to the property requirements of ASTM C 270 provide strengths that exceed the values listed in Table 2.2. High strength Type S and Type M mortar cements allow the specifier to accommodate special application requirements related to load bearing masonry, masonry below grade level, and masonry for paving, without compromising the advantages of simplified batching.

4) Workability

Workability is the mason's appraisal of the mortar's ability to cling to head joints, slide smoothly off the trowel, and evenly support the placement of units. Mortar of proper workability is soft but has good body; it spreads readily and extrudes from joints without smearing or dropping. Additionally, the masonry mortar needs to retain these properties for a reasonable length of time at whatever ambient conditions exist at the job site. That length of time that the mortar retains its workability is often termed its board life. The plasticizers contained in mortar cements contribute to their workability and board life. Fineness, time of setting, air content, and water retention requirements for mortar cements are specification properties that relate to consistent performance with respect to workability. The importance of workability is apparent when one considers that workmanship is a key element in achieving quality masonry construction.

5) Durability

Expansion of mortars due to unsound ingredients can cause serious disintegration of masonry. Soundness of a cementitious material is measured by the autoclave expansion test. This test produces reactions in any unsound ingredients and simulates a long period of exposure for the cementitious material. Conformance of mortar cement to the autoclave expansion limits of ASTM C 1329 assures that there will be no significant expansion of hardened mortar in a wall due to unsoundness.

2.3 Method of Construction

Brick masonry houses are structures defined by vertical and horizontal elements, respectively walls and floors. Since the main service loads are applied on the floors the seismic forces will be mainly concentrated at each floor level. Floors should be rigid in their plane to distribute the seismic load among the vertical wall elements in proportion to their stiffness. Such floors are referred to as horizontal diaphragms. However diaphragms alone will be inadequate unless good connection between them and the supporting walls exists. When constructing RC slabs, casting of bond-beams just below floor level is economic and efficient solution. Good floor to wall connection can also be achieved by designing steel ties between timber floor joists and supporting wall.

In EC6 are discussed the following types of masonry walls, as shown on Fig. 2.4.

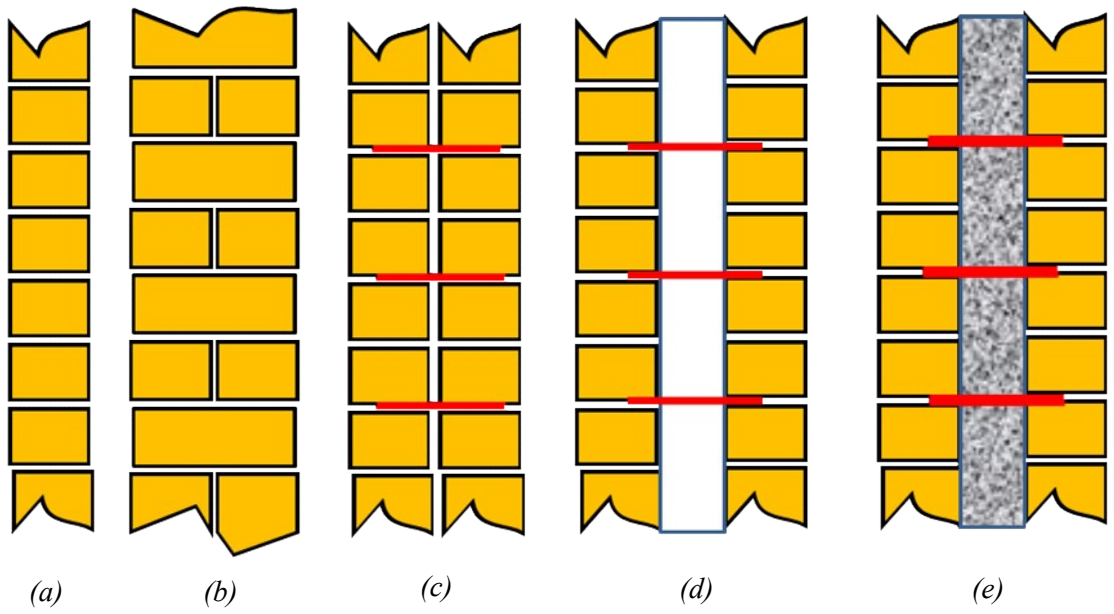

Fig. 2.4. *Cross section of different types of masonry walls; a) single leaf (half brick), b) single leaf (whole brick), c) double leaf, d) cavity wall, e) cavity wall (infilled with concrete)*

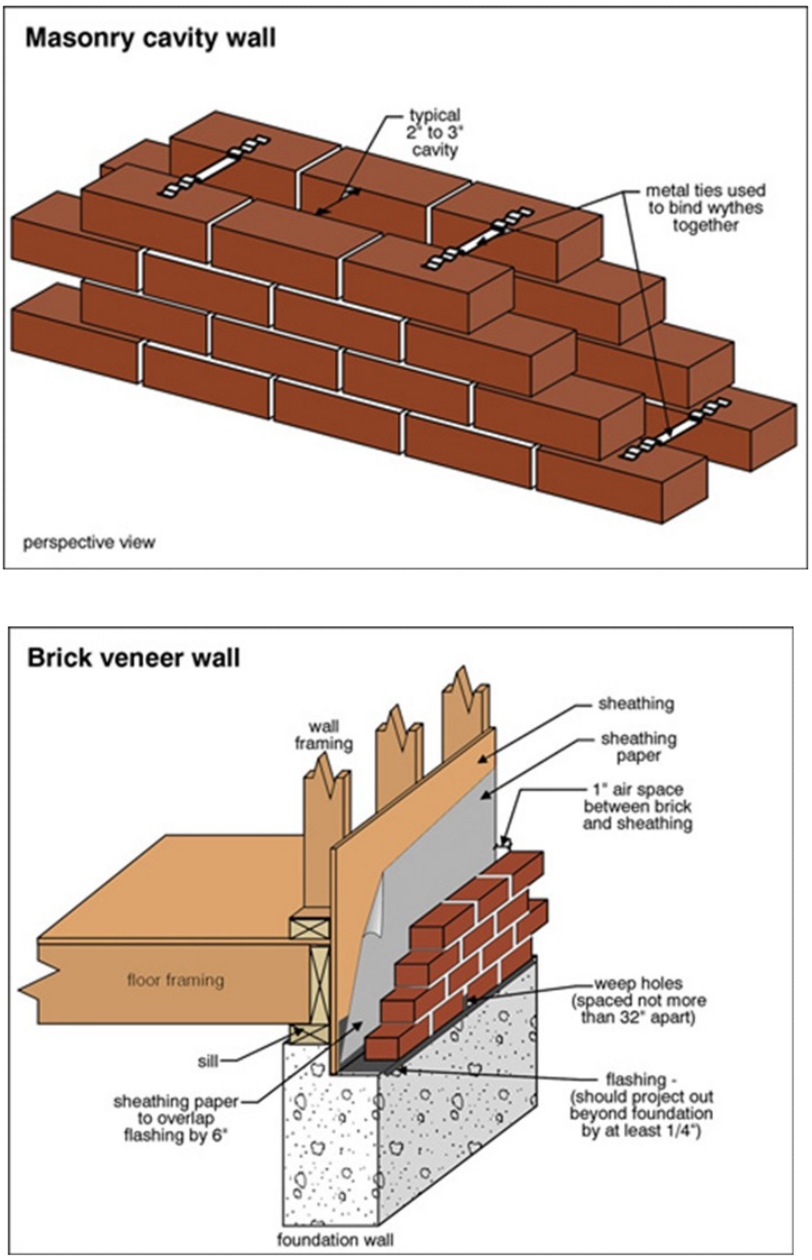

Fig.2.5. *Construction process of masonry cavity wall and veneer wall (Carson Dunlop 2014)*

2.3.1 Single-Leaf Wall

Defined as a wall without continuous vertical joint or cavity

2.3.2 Double-Leaf Wall

Defined as a wall constitued from two parallel leaves and a joint between them max 25 mm, filled with mortar. The leaves can be tied together with steel wall ties to achieve solid wall cross section.

2.3.3 Cavity Wall

Defined as a wall constructed of two parallel single-leaf walls, tied together with wall ties or bed joint reinforcement (Fig. 2.5). One or both leaves can be load-bearing. The cavity between the leaves can be filled, or partially-filled, with non-load bearing insulation material. There is also grouted cavity wall that has a cavity in between the two leaves having a space min of 50 mm apart and are tied securely in place with steel wall ties and bed joint reinforcement, and with a cavity filled with concrete.

2.4 Unreinforced and Reinforced Masonry

2.4.1 Unreinforced Masonry

Unreinforced clay brick masonry is a traditional form for construction of low-rise houses that has been extensively practiced in almost every part of the world. With the increased popularity and availability of reinforced concrete, improved masonry forms of construction, like confined and reinforced masonry became more common for low-rise houses. However traditional houses with load-bearing system of unreinforced burnt clay brick walls are still being constructed in many areas of Asia, Indian Subcontinent and Latin America. This type of housing can be vulnerable to the earthquake shaking unless all rules and recommendations in this guide are followed. Brick masonry should be constructed following simple instructions for quality workmanship:

In dry and hot climate, masonry units should be soaked in water before the construction in order to prevent quick drying and shrinkage of cement based mortars masonry units should be assembled together in overlapped fashion (Fig. 2.6) so that the vertical joints are staggered from course to course. To ensure adequate bonding the units should overlap by a length equal to 0.4 times the height of unit or 40 mm, whichever is the greater. At the corners and wall intersections the overlap should be min the width of the units. To ensure adequate bonding the units should overlap by a length equal to 0.4 times the height of unit or 40 mm, whichever is the greater. At the corners and wall intersections the overlap should be min the width of the units.

Same type of masonry units and mortar should be used for structural walls in the same storey. Bracing walls should be constructed in the same time as the load-bearing walls. The thickness of individual walls is kept constant from storey to storey. In cases where general purpose mortar is going to be used, the mortar joints thickness should be between 8 and 15 mm. In seismic zones, it is recommended that the minimum thickness of load-bearing walls is 240 mm. To ensure

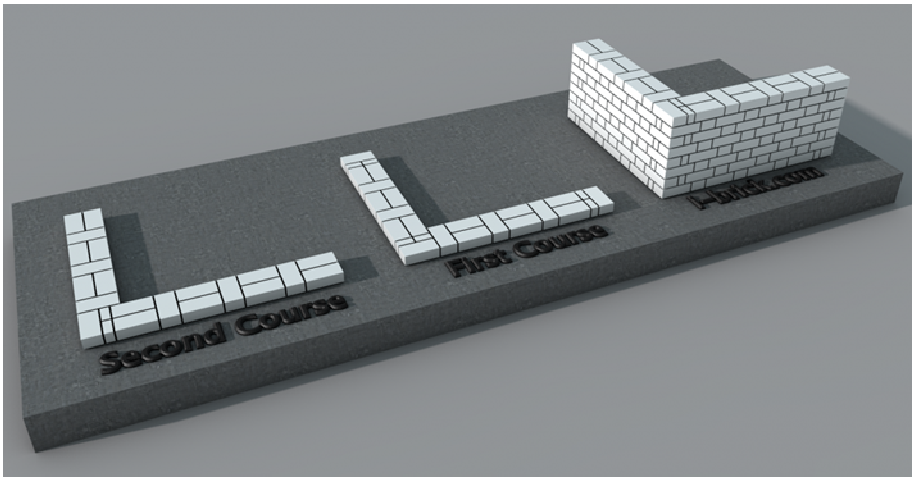

(a) Flemish bond for one brick thick wall

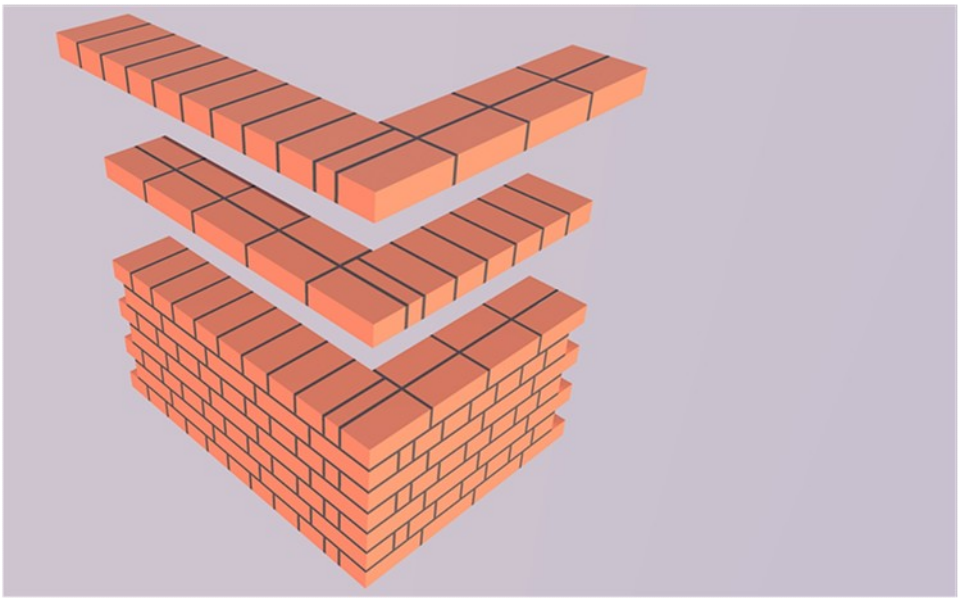

(b) English bond for one brick thick wall

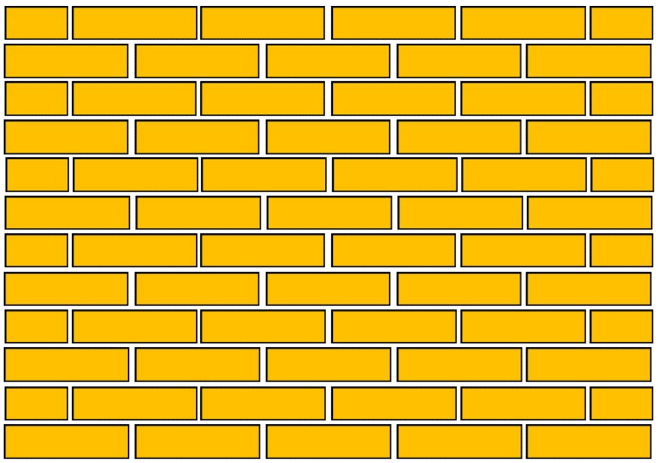

(c) Stretcher bond for half brick thick wall

Fig. 2.6. *Different types of masonry bonds (I-brick 2015)*

stability of walls, the ratio of the effective wall height to wall thickness should be max 15. Openings in plain masonry walls should be limited to ensure load bearing capacity. Therefore the length of a structural wall should be at least 1/2 of the greater clear height of the openings adjacent to the wall.

2.4.2 Behavior of Unreinforced Masonry

Masonry is a complex material, because it is defined as a composition of bricks and mortar. The possibility of combining these elements with different qualities and geometry give masonry a wide range of alternatives of mechanical behavior and structural performance. It is well known that masonry has a good performance when resisting and transmitting compressive loads and a poor performance to resist tensile demands. In particular, the constituent elements of masonry (bricks and mortar) have a strong non-linear response when subjected to high demand loads and, normally, have an anisotropic behavior. There is also a special issue to define the mechanical behavior of the contact zone between brick and mortar, which is highly non-linear. Moreover, normally earthquake loads demand a non-linear response in buildings and their structural components.

The in-plane shear strength of a URM wall depends on the failure mode of the wall, which is governed by a number of variable parameters, such as masonry aspect ratio (L/H), vertical compression on the masonry (σ_n), compressive strength of the masonry (f'_{mc}), tensile strength (f_{tu}), shear strength (τ_u), masonry elastic modulus (E_{me}), and masonry shear modulus (G_{me}). These variables control the inelastic mode of failure of masonry shear walls. The lateral strength of masonry shear walls is limited by flexural cracking, rocking followed by toe crushing, diagonal shear cracking, and sliding shear at the bed-joint (see more detail in Sec 5.1 on Chapter 5).

2.4.3 Reinforced Masonry

A lot variety of reinforced masonries are seen in different parts of the world. They can be commonly divided into three categories:

1. *Internally Reinforced Masonry Wall*
2. *Confined Masonry Wall*
3. *Externally Reinforced Masonry Wall*

In following paragraphs, these three types will be discussed briefly.

1) Internally Reinforcement Masonry Wall

This type of masonry is reinforced with steel bars embedded in the mortar. This reinforcement is placed in the horizontal joints and/or in the brick holes and then filled with grout. The horizontal reinforcement helps to improve the resistance to horizontal loads (shear failure) and the vertical

reinforcement helps to improve the flexural resistance. In North America and Europe, this type of masonry is widely used. Unfortunately, in most developing countries, specially in Aisa, Latin America and Africa, this type of masonry is not popularly used, especially because the grout filling for vertical bars is not well done. A general scheme of reinforced masonry is displayed in Fig. 2.7.

2) Confined Masonry Wall

This is a special type of masonry which takes into account the confinement of the masonry within a reinforced concrete frame. This confinement is materialized with vertical tie columns and a horizontal bond beam [Fig. 2.8(a)]. Normally, the codes define the requirements for the maximum area to be confined in order to have a good structural performance. In seismic countries, this type of masonry is widely used and, sometimes, obligatory. In this type of masonry the distribution of steel reinforcement on the intersections between tie columns and bond beams is very important. It is also important to note that there are differences in this type of masonry, depending on how the wall is built. If the masonry is built before the reinforced concrete frame, then the structural system masonry is called "confined masonry". If the masonry is built after the reinforced concrete frame, then the structural system is called "infilled frame" [Fig. 2.8(b)].

3) Externally Reinforcement Masonry Wall

Externally reinforcement of masonry walls are done primarily by attaching FRP sheets on the surface of the walls in different configurations, as shown in Fig. 2.9.

2.5 Masonry Strengthening and Retrofitting

The performance of the building subject to an earthquake motions is governed by the inter-connectivity of structural components as well as the individual component's strength, stiffness and ductility. Thus the details to provide seismic resistance can be classified in two categories:

1) Details for Complete Load Path

- Provide wall to wall connection ie. tying of walls
- Provide means for walls to foundations connection
- Provide connection of bond beams to roof
- Provide connection of walls to bond beams

Provide stiffness in their plane floors/roofs

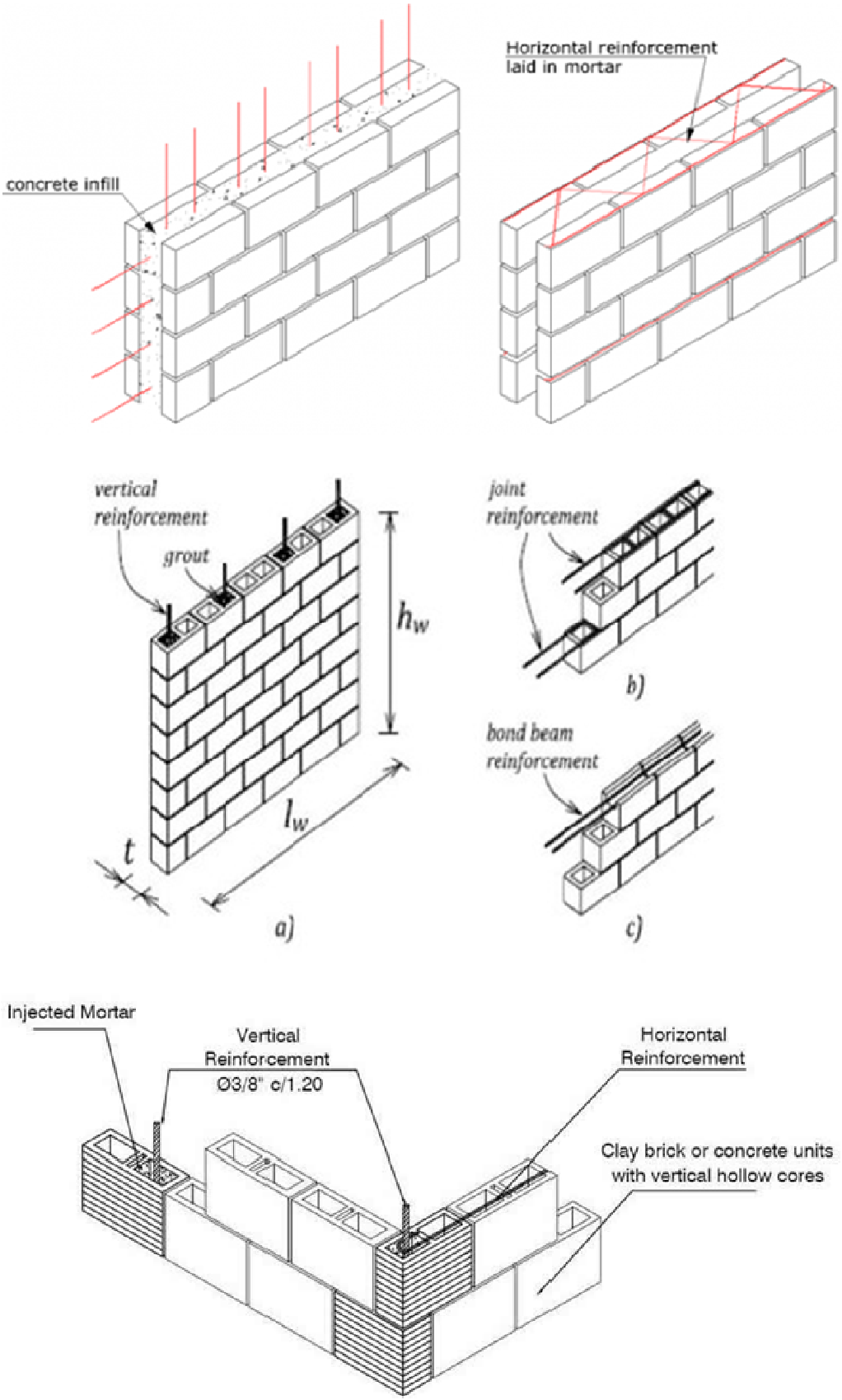

Fig. 2.7. *Construction process of various types of internally reinforced masonry wall (Sam 2011).*

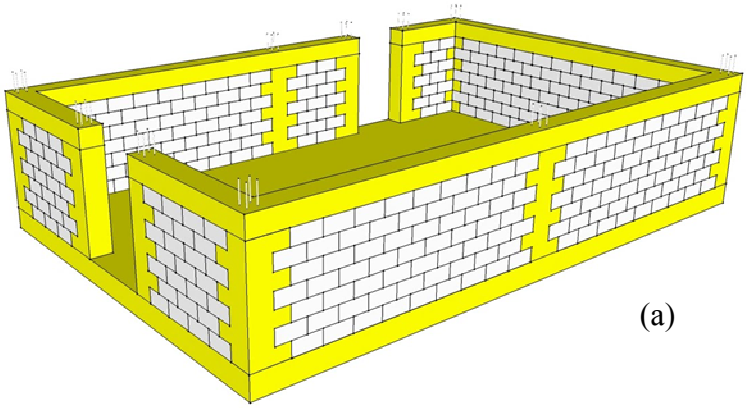

(a)

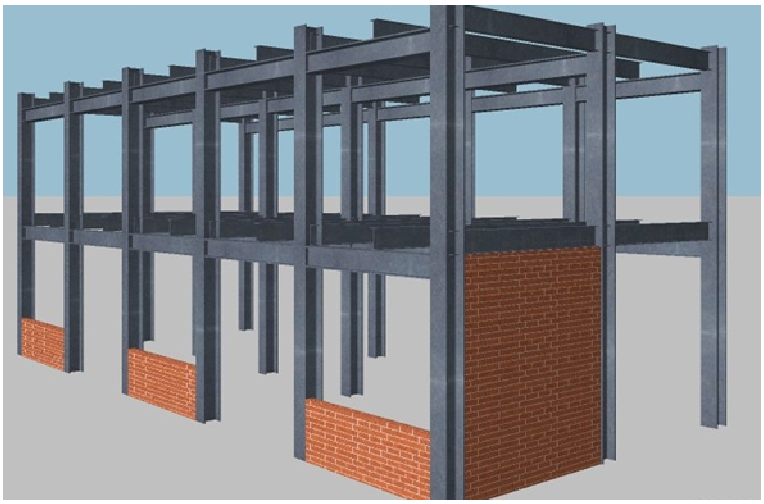

(b)

Fig.2.8. *a) Confined masonry wall, b) In-filled masonry wall (The Global Studio)*

2) Details to Improve Structural Components Strength and Ductility

- Improve the compressive strength of structural components
- Improve the flexural strength of structural components
- Improve the shear strength of structural components
- Improve the ductility of the structural components

2.5.1 Retrofitting Materials

For external retrofitting, there are two types of FRP materials are generally used; they are 1) Synthetic fibers and 2) Natural fibers. Following sections will give more detail on these two types of fibers.

1) Synthetic Fibers

A fiber reinforced polymer (FRP) is a composite material consisting of a polymer matrix imbedded with high-strength fibers, such as Glass, Aramid, Carbon, Natural fiber etc to achieve

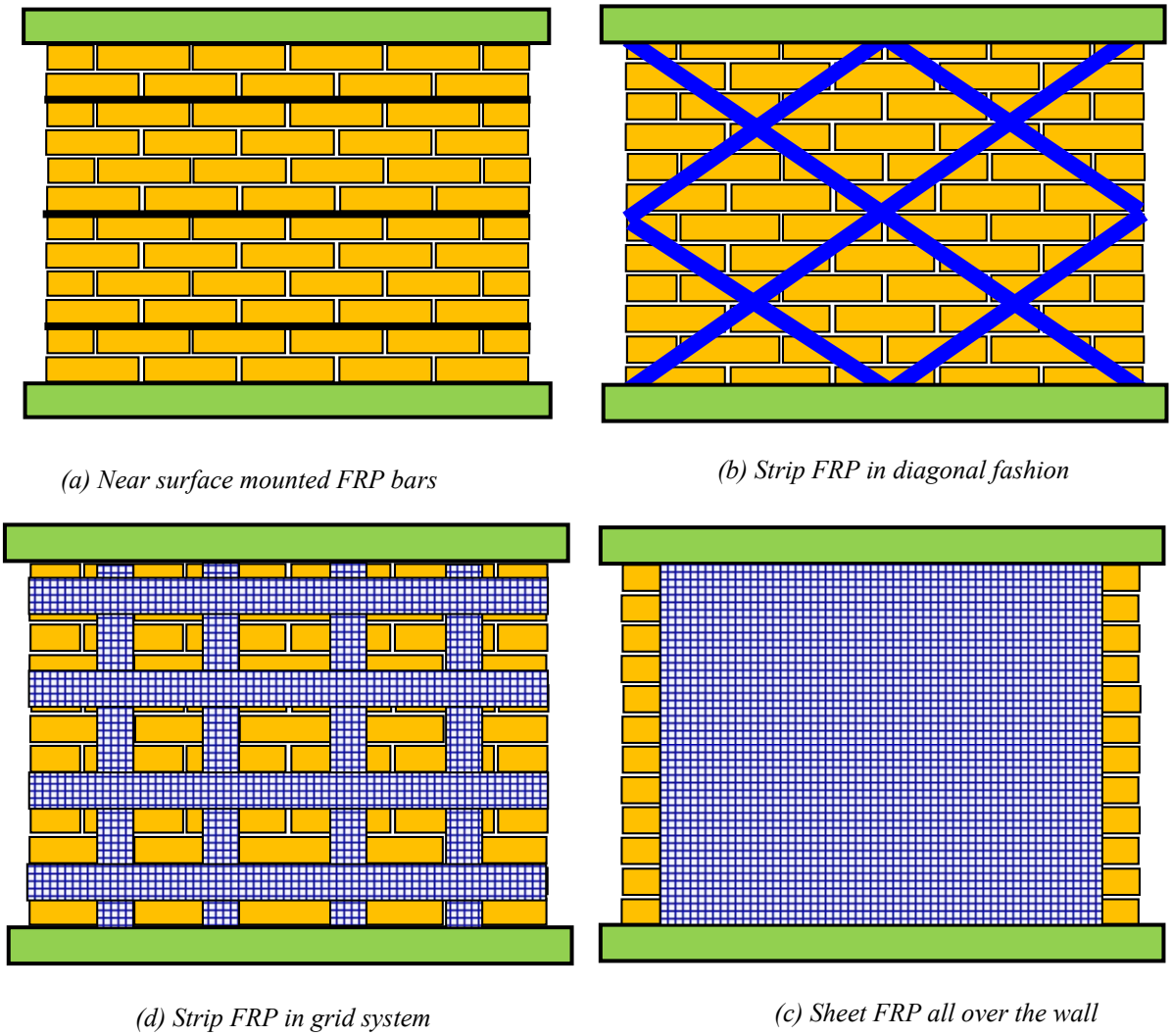

(a) Near surface mounted FRP bars

(b) Strip FRP in diagonal fashion

(d) Strip FRP in grid system

(c) Sheet FRP all over the wall

Fig. 2.9. *Different techniques of FRP installation on masonry wall*

certain properties better than either of the base materials (Fig. 2.10). The one success of the FRP industry has been its use for repair and strengthening. One reason for the success is the light weight. However, the benefit comes from the reduction in handling costs; despite additional material costs, FRPs are easy to install (Burgoyne & Balafas 2007). The use of FRPs as a shear reinforcing material for RC members is becoming increasingly popular since the early 1990s, due to their various advantages that include low weight to strength ratio, non-corrosiveness, minimum disruption to the use and no significant change in the geometry. Besides high strength and high stiffness, these composites have long fatigue life and adaptability to the intended function of the structure. The aim of seismic retrofitting is to upgrade the ultimate strength/deformation of the structure by improving the structure's ability to undergo inelastic deformation without fully collapsing during an earthquake. However, to date the number of primary structural applications of FRPs in construction remains relatively low and there appears to be a number of issues contributing to their slow uptake by the construction industry. Issues

such as cost, absence of design codes, lack of industry standardization, poor understanding of construction issues by composites industry, lack of designers experienced with polymer composite materials and civil/building construction are commonly claimed to place these materials at a disadvantage when considered against traditional construction materials. The practical applications of FRPs to URM are very few and are being used for the reinforcement of old masonry structures, mostly in Italy and Greece.

2) Natural Fibers

Research on natural fiber composites has incepted long ago but has not received much attention until late in the 1980's. There is enough potential for agro based product as an additives / reinforcement in the formation of composite materials. Natural fibers offer many technical and ecological benefits for their use in reinforcing composites. Many types of natural fibers have been investigated for use in plastics including cotton, jute, straw, flax, hemp, wood, sugarcane, bamboo, grass-, kenaf, sisal, coir, rice husks, wheat, barley, oats, kapok, mulberry, banana fiber, raphia, pineapple leaf fiber and papyrus etc (Malhotra et al. 2012) (Fig. 2.10). These materials are predominantly used as a replacement for conventional synthetic petroleum based fibers. Petroleum based composites; primarily glass and carbon as well as few bio-fiber composites are found in countless industries including: aerospace, leisure, construction, sport, packaging, and automotive industries, (Holbery et al. 2006, Bledzki et al 2006 and Mohantya et al. 2000). This serves a two-fold benefit to the industries; to lower the overall weight of the product thus increasing fuel/cost efficiency and to increase the sustainability of their manufacturing process. Recently, car manufactures have been interested in incorporating natural fiber composites into both interior and exterior parts. Many companies such as Mercedes Benz, Toyota and DaimlerChrysler have already accomplished this and are looking to expand the uses of natural fiber composites (Westman et al. 2010). A major goal of natural fiber composites is to alleviate the use of expensive fibers which has a relatively high density and is dependent on nonrenewable sources. Natural fibers presently have many advantages compared to synthetic fibers which make them attractive as reinforcements in composite materials. They come from abundant and renewable resources, which ensures a continuous fiber supply and a significant
saving in material cost (Arpitha and Sonjoy 2014). Natural fibers can cost as little as $1.50/kg, and can be grown in just a few months. Natural fibers are also significantly lighter than glass, with a density of 1.15-1.50 g/cm³ versus 2.4g/cm³ for E-glass (Pickering 2008). In parallel to these developments there have been many advances in biodegradable polymers, both thermoplastic and thermosetting in nature. Composites using natural fibers and bio-based resins are poised to see explosive development in the next ten years (NGCC 08).

Table 2.4 *Selected properties of natural and synthetic fibers (Al-Bahadly. 2013)*

Fiber	Density (g/cc)	Tensile Strength (MPa)	Elastic Modulus (GPa)	Elongation (%)	Moisture absorption (%)	Cost ($/kg)
Cotton	1.5 - 1.6	40-70	0.6 – 1.2	3.0-10.0	8-25	3.67
Jute	1.3 – 1.5	35-80	1.0-3.0	1.2-3.0	12	1.50
Flax	1.4- 1.5	80-90	5.0-7.0	1.5-4.0	7	1.25
Kenaf	1.45	93	5.3	1.45	8	1.20
Sisal	1.3-1.5	51-70	1.5-300	2-5	11	1.15
Coir	1.2-1.3	15-22	4.0-6.0	20-40	10	0.90
Carbon	1.4	3500-4000	230	1.8	-	4.75
Aramid	1.35	3000-3150	170	2.1	-	3.50
E-glass	2.55	1500-2400	73	2.2	-	3.25
PET	1.75	700-900	10	10	-	2.75
Nylon	1.95	50-100	1.2-2.8	15-30	-	1.75

Construction materials are a major source of CO emissions and as a consequence raise the carbon foot-print of a building. Many construction materials, such as concrete, bricks, and blocks, use large amounts of energy in their production and transport. It has been suggested that 66 per cent of total energy consumption is accounted for by construction and use of buildings (Woolley et al, 2002). Natural fibers are good candidate*s* to substitute the synthetic fibers such as E glass as they have inherently lower embodied energy. It is estimated that there are some 2.3million tons of glass fibers devoted to various applications around the globe so there are a number of opportunities for natural fibers to be used in place of existing glass fibers. Natural fibers have several advantages over synthetic fibers: low density, low cost, high toughness, acceptable specific strength properties, good thermal properties, low embodied energy, reduced tool wear, reduced irritation to the skin and respiratory system, and they also have a low energy requirement for processing. In addition they are biodegradable or recyclable depending on the selected matrix (NGCC, 2008). Though the strength of bio-fibers is not as great as conventional fibers, the specific properties are comparable and they are compatible with conventional resins. Table 2.4 gives selected properties of natural and synthetic fibers.

2.5.2 Retrofitting Techniques

The use of FRPs as a shear reinforcing material for RC members is becoming increasingly popular since early 90s due to its various advantages that includes low weight to strength ratio, minimum of disruption to the use and virtually no change in the geometry. The aim of seismic retrofitting is to upgrade the ultimate strength of the building by improving the structures ability

Fig. 2.9. *Common types of fiber sheet (NGCC, 2008)*

to undergo inelastic deformation without fully collapse during an earthquake. This can be achieved by changing the structural system such that the energy is transferred along alternative load paths, or alternatively, increasing the ductility in the individual elements that make up the structural system (Zhuge 2010). The application of FRPs to URM is one of the methods that attempt to improve a structures load carrying capacity and integrity during an earthquake event.

Externally bonded PET FRP with a large fracture strain is one of the retrofitting techniques that has drawn a significant attention as an unique alternative to CFRP or GFRP due to its pronounced ductile behavior and relatively low material cost, without compromising the other advantages of FRP. The main objective of using FRPs is to enhance performance of structure at normal loading condition and to offer greater resistance at the time of severe loading. Neither too much stiffness nor the very high strength materials will be coherent with the overall performance of the masonry structures. It is commonly observed that material with high stiffness produces very little deformation prior to collapse and the failure if any will normally be brittle and

explosive in nature, which is not an expected failure mode from a well performed structure. On the other hand too soft material with nominal strength will not be well suited with the purpose of strengthening.

2.5.3 Behavior of Externally Strengthened Masonry

When FRPs are bonded to the surface of the wall, a compressive crushing type of failure is quite common (Hamid et al. 2005; Wang et al. 2006). Also, premature debonding or fracture of FRP was commonly observed during the test and, in general, FRP could not reach its ultimate strength (Ehsani et al. 1997; Stratford et al. 2004; ElGawady et al. 2005). Experimental tests indicate that the failure patterns are affected by the strength, orientation, amount and anchorage length of FRP (Santa-Maria et al. 2006; Alcaino and Santa-Maria 2008; Marcari et al. 2007). In general, the possible failure mode for masonry strengthened with FRP can be a combination of several mechanisms (CNR DT200 R1/2013) such as, excessive cracking due to tensile stresses in the wall, crushing of masonry in the compression zone, shear-slip of masonry, FRP debonding, and FRP rupture.

2.6 Summary

From an exhaustive literature review on both unreinforced and reinforced masonry walls mentioned in forgoing sections, the following outlines can be made:

1) Although masonry structures are seen as fragile in nature and have very poor seismic performance, they are still being constructed in different parts of the world, as they are low cost in material and in construction in comparison with traditional RC and steel structures.
2) Since, it is not possible to fully replace all of the masonry structures (and even impossible for historical masonry buildings), methods for retrofitting/strengthening them are quite common now a day and are very new and cost-effective retrofitting techniques are emerging with time.
3) External strengthening with FRPs is one of the techniques that should be addressed with sufficient importance as the damage of human lives and properties is enormous during an earthquake as has been seen in Nepal, where a good number of residential buildings are masonry.

References

ACI 440. (2008). “Guide for the design and construction of externally bonded FRP systems for strengthening concrete structures.” *American Concrete Institute*, Farmington Hills, MI 48331 U.S.A.

Alcaino, P. and Santa-Maria, H. (2008), “Experimental Response of Externally Retrofitted Masonry Walls Subjected to Shear Loading” *J. Compos. Constr.*, 12(5), 489– 498.

ASTM C 91 (2003). “Standard specification for masonry cement” *ASTM international.* USA.

ASTM C 1012. (2002) “Standard test method for length change of hydraulic cement mortars exposed to a sulfate solution”. *ASTM international.* USA.

ASTM C 151. (2000). “Standard test method for autoclave expansion of portland cement” *ASTM international.* USA.

ASTM C 1329 (2003). “Standard specification for mortar cement” *ASTM international.* USA.

ASTM C 150. (2002) “Standard specification for portland cement” *ASTM international.* USA.

ASTM C 1072. (2000). “Standard test method for measurement of masonry flexural bond strength” *ASTM international.* USA.

ASTM C 1148. (2002). “Standard test method for measuring the drying shrinkage of masonry mortar”. *ASTM international.* USA.

ASTM C 270 (2003). “Standard Specification for Mortar for Unit Masonry” *ASTM international.* USA.

A179 (1994). “Mortar and Grout for Unit Masonry” *Canadian Standards Association.*

ACI 318-08 (2008). “Building code requirements for structural concrete and Commentary.” *American Concrete Institute*, Farmington Hills, MI 48331 U.S.A.

A 3002 (2003). “Masonry cement” *Canadian Standards Association.*

BIA (2006). “Technical note on brick construction”. *Brick Industry Association, Reston, Virginia.*

BIA (2007). “Specifications for and classification of brick”. Brick Industry Association, Reston, Virginia.

Bledzki, A. K., Faruk, O. and Sperber, V. E.(2006). “Cars from Bio-Fibres.” *Macromolecular Material Engineering, 2006, 291, 449–457.*

CNR-DT200. (2013). “Guide for the Design and Construction of Externally Bonded FRP Systems for Strengthening Existing Structures.” *CNR-DT 200 R1,* Italian National Research Council, Italy.

Carson Dunlop. (2014). “Brick Houses- solid masonry vs brick veneer” http://www.carsondunlop.com/resources/articles/brick-houses-solid-masonry-vs-brick-veneer/

Dubovoy, V. S., and Ribar, J. W. (1990). “Masonry cement mortars-a laboratory investigation” *Research and Development Bulletin* RD0095, PCA, Skokie, IL.

Eurocode 6 (2005). “Design of masonry structures - Part 1-1: General rules for reinforced and unreinforced masonry structures”. *EN 1996 -1 -1: 2005, CEN, Brussels.*

Eurocode 8 (2005). “Design of structures for earthquake resistance.”. *EN 1996 -1 -1: 2005, CEN, Brussels.*

Ehsani, M. R., Saadatmanesh, H., and Al-Saidy, A. (1997). “Shear behavior of URM retrofitted with FRP overlays.” *J. Compos. Constr.*, 1(1), 17– 25.

ElGawady, M. A., Lestuzzi, P., and Badoux, M. (2005). “ Performance of masonry walls under in-plane seismic loading.” *TMS Journal, 23(1),*85-104.

FEMA 356. (2000). “Prestandard and commentary for the seismic rehabilitation of buildings.” *Federal emergency management agency*, Washington, D.C.

Hamid, A., EI-Dakhakhni, W. W., Hakam, Z., and Elgaaly, M. (2005). "Behaviour of composite unreinforced masonry-fiber-reinforced polymer wall assemblages under in-plane loading." *J. Compos. Constr.*, 9(1), 73–83.

Holbery, J. and Houston, D. (2006). "Natural-Fiber-Reinforced Polymer Composites in Automotive Applications." JOM, 2006, 11, 80-86.

Isberner, Albert W. (1974). "Properties of masonry cement mortars" *Research and Development Bulletin* RD019, Portland Cement Association.

I-Brick. (2015). "Brickwork help & advice" http://www.i-brick.com/flemish-bond-brickwork

Mohantya, A. K., Misraa, M. and Hinrichsen, G. (2000). "Bio-fibres, bio-degradable polymers and bio-composites: an overview." *Macromolecules and Material Engineering, 2000, 276/277, 1-24.*

Marcari, G., Manfredi G., Prota A. and Pecce, M. (2007). "In-plane shear performance of masonry walls strengthened with FRP." *Elsevier J. of Comp.* Part B 38 (2007) 887–901.

NGCC., Sustainable FRPs – naturally derived resins and fibres, NGCC Technical Sheet 08, *Network group for composites in construction*, 2008.

PCA (2002). "Masonry information, mortar cement: product data sheet". *Portland Cement Association,* Skokie, IL.

PCA (2004). "Masonry information: masonry mortar". *Portland Cement Association*, Skokie, IL

Ritchie, T., and Davison, J. I. (1963). "Factors affecting bond strength and resistance to moisture penetration of brick masonry," *Symposium on Masonry Testing* - STP320, ASTM , West Conshohocken, Pennsylvania.

Stratford, T., Pascale, G., Manfroni, O., and Bonfiglioli, B. (2004). "Shear strengthening masonry walls with sheet glass-fiber reinforced polymer". *J. Compos. Constr.*, 8(5), 434– 443.

Santa Maria, H., Alcaino, P. and Luders, C. (2006). "Experimental response of masonry walls externally reinforced with carbon fiber fabrics" *Proc. of the 8th U.S. National Conf. on Earth. Eng.,* April 18-22, 2006, CA, USA, p-1402.

Sam. (2011). http://www.archexamhandbook.com/intent/about/

The Global Studio. http://www.theglobalstudio.org/

Wang, Q., Chai, Z., Huang, Y., Yang, Y. and Zhang, Y. (2006) "Seismic shear capacity of brick masonry wall reinforced by GFRP." *Asian Journal of Civil Engg. (Building And Housing)*, 7(6), 563-580.

Westman, M. P., Laddha, S. G., Fifield L. S., Kafentzis T. A., and Simmons K. L. (2010). "Natural fiber composites-a review". US Department of Energy. Pacific Northwest National Laboratory. PNNL-19220.

WHE (2011). "Unreinforced brick masonry construction" World Housing Encyclopedia, a joint project *by the Earthquake Engineering Research Institute (EERI) and the International Association for Earthquake Engineering (IAEE).*

Zhuge, Y. (2010). "FRP-retrofitted URM walls under in-plane shear: review and assessment of available models" *J. Compos. Constr.*, 14(6), 743– 753.

PART-2

Chapter 3

Interface Shear and Tensile Strength

3.1 Interface Shear Strength

Shear failure is the dominant mode of failure observed in many masonry buildings subjected to lateral loading due to earthquakes, wind (in tall and slender structures), support settlements or unsymmetrical vertical loading. Lateral loading can produce both diagonal cracking failures, and shear failures of the horizontal joints. The joint resistance is of particular concern in the analysis of load-bearing unreinforced masonry structures that are rather common among older buildings in many countries in the world. The shear generally acts in combination with compression, which is caused by the self-weight and floor loads. Confinement by, for instance, structural frames to in-fill walls may also lead to shear compression.

The present state of knowledge concerning shear strength and shear load-displacement behavior of masonry is far less advanced than that concerning masonry behavior in compression, even though shear failure is an important, often governing mode of failure in many masonry buildings (Van Zijl 2004). This lack of understanding is reflected by the low values of shear resistance allowed by the present U.S. building codes (ASCE 31-02). Information on the post-peak behavior, and on the deformations associated with pre-peak and post-peak responses are also lacking. Only recently, the term "softening" and "dilatancy" were introduced in the research community (Lourenço et al. 1998 and Van Zijl 2004). Knowledge of such behavior is essential, if adequate analytical models are to be developed to describe the in-plane behavior of masonry walls. Most of the research conducted to date regarding the masonry shear behavior has been limited to determining the peak shear stress and its affecting parameters.

A variety of experimental approaches (Fig. 3.1) have been adopted in the last two decades to determine the shear behavior of joints of unreinforced masonry. A widely used approach is the compressive loading of a prismatic masonry specimen which contains a single joint at an angle θ, to the applied load, as illustrated in Fig. 3.1(a) (Nuss et al. 1978; Hamid & Drysdale 1980). The nature of this force-controlled test makes it impossible to obtain data in the post-peak range, as

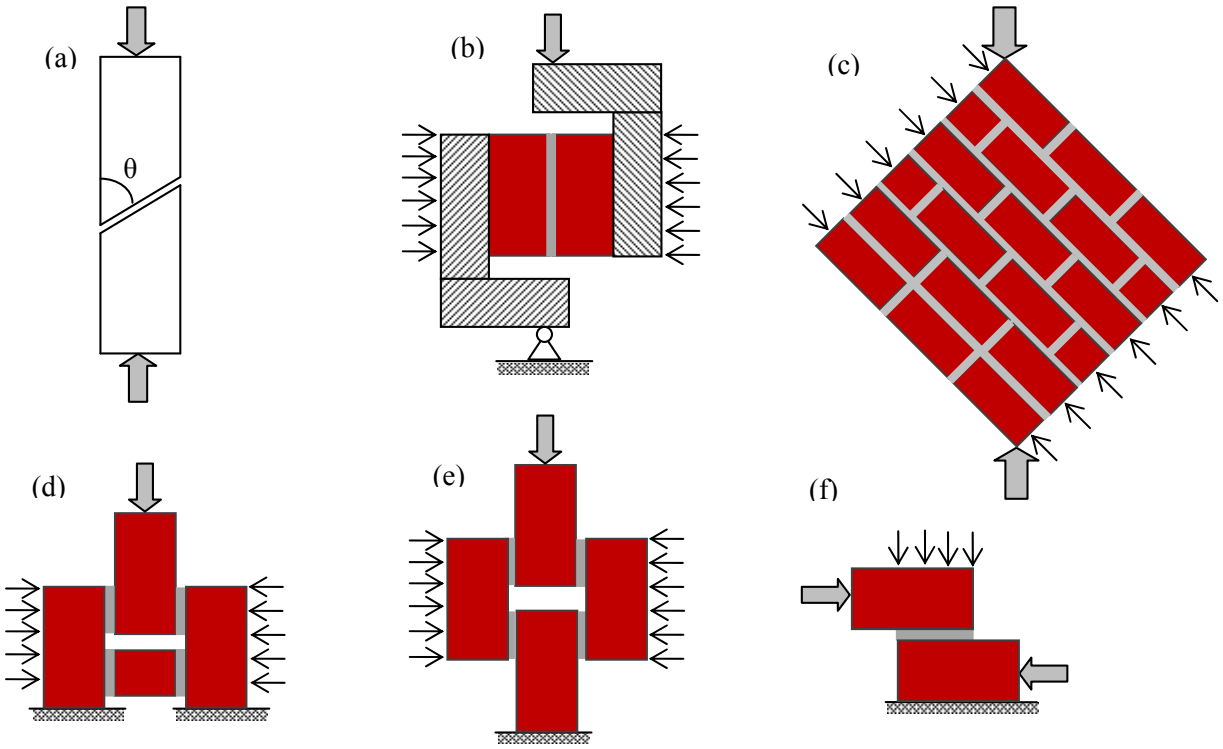

Fig. 3.1. *Different type of shear test specimens: (a) Nuss shear test(1978); (b) van der Pluijm test(1993); (c) Diagonal tension test; (d) Triplet test; (e) Meli test(1973); and (f) Direct shear test*

the specimen collapses in an unstable manner after attaining its strength. Studies using this approach have, however, given valuable information concerning the factors (including mortar type) which influence the peak shear stress.

Van der Pluijm (1993) presents the most complete characterization of the masonry shear behavior, for solid clay and calcium-silicate units. The test set-up shown in Fig. 3.1(b) allows to apply a constant confining pressure upon shearing. The confining (compressive) stresses were applied at three different levels, namely 0.1, 0.5 and 1.0 MPa. Thereby, the specimen edges could translate in the direction normal to the shearing deformation. The uplift, or displacement normal to the shear joint, which is known as dilatancy, was also measured. Armaanidis (1998) measured a dilatation angle between 23.5° to 34.5° for limestone using a direct shear test. He proposed that the shear strength at the weak discontinuities of limestone be a combined effect of both the internal friction angle(ϕ) and the dilatancy angle(φ) and , proposed the following expression:

$$\tau_u = c + \sigma_n \tan(\phi + \varphi) \qquad (3.1)$$

Hansen (1999), Gottfredsen (1997) and Chaimoon & Attard (2009) also used the same experimental technique in their study.

Many researchers (Yokel & Fattal 1975, Calvi et al. 1985, Gabor et al. 2006) have used the test configuration shown in Fig. 3.1(c) to study the shear strength of masonry subjected to diagonal compression. The concentrated diagonal load creates in-plane shear stress along the joints of the specimen. The distribution of normal and shear stresses along any given joint is strongly nonuniform, with the result that shear strength determined from this test represents an average value of progressive failure events, because of the stress redistribution during the failure process, rather than reflecting a true material property. The post-peak behavior and deformations cannot be obtained realistically by mean of this experimental configuration.

The triplet test configuration shown in Fig. 3.1(d) was adopted by Lourenço et al. (2004), as recommended by European Standard EN 1052-4. This test was conducted to verify the Mohr-Coulomb criterion with a cohesion value of the order of 1.4 MPa, and the initial friction coefficient ($\tan\phi$) of 1.03. Copeland & Saxer (1964) used the same specimen configuration to identify the parameters affecting the shear bond between brick and mortar.

Meli (1973) used the test configuration shown in Fig. 3.1(e) to investigate bond and friction of joints with different unit types. A linear variation of the shear strength with confining pressure was observed. Bond strength was found to vary with the mortar and unit types. Hamid & Drysdale (1980) also used the test configuration shown in Fig. 3.1(e) to study the shear response of both grouted and ungrouted concrete masonry. Their results showed that the coefficient of friction decreased with an increase in the confining stress and that grouted specimens yielded friction coefficients that were considerably higher than ungrouted specimens. Data concerning the deformation in the direction of the shear load showed that ungrouted masonry has a considerably higher initial shear stiffness in comparison to grouted concrete masonry. With the increase in normal stresses both the shear strength and the shear stiffness increase. The post-peak frictional response under shear loading that was applied in the same direction as the initial shear force was also determined.

Abdou et al. (2006), El-Sakhawy et al. (2002) and Atkinson et al. (1989) conducted direct shear tests on masonry couplets as shown in Fig. 3.1(f). They used a servo-controlled system to measure the shear load-displacement characteristics for different types of brick and mortar. Abdou et al. (2006) tested both hollow and solid bricks, and found that the shear stiffness of masonry with hollow bricks is higher than that of masonry with solid bricks, because of the mortar that entered inside the holes and acts as an abutment, thus giving more shear resistance than the solid brick. He also found that the ultimate shear strength and residual friction are independent of the brick types. Only one type of mortar was used (20 MPa), so no direct correlation between mortar grade and shear strength could be established. The joint failure could

Table 3.1 *Various experimental results on interface shear stress-slip test*

Author's Name & Test Method	f'_{cm} MPa	E_m GPa	f'_{cb} MPa	σ_n MPa	τ_u MPa	τ_r MPa	c MPa	ϕ_i Deg	ϕ_r Deg	t_m mm
Hansen (1999) for solid clay bricks with couplet Specimen (see Fig. 3.1b)	3.8	2.8	32.0	0.1	0.7	0.08	0.68	23.9	40.1	12
				0.2	0.79	0.17				
				0.5	0.89	0.42				
	11.5	8.4	26.0	0.1	1.2	0.06	1.2	17.2	41.7	12
				0.2	1.29	0.21				
				0.5	1.34	0.43				
	19.0	13.9	25.0	0.1	1.11	0.13	1.08	17.5	45.4	12
				0.2	1.05	0.23				
				0.5	1.21	0.49				
Hansen (1999) for perforated clay bricks with couplet Specimen (see Fig. 3.1b)	3.8	2.8	46.0	0.1	0.69	0.12	0.68	45.0	45.8	12
				0.2	1.00	0.23				
				0.5	1.15	0.50				
	11.5	8.4	46.0	0.1	0.70	0.29	0.68	31.0	53.7	12
				0.2	0.84	0.32				
				0.5	0.96	0.63				
	19.0	13.9	80.0	0.1	0.28	0.08	0.19	62.2	38.0	12
				0.2	0.72	0.13				
				0.5	1.11	0.40				
Chaimoon (2007) for solid clay bricks with frog marks on couplet Specimen (see Fig. 3.1b)	7.3	6.2	11.1	0.2	0.70	0.28	0.43	30.4	38.9	10
				0.4	0.82	0.40				
				0.8	1.02	0.66				
	16.8	11.3	11.1	0.2	0.3	0.24	0.18	39.8	40.3	10
				0.4	0.67	0.37				
				0.8	0.87	0.64				
Lourenço et al. (2004) for hollow clay bricks with triplet Specimen (see Fig. 3.1d)	30.3	22.2	31.8	0.2	1.5	0.26	1.39	37.6	32.5	25
				0.6	2.0	0.37				
				1.0	2.31	0.54				

Table 3.1 *Continued*

Author's Name & Test Method	f'_{cm} MPa	E_m GPa	f'_{cb} MPa	σ_n MPa	τ_u MPa	τ_r MPa	c MPa	ϕ_i Deg	ϕ_r Deg	t_m mm
Van der Pluijm (1993) for solid clay bricks with couplet Specimen (see *Fig. 3.1b*)	9.0	6.0	11.0	0.1	0.89	0.08	0.87	42.9	37.2	15
				0.5	1.31	0.37				
				1.0	1.69	0.74				
Abdou et al. (2006) for hollow clay bricks with couplet Specimen (see *Fig. 3.1f*)	20.0	14.7	24.0	0.36	1.62	0.82	1.50	23.9	41.7	10
				0.57	1.82	1.17				
				1.03	1.94	1.37				

Note: f'_{cm}, f'_{cb} = Uniaxial compressive strength of mortar and brick respectively; E_m = Young's modulus of mortar; σ_n = Normal pre-compression; τ_u = Ultimate shear strength; τ_r = Residual shear stress; c = interface cohesion; ϕ_i = Initial friction angle; ϕ_r = Residual friction angle; t_m = thickness of mortar.

be well represented by the Mohr- Coulomb criterion when a shear load is applied together with compression. Atkinson et al. (1989) conducted a series of tests on various types of brick and mortar, for both static and cyclic loading. Some of the results along with their test methods are given in Table 3.1 and Fig. 3.2.

The previous studies on joint shear behavior, while providing insight into some of the parameters influencing the shear strength, do not, in general, provide the detailed information related to the constitutive behavior which would be required to set-up analytical models for simulating the structural response under different loading conditions. Such a model will require definitions of: (1) shear stiffness for initial loading states; (2) peak and residual stresses; and (3) the effect of materials properties and normal loads on shear strength/stiffness and dilatancy. As in the case of rock joints (Goodman 1976, Armaanidis 1998), dilatancy is the normal expansion or contraction upon shearing.

A complex relationship exists among joint normal stiffness, normal displacement, and shear displacement (Van Zijl 2004). Dilatancy can produce an increase in the normal load resulting in an increase in shear strength, when the normal boundary condition is

displacement-controlled. This applies, for example, to in-fill panels where the stiffness of the frame enclosing the panel affects its normal displacements. An evaluation of the dilatancy requires the measurement of both normal and shear displacements, prior to and after the peak shear stress. It was also observed that the effect of dilatancy under high compression is marginally small and can be neglected (Gabor et al. 2006).

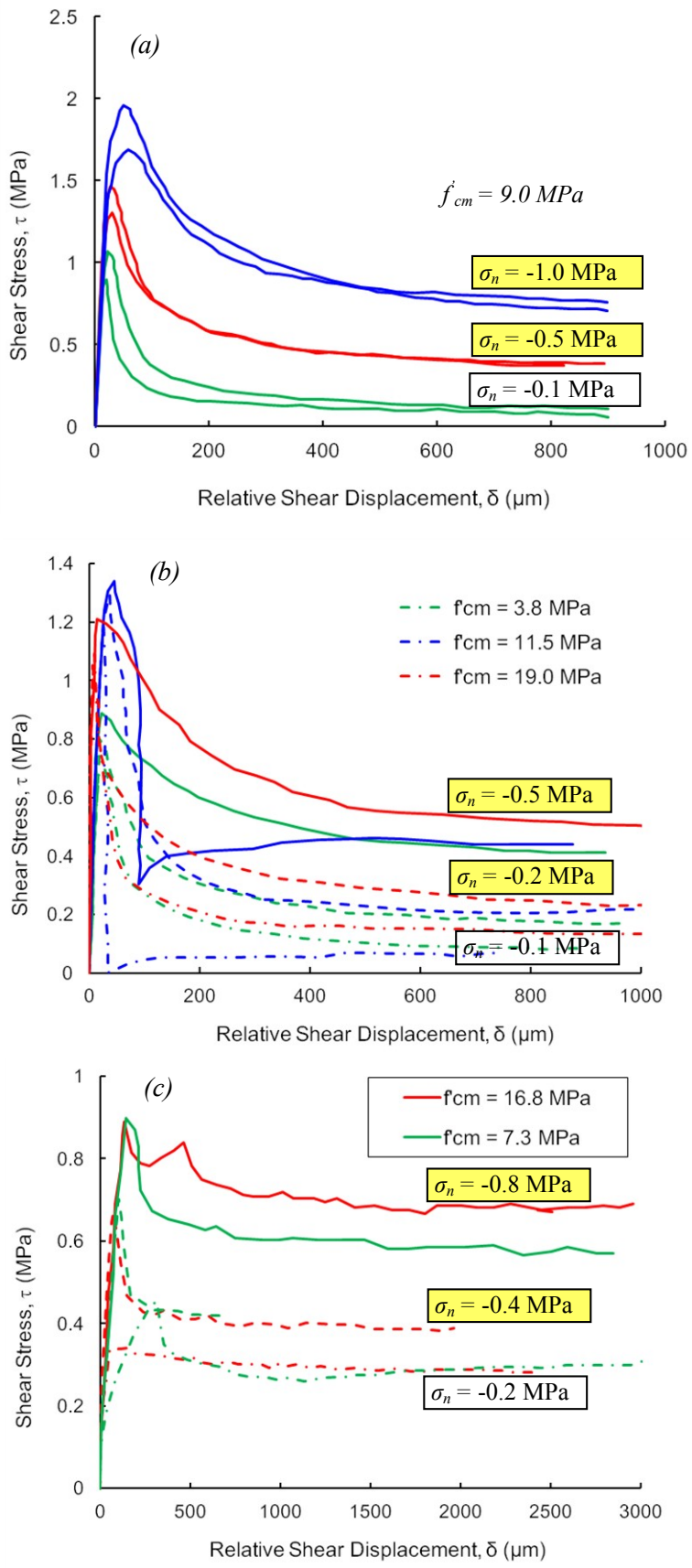

Fig. 3.2. *Shear-slip relationship from different experimental results: (a) Van der Pluijm (1993); (b) Hansen (1999); (c) Chaimoon (2007); for solid clay bricks*

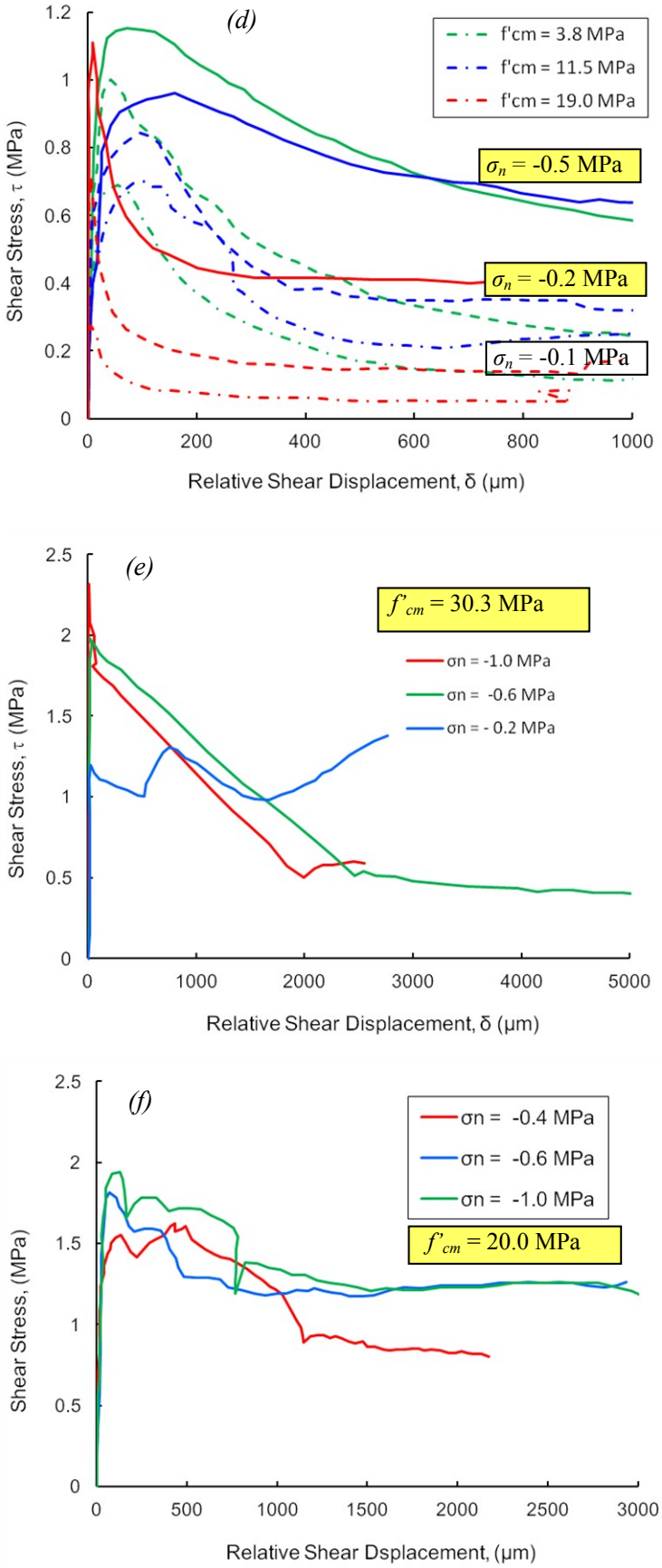

Fig. 3.2. *Shear-slip relationship from different experimental results (d) Hansen (1999); (e) Lourenco et al. (2004); (f) Abdou et al. (2006) for perforated clay bricks*

This research work examines the shear failure mode occurring in horizontal joints, and the shear stress-slip behavior of unreinforced brick masonry under static loading. Nonstandard tests were conducted on four series of masonry samples; triplet shear specimens [Fig. 3.1(d)] were used, in order to study the effect of mortar strength on joint shear behavior. At the outset, this chapter describes the experimental apparatus and the sample preparation procedures. Then the experimental program is outlined. This is followed by a description of the experimental results. An analytical approach has been taken to correlate the shear strength with confining pressure and mortar strength. Finally, macro mechanical model for shear stress-slip is proposed with numerical examples. Finally some exhaustive conclusions are drawn on the basis of the observed results.

3.2.1 Experimental Program

The materials used in the preparation of the triplet shear test specimens included one type of wire-cut clay brick, and four types of mortar with different proportions and strengths, indicated as E, M, S, N respectively. The brick used here, had an actual dimension of 250 × 120 × 70 mm. Bricks were immerged in water the day before the construction of the tested specimen assembly. They were then dried in normal laboratory conditions for at least 1 day prior to build the specimens, to ensure saturation degree of 80%. The brick compressive strength was 17 MPa. The three types of ordinary mortar (M, S, N) used were prepared following the provisions of ASTM C270 for the construction of masonry walls. The type E mortar was prepared as high strength mortar, with comparatively low water cement ratio. The reason for choosing these mortar types was to study the effect of mortar types and strength on the shear strength. The workability of the

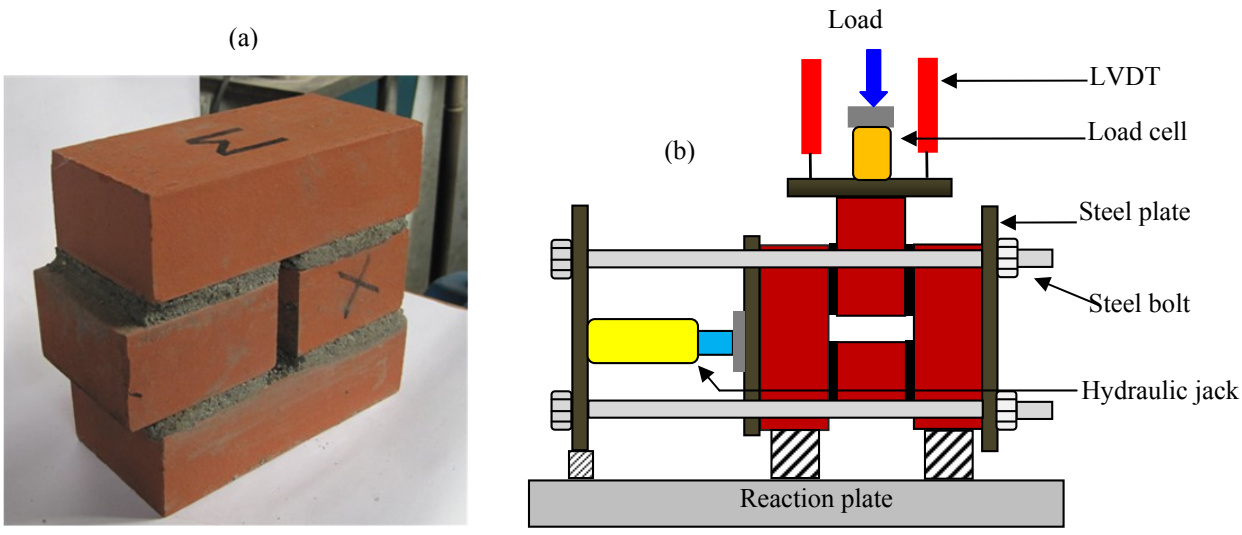

Fig. 3.3. *(a) A typical triplet shear specimen, (b) Schematic diagram of instrumentation*

mortar was monitored using the flow test (ASTM C 1437). For each batch of mortar type used in the construction of the specimens, 10 cylinders (∅ = 50mm) were cast to determine the compressive and splitting strength of the mortar. Table 3.2 summarizes the results for the four types of mortar used in the present investigation.

3.2.2 Specimen Preparation

The specimens were built with two full bricks, one ¾ brick and one quarter brick bonded together by a 10 mm- thick mortar joint, as shown in Fig. 3.3(a). To ensure the correct dimension of the mortar joints, a timber block that was thicker than the bricks by 10 mm was placed over the first brick. More than the needed amount of mortar was then placed on the top face of the brick with a trowel. The one ¾ brick (170mm) was then placed in such a way that a small portion of it (60 mm) exceeded the bottom brick, and rested on the timber block. Another quarter brick was then placed 30 mm apart from the ¾ brick. The second brick was then placed on these two cut bricks, tapped with a wooden mallet, and leveled in two directions with a sprite level to create a 10 mm-thick mortar joint. The mortar in excess, that squeezed to the sides, was removed with a trowel, and the sides of the mortar joint were flattened at the same level of bricks

Fig. 3.4. *Instrumentation and test setup of shear specimen*

on all sides. The timber block was then removed and the specimen was left in place for 5 days, to allow the mortar to develop sufficient strength. During these 5 days, the specimens were covered with thin plastic sheet for curing. After the 5 days of initial curing, the plastic sheet was removed. The specimens were then left for additional 23 days to cure under in ambient conditions in the laboratory before testing , that began at 28 days from construction.

3.2.3 Instrumentation and Test Setup

Five specimens for each mortar type were built and cured for 28 days. Before testing, the length of the mortar joint was measured. Two steel plates were attached on both sides of the specimen and kept in position with four bolts. A uniform confining pressure was exerted on the specimen using a manually controlled hydraulic jack having a load gauge. When the expected level of pressure was reached, the specimen was ready for the shear test. Four linear displacement (LVDT) gauges were attached on the top of the ¾ brick that will be load for shear [Fig. 3.3(b)] on opposite sides of joints to record the shear displacement. The specimen was designed in such a way, that the applied load be transferred through the upper ¾ brick as shear, and the confining pressure be carried out by both the top and bottom bricks. The area resisting to shear and compression was calculated accordingly. Fig. 3.4 shows the loading and support arrangements used for testing of the specimens. Synthetic elastomers were used to ensure a uniform load distribution over the area and supports.

3.2.4 Testing and Measurements

For each type of mortar five specimens were tested with a constant confining pressure of 0.25, 0.50, 1.0, 1.25 and 1.50 MPa respectively, resulting in a total of twenty specimens. At the beginning the required confining pressure is applied through the hydraulic jack. Then specimen was transferred under the actuator of a universal testing machine to apply the shear load as compression. The maximum loading capacity of the vertical actuator is 1000 kN. The shear load was applied at a rate

of 0.05 mm, and the corresponding shear displacement was measured by mean of four LVDTs attached to two opposite sides of the specimen [Fig. 3.3(b)] and recorded through a data logger. The confining pressure was kept almost constant throughout the entire loading process. Fig. 3.5 gives a confining pressure as a function of time for some of the specimen tested; the plots show that there is little fluctuation of the confining pressure. This is due to the fact that when two rough surfaces of brick and mortar slide over each other, dilatancy takes place, which causes an increase in volume, and thus pressure on the steel plate. This excess pressure somehow contributes to the overestimation of the shear strength at the interface, but for the sake of

simplicity of the analysis, the dilatancy effect is neglected in the numerical modeling. A more detailed explanation of this exclusion is given in the subsequent paragraph.

Table 3.2 *Specification of mortar used in triplet shear test specimen*

Mortar type	Cement : Sand (by volume)	Water/Cement (by weight)	Compressive strength (MPa)	Splitting tensile strength (MPa)	Young's modulus (GPa)	Poisson's ratio ν	Flow (mm)
E	1 : 2.25	0.50	28.5	3.0	26.0	0.186	170
M	1 : 2.75	0.70	20.0	1.7	19.3	0.156	212
S	1 : 3.5	0.86	12.5	1.5	15.7	0.200	221
N	1 : 4.0	0.95	10.0	0.9	14.5	0.188	190

3.2.5 Test Results and Discussion

It is quite obvious that the ultimate shear strength increases with increasing confining pressure normal to the shearing surface. However, this is not the only governing factor that influences the shear strength of the brick-mortar interface. The other factors are: 1) characteristics of bond between mortar and brick; 2) characteristics of brick and mortar; 3) coefficient of friction between the two sliding surfaces; and 4) the overall quality of the joint. Since, during the fabrication of the specimens, an overall uniformity was difficult to be attained, some inconsistencies are inevitable. Fig. 3.6(a) and Fig. 3.6(b) show the nominal shear stress as a function of the shear displacement for some of the tested specimens. According to the figures, it is plain to see that just before the peak shear stress the stiffness is very high, with very little shear deformation. The interlocking between the grains of the brick and the mortar under confining pressure, is the main reason for the high stiffness of the shear load-displacement relationship. There is a barely detectable hardening phase, but just for a short range before the peak load. As the imposed shear displacement overcomes the interlock between brick and mortar, a phenomenon of volume increase (dilatancy) takes place, and give rise to a much higher strength than expected. In the present study, the effect of dilatancy was not considered, due to the fact that at a confining pressure higher than 0.5 MPa, this dilatancy becomes marginally small, the effect of internal friction dominates over dilatancy (Armaanidis 1998), and therefore makes it possible to evaluate the shear strength by mean of the Mohr-Coulomb criterion. Moreover, the high confining pressure restricts the upward dilatant deformation of the specimen, and turns it into deformation of brick and mortar by squeezing them laterally, at constant volume.

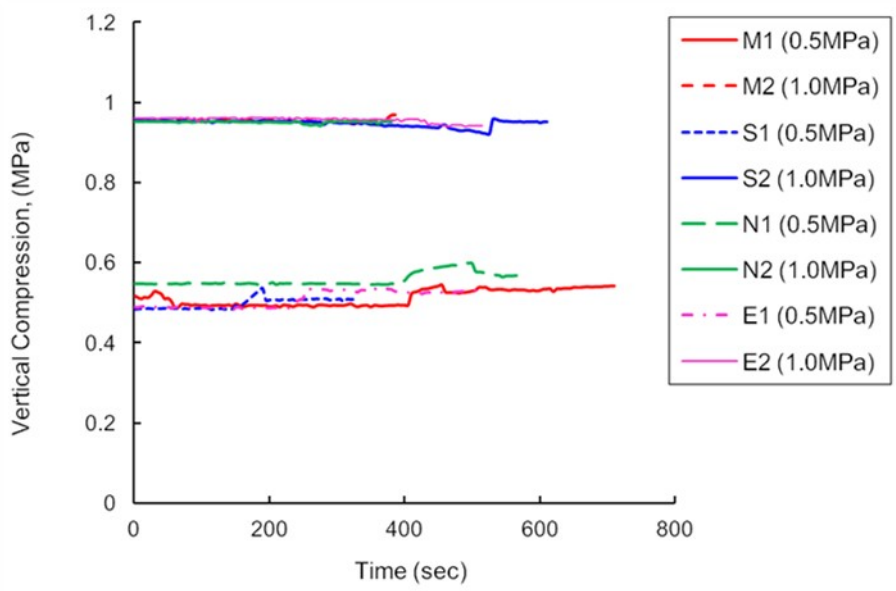

Fig. 3.5. *Time history of the vertical load for each specimen*

As previously mentioned, the interface behaves like a quasi-brittle material, and exhibits a very small hardening branch, that appears between the elastic limit and the peak stress. The post-peak damage and release of strain energy is quite evident, as the stress drops gradually. After the initial damage, the shearing surface readjusts and relocates its position for new sliding resistance, after losing the cohesive bond at the brick-mortar interface. This stage is called residual stress, and depends mainly on the interface static friction and confining pressure; in the following, it will be indicated as residual shear strength. After reaching the residual shear strength, the relative movement between the two sliding surfaces turns into a rigid body movement, with very little (or no) relative shear deformation. This stage can be considered as a complete failure stage, and the whole phenomenon can be indicated as dynamic friction, something that is beyond static equilibrium and static analysis.

In this study, two important parameters, confining pressure and mortar strength were noticed as major factors contributing to the shear capacity at the brick-mortar interface. The increase in shear strength with increasing confining pressure, for different mortar strengths (N, S, M and E) can be seen in Fig. 3.7(a). The experimental parameters found from the triplet shear test are given in Table 3.3. It is quite evident from Fig. 3.7(a) that the shear strength does increase with increasing confining pressure in a rather nonlinear fashion for different mortar strengths, which is incompatible with Mohr-Coulomb criterion but consistent with the Mohr-Coulomb failure envelop or rupture line. For a specific material, the rupture line may be a curve as shown in Fig. 3.8.

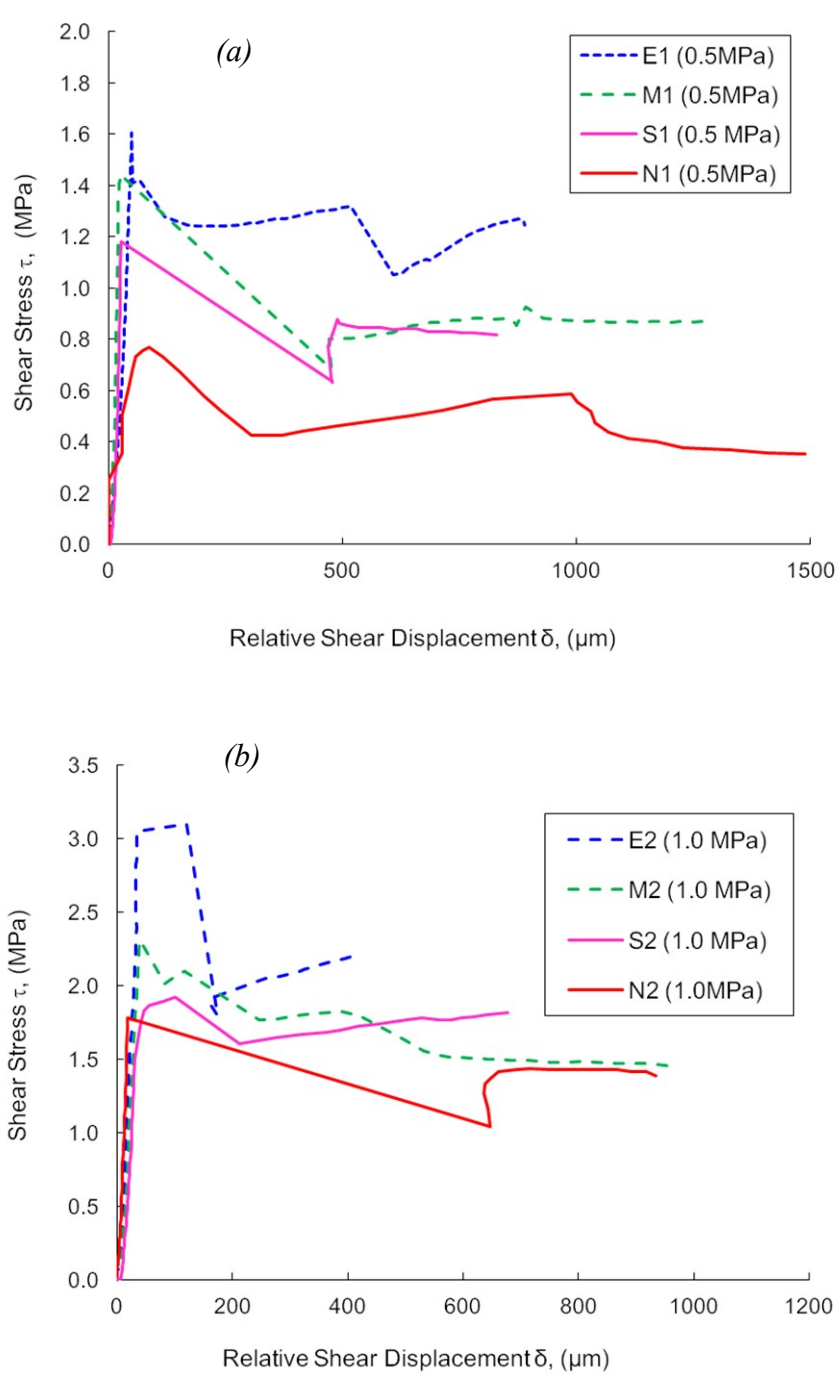

Fig. 3.6. *Experimental results of shear stress vs. shear deformation: (a) for 0.5 MPa; (b) for 1.0 MPa of confining pressure.*

The Fig. 3.7(a) also indicate that the strength of mortar have a significant role on the peak shear stress. The other two parameters namely as cohesion *c* and internal friction angle ϕ which are the inherent properties of the interface between brick and mortar, also varies with the mortar strength and confining pressure. The cohesion *c* is independent of normal stress and only increases little with increasing mortar strength where as the friction angle ϕ is dependent on normal stress, but cannot be verified independently at this present stage of knowledge.

Table 3.3 *Shear strength parameters from triplet shear test*

Mortar Grade	σ_n MPa	f'_{cm} MPa	f'_{cb} MPa	τ_u MPa	τ_r MPa	c MPa	ϕ_i deg	ϕ_r deg
	0.25			0.84	0.42			
	0.50			1.60	0.94			
E	1.00	28.5	17.0	3.04	1.88	0.23	69.4	61.5
	1.25			3.50	2.25			
	1.50			--	--			
	0.25			0.67	0.46			
	0.50			1.32	0.80			
M	1.00	20.0	17.0	2.34	1.60	0.16	65.6	56.8
	1.25			2.62	1.78			
	1.50			2.85	1.89			
	0.25			0.47	0.35			
	0.50			0.97	0.74			
S	1.00	12.5	17.0	1.87	1.48	0.19	56.3	56.3
	1.25			2.11	1.68			
	1.50			2.30	1.77			
	0.25			0.33	0.25			
	0.50			0.78	0.56			
N	1.00	10.0	17.0	1.67	1.13	0.12	60.8	49.4
	1.25			2.01	1.50			
	1.50			2.28	1.61			

Note: f'_{cm}, f'_{cb} = Uniaxial compressive strength of mortar and brick respectively; σ_n = Normal pre-compression; τ_u = Ultimate shear strength; τ_r = Residual shear stress; c = interface cohesion; ϕ_i = Initial friction angle; ϕ_r = Residual friction angle.

The relationship between confining pressure and residual shear strength is shown in Fig. 3.7(b). It is quite interesting to notice that once the interface cohesion is lost, the ratio of residual shear strength to confining pressure (or residual friction coefficient) increases to an almost constant rate, that is independent of the mortar strength.

The failure modes of the shear test specimens were predominantly interface failures. In all cases, the mortar separated from either the inner brick or the outer, or both. No substantial damages was seen on the brick surfaces; rather, some small mortar pieces appeared to remain attached to the brick surfaces (Fig. 3.9), something that indicates that if the brick strength is higher than the mortar strength, damage takes place within the mortar. During the increase of the shear load, a

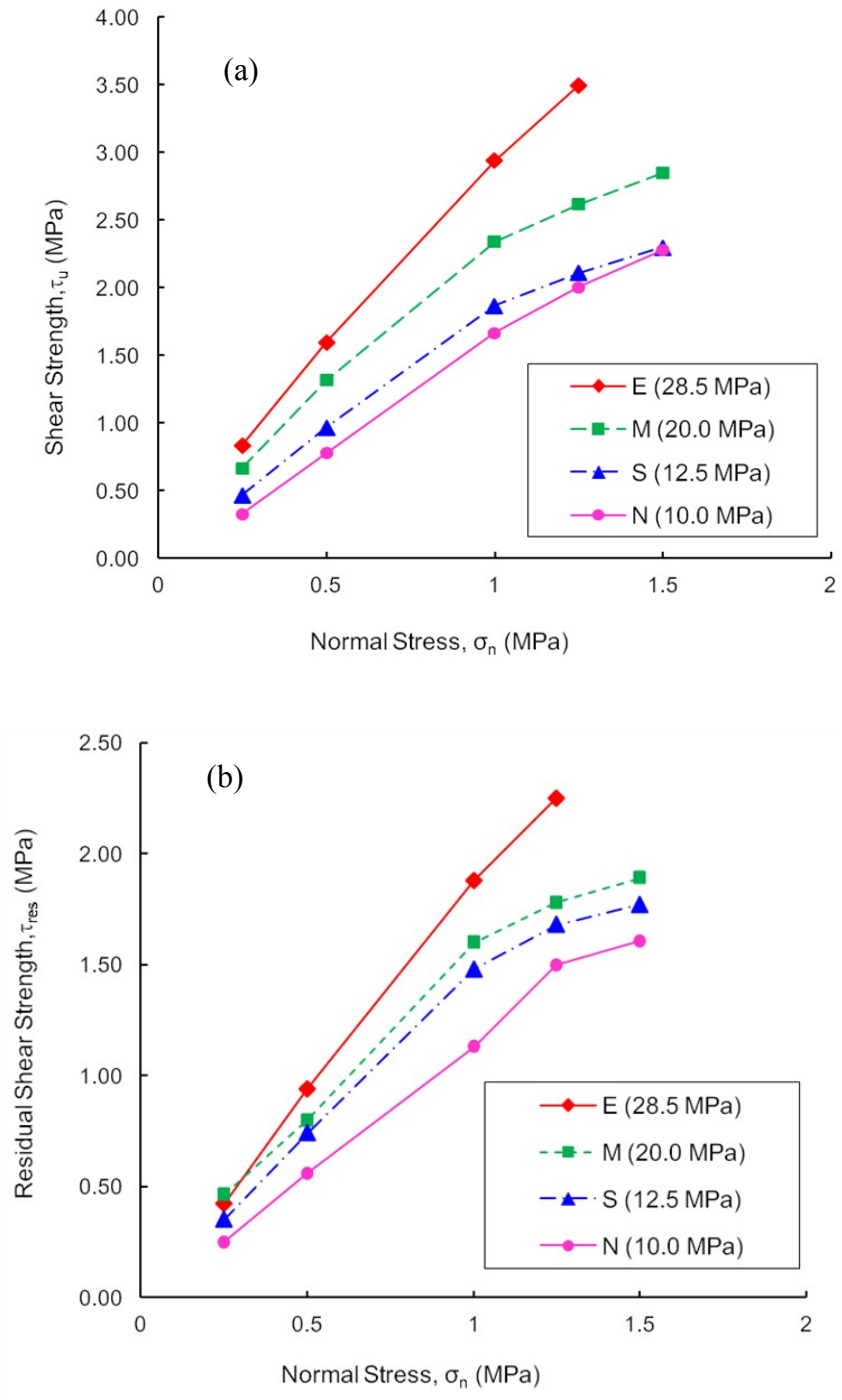

Fig. 3.7. *Effect of normal stress: (a) variation of shear strength with normal stress; and (b) variation of residual shear strength with normal stress*

minor crack was observed, propagating almost halfway into the depth of the outer bricks at the peak shear load. This crack can be regarded as a flexural crack. Since the crack does not reach the interface, its effect on the average shear strength at the interface is not very significant.

3.2.6 Shear Strength and Shear Stress-Slip Relationship

The shear capacity of masonry joints with moderate confining pressure can be predicted by the Mohr-Coulomb criterion (Lourenço et al. 2004), which establishes a linear relationship between the shear strength τ_u and the normal compressive stress σ_n (see Table 3.3), by $\tau_u = c + \sigma_n \tan\phi$. Here, c represents the cohesion between the brick-mortar interface and $\tan\phi$ is the tangent of the friction angle of the interface. This relationship can be observed in other experimental findings, as shown in Table 3.1, in which the Mohr-Coulomb criteria obtained from the test results of each mortar strength cases is shown. It can be observed in Fig. 3.7(a) that the shear strength increases with both confining pressure and mortar strength in a nonlinear fashion. The value of interface cohesion c represents the quality of bond between the brick-mortar interfaces. The increase in mortar strength will increase the interface cohesion but this is not the only factor that controls the interface cohesion. There are other influential factors like the type of brick, the surface roughness of the brick, the absorption of the brick, as well as the brick strength, that also affects the quality of the interface cohesion. Since, both this and the previous studies did not deal specially with those parameters explicitly; a clear idea about their influence on the interface cohesion is still open to investigate.

The internal frictional angle ϕ at the interface is a function of material properties, as well as surface properties of the two sliding surfaces. In static conditions it should, by definition, be equal to a constant that is called the coefficient of static friction. During the evolution of sliding under compression, however, both the two sliding surfaces undergo substantial deformation, and after the loss of interface cohesion, the value of the frictional angle is different from the static one. Until (and unless) an accurate analysis of the brick surface texture, abrasion characteristics

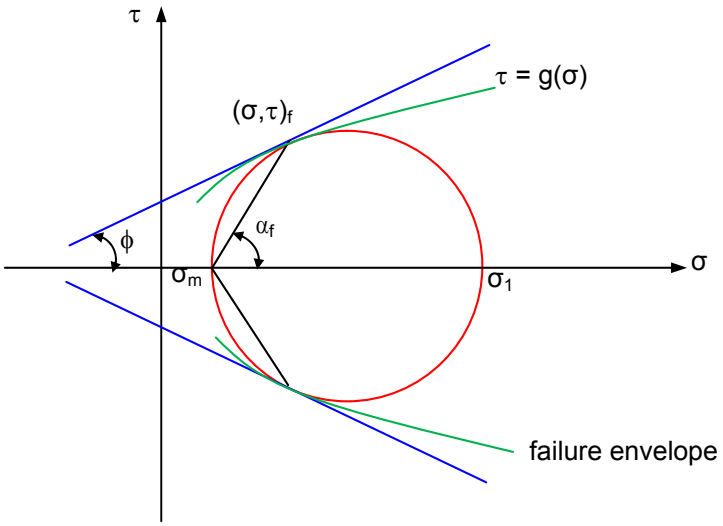

Fig. 3.8. *Mohr-Coulomb failure envelopes*

***Fig. 3.9**. Failure surface of a typical shear specimen*

of both brick and mortar, and pore structure of the brick are explicitly carried out, conclusive remarks cannot be drawn on the relationship between the static and dynamic coefficient of internal friction as a function of brick and mortar characteristics. The residual shear strength is defined as the constant value after the shear strength, from which the residual friction angle can be obtained. Both the initial and the residual frictional angles are somehow independent of mortar strength. The later lies around 45° as in the case of the Authors' experiments [Fig. 3.7(b) and Table 3.3] with some scattering though. Fig. 3.6 shows some of the shear stress-slip relationships. The pre-peak stiffness does not change noticeably with the increase of confining pressure; rather, a change in stiffness is observed with the increase of mortar strength. High strength mortar offers strong interface cohesion, which in turn increases the interface stiffness. On the other hand, higher confining pressure levels merely increase the shear capacity of the interface, with the stiffness almost constant. Nevertheless, it cannot be concluded that the confining pressure has no effect on interface stiffness, unless more tests are carried out.

3.2 Interface Tensile Strength

Another important failure mode of the unreinforced masonry walls is the tension failure in the brick-mortar joint. For better understanding to this phenomenon, an experimental study is carried out on brick couplet specimens. Researchers and standards have suggested different kinds of specimens and test procedures to determine the flexural bond strength. These include the test on wallets (small walls), the bond wrench test, the Brench test, the direct tensile test, and the crossed couplet test. Each of these tests has its own merits and demerits. In this work a test

method is conducted to determine the tensile bond strength by crossed couplet specimens. Test results are used to develop numerical model for tensile cracking in this quasi-brittle material. It is defined in terms of normal stress on the average crack plane and corresponding normal relative displacement. A crack surface in stress space determines the crack initiation in pure tension and complete crack opening with the cessation of stress transfer across the crack plane. The numerical model thus developed can be applied directly as constitutive law of a brick-mortar interface. Model is tested against analytical as well as experimental data.

Direct tensile stresses can arise in masonry as a result of in-plane loading effects. These may be caused by wind, by eccentric gravity loads, by thermal or moisture movements or by foundation movement. The continuous bed joints that divide masonry into equal horizontal layers have been shown to be the weakest plane for tension for unreinforced masonry. Because the bed joint tends to be a major plane of weakness and is an obvious axis, the bed joint and the direction normal to it (head joint) are considered to be the principal directions for the formulation of tensile strengths. The tensile resistance of masonry, particularly across bed joints, is low and variable and therefore is not generally relied upon in structural design. Nevertheless, it is essential that there should be some adhesion between units and mortar, and it is necessary to be aware of those conditions which are conducive to the development of mortar bond on which tensile resistance depends. The mechanism of unit-mortar adhesion is not fully understood but is known to be a physio-chemical process in which the pore structure of both materials is critical. It is known that the grading of the mortar sand is important and that very fine sands are unfavorable to adhesion. In the case of clay brickwork the moisture content of the brick at the time of laying is also important: both very dry and fully saturated bricks lead to low bond strength.

Masonry panels used essentially as cladding for buildings have to withstand lateral wind pressure and suction. Some stability is derived from the self-weight of a wall, but generally this is insufficient to provide the necessary resistance to wind forces, and therefore reliance has to be placed on the flexural tensile strength of the masonry. If a wall is supported only at its base and top, its lateral resistance will depend on the flexural tensile strength developed across the bed joints. If it is supported also on its vertical edges, lateral resistance will depend also on the flexural strength of the brickwork in the direction at right angles to the bed joints. The strength in this direction is typically about three times as great as across the bed joints. If the brick-mortar adhesion is good, the bending strength parallel to the bed joint direction will be limited by the flexural tensile strength of the units. If the adhesion is poor, this strength will be limited mainly by the shear strength of the unit-mortar interface in the bed joints. The flexural tensile strength of clay brickwork ranges from about 2.0 to 0.8MPa in the stronger direction, the strength in

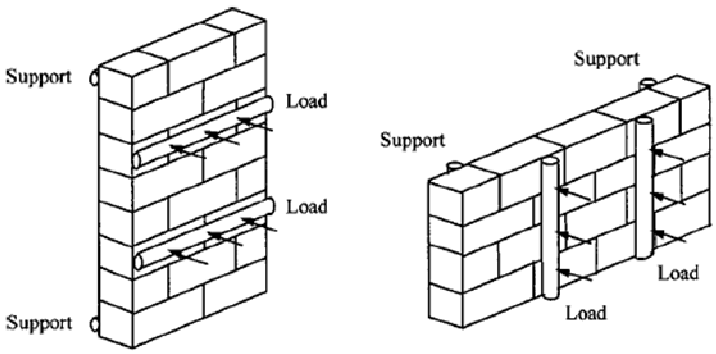

Fig. 3.10 *Testing arrangement of wallettes (BS 5628) :(a) plane of failure parallel to bed joint; (b) plane of failure normal to bed joint*

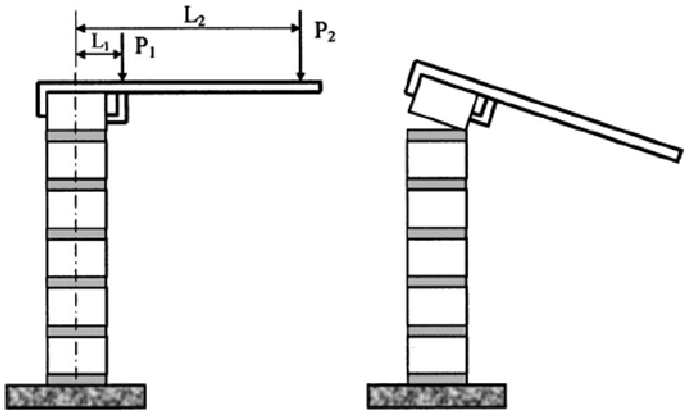

Fig. 3.11. *Bond wrench shown in position before test and after bond failure (ASTM C1072)*

bending across the bed joints being about one-third of this. As in the case of direct tension, the strength developed is dependent on the absorption characteristics of the bricks and also on the type of mortar used. Calcium silicate brickwork and concrete block work have rather lower flexural tensile strength than clay brickwork, that of concrete block work depending on the compressive strength of the unit and the thickness of the wall.

BS 5628 describes the testing of small brick/ block wall specimens (wallets) under four-point loading as a standard test for determination of the flexural bond strength of masonry bed joints. The wallets test arrangement is shown in Fig. 3.10, for planes of failure parallel and normal to the bed joint. The test specimens in Fig. 3.10 do not give the direct tensile bond strength, but many engineers regard it as of practical importance. The test provides an index of wall strength derived from its flexural performance. The difficulty with the BS 5628 test is the large specimen needed for the test and the test setup, which makes it cumbersome to perform. A bond wrench test developed in Australia has been in use for several years for laboratory research on bond strength, as a quality control tool for newly built masonry, and for in situ measurement of bond

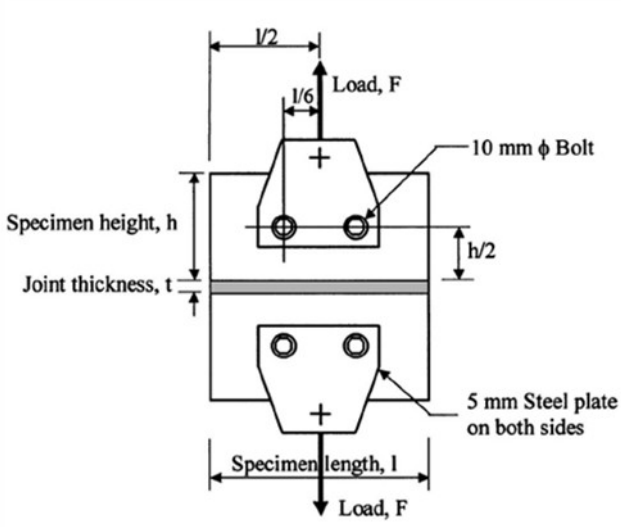

Fig. 3.12. *Direct tensile test as performed by Riddington and Juke (1994)*

on existing structures. The test is specified in the Australian Code of Practice AS 3700. In the United States, the use of bond wrenches in the laboratory is now covered by ASTM C 1072 (2000) and C 1357 (2002). Based on the Australian bond wrench test, the U.K. Building Research Establishment (BRE) in Digest 360 (BRE 1991) covered the technical background of results for a bond wrench test called "Brench" (Fig. 3.11). BRE claimed that the Brench test could be used for investigating suspect masonry, for quality control of a new work, and for laboratory investigation of bond strength. Riddington and Jukes (1994) used direct pull tests, bending tests on stacks, and wrench tests to determine and compare results of bond strength. Various brick and mortar combinations were used. For the direct pure tensile test, they used bolts through the brick thickness to apply the load Fig. 3.12. They concluded that a direct tensile test is more likely to produce a representative value for bond strength than a bending or wrench test, provided that a stress multiplication factor is applied to the average failure stress value obtained. The stress multiplication factor accounts for the difference between the average and maximum stress across the joint, as indicated by a finite-element analysis for the particular loading arrangement Jukes et al. 1997. Held and Andersen (1983) used crossed couplet specimens (ASTM C 952) to establish bond strength. Sinha (1967) conducted direct tensile tests to determine bond strength. Sinha's results, while suffering from a high degree of variability, show a variation in the tensile bond strength as the moisture content of the mortar varies. The bond strength tends to increase for wetter mortars, until the saturation moisture content is approached, when strength falls off rapidly.

The test method adopted in this research work is based upon direct tensile test, for its simplicity and acceptability stated by ASTM C 952-02. The specimen is constructed from two units in a

cross-shaped configuration, and failure is induced by direct tension under two-point loading as shown in Fig. 3.13. Testing was carried out on one types of clay brick, and four different types of mortars. The cross-shaped test specimens were found to be easy to construct and test, with results showing a good degree of consistency.

Table 3.4 *Specification of mortar used in cross-bond specimen*

Mortar Type	Cement : Sand (by Volume)	Water/Cement (by Weight)	Compressive strength (MPa)	Splitting Tensile Strength (MPa)	Flow (mm)
E	1 : 5.75	0.55	28.5	3.0	154
M	1 : 6.75	0.70	20	1.7	140
S	1 : 8.5	0.87	12.5	1.5	186
N	1 : 4.5	1.00	10.0	0.9	138

Strength is investigated herein using a macro-mechanics approach, which is more adaptable to incorporating the analytical model that are important for numerical analysis than is the micromechanics approach. Thus the material is taken to be globally homogeneous, and the effects of the constituent materials are detected only as averaged properties of the composite material. As is

shown later, the strength of the assemblage may be described by a linear combination of the resistances of the constituent materials.

3.2.1 Experimental Procedure

The materials used in the construction of the cross-bonded specimens included one type of wire-cut clay brick, and four types of mortar of different proportions and strengths, (E,M,S,N). The brick used had an actual sizes of 21×102×65 mm. All bricks used were inundated in water one day before of fabrication. They were then dried under normal laboratory conditions for at least 1 day prior to use to ensure 80% saturation according to ASTM. The brick compressive strength was 17 MPa. The four types of were mortar used as recommended by the ASTM C270 for construction of masonry walls. The reason for choosing these mortar types was to study the effect of changing mortar proportions and strength on the tensile bond strength.

The workability of the mortar was monitored using the flow test (ASTM C 1437). For each batch of mortar type used in the construction of the specimens, ten 50 mm cylinder were cast to determine the compressive and splitting strength of the mortar. Table 3.4 summarizes the results for the four types of mortar used in the investigation.

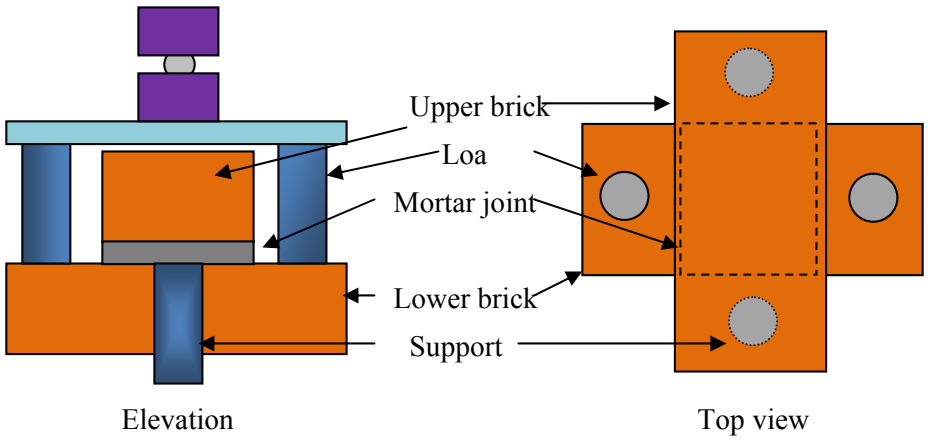

Fig. 3.13. *Crossed-brick test assembly (ASTEM C 952)*

3.2.2 Specimen Preparation

The specimens were constructed with two bricks bonded together by a 10 mm rectangular mortar joint in a crossed arrangement to try to reproduce the way that is stated in ASTM C 952. The first brick was placed in between two pieces of a timber blocks that was thicker than the brick by 10 mm. More than the needed amount of mortar was placed on the top face of the brick with a trowel. The second brick was then placed in crosswise over the lower brick in such a way that the extended ends rest on the wooden blocks. The top brick was then tapped with a wooden mallet and leveled in two directions with a sprite level to create a 10- mm-thick mortar joint.

Fig. 3.14. *Experimental setup of crossed-brick test*

Fig. 3.15. *Arrangement of strain gages over the specimen*

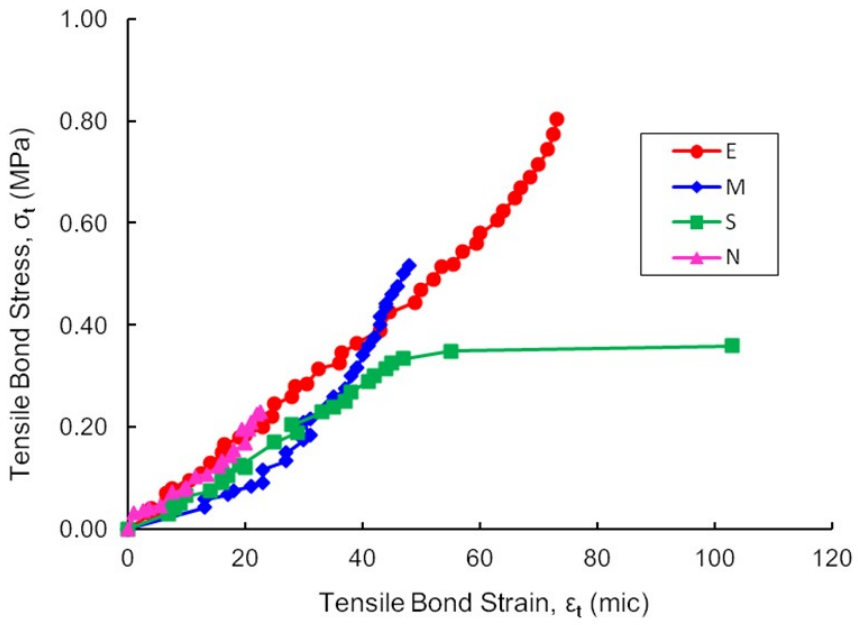

Fig. 3.16. *Tensile stress-strain relationship of brick-mortar interface from cross-bond test specimens*

After 1 min the wooden blocks were removed and the access mortar cut away from all four edges of the mortar with a trowel, and the sides of the mortar joint were flattened level with the bricks from all sides. The specimens were covered for 7 days with thin plastic sheeting for curing. After the 7 days the specimens were then left for an additional 23 days to cure under ambient conditions in the laboratory before testing at 28 days from construction.

3.2.3 Test Arrangement

Eight crossed-brick specimens were finally tested in accordance to the specification ASTM C 952. Before testing, the length of the mortar joints was measured. Fig. 3.14 shows the loading and support arrangements used for testing the specimens. The specimens were loaded to failure by applying the load at a standard displacement rate of 0.5 mm/min.

3.2.4 Instrumentation and Measurements

Two mechanical strain gages were also attached at the brick-mortar interface level to record the strain with the increase of bond stress (Fig. 3.15). The applied load was recorded through the data logger attached to the testing machine. Load was applied until full separation of the two bricks from each other. The bond strength was calculated from the peak load divided by the gross bond area. Graph was plotted from the bond strain verses the bond stress. Since the brick and mortar are two different materials, with two different stiffnesses, the recorded strain will definitely gives the combined strain of these two composites. Whereas the stress that will go through the weakest plain, must pass through the interface, as it is the pre-determined plane of weakness.

Table 3.5. *Results of direct tensile test on interface*

Mortar Type	Cement : Sand (by Volume)	Compressive strength (MPa)	Splitting Tensile Strength (MPa)	Direct tensile Strength (MPa)	Strain at Ultimate Stress (%)
E	1 : 5.75	28.5	3.0	0.70	73
M	1 : 6.75	20	1.7	0.36	38
S	1 : 8.5	12.5	1.5	0.29	26
N	1 : 4.5	10.0	0.9	0.22	24

3.2.5 Test Results and Discussion

The results of the experimental test program are shown in Table 3.5. In this table, the values of tensile bond strength, f_{ti}, and corresponding strain, ε_{ti}, for different mortar strengths are presented. It is evident from the Table 3.5 that higher tensile bond strength results from a higher compressive strength of mortar. Fig. 3.16 gives a typical stress-strain characteristic normal to the bed joint. It shows the relative inconsistency in the stiffness for different mortar strengths. The mechanical properties of the constituent materials (i.e. brick and mortar) have no direct effect on this inconsistency, rather it is the other physical properties that affect the stiffness. Surface roughness and initial rate of absorption (IRA), workmanship, such as pressure applied to the mortar bed during placing and net coverage of the mortar over the two brick surfaces, affect the tensile stiffness of the interface. The above factors can also affect the tensile bond strength as well, as can be seen from the Fig. 3.17. Lower strength mortars offer lower bond strengths but

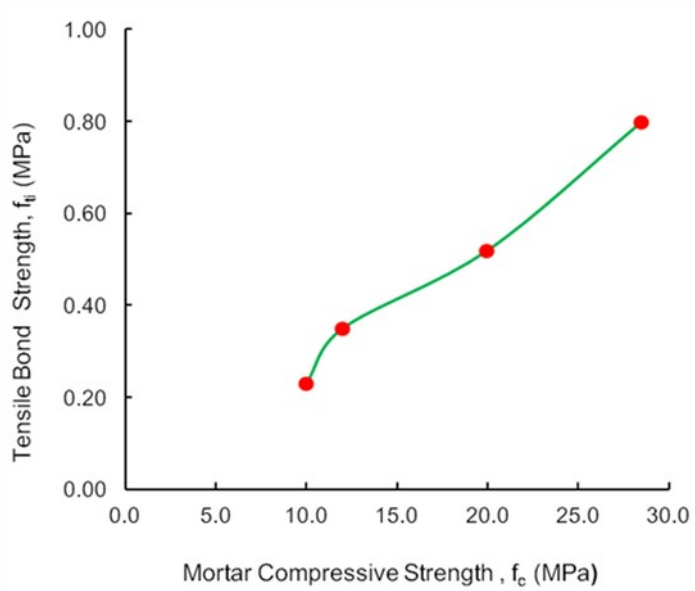

Fig. 3.17. *Tensile bond strength versus mortar compressive strength*

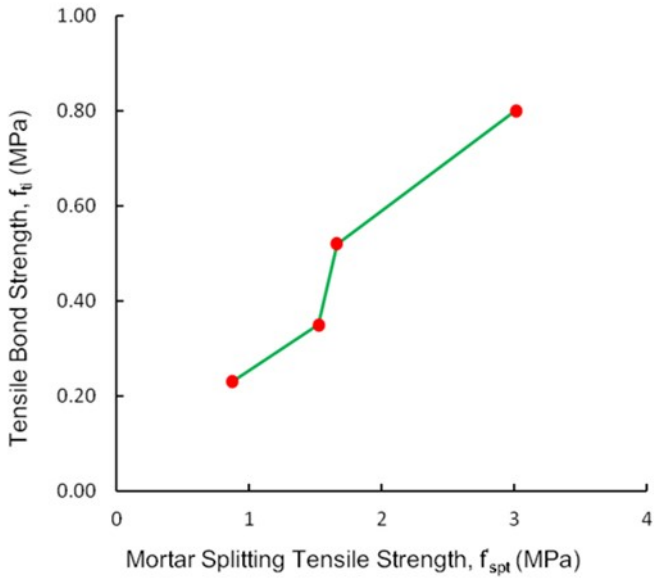

Fig. 3.18. *Tensile bond strength versus mortar splitting tensile strength*

not in a consistent manner. A relationship between mortar compressive strength and tensile bond can also be seen in Fig. 3.17**.** There is a linear relationship between the two but consistency can be seen again for the low strength mortars. The same linear variation of the tensile bond strength with the splitting tensile strength of mortar can be seen in Fig. 3.18 with the same nature of inconsistency for the low strength mortars. Khalaf (2005) also reported such kind of linear relationships for flexural bond strength test on clay brick couplets. Reddy and Gupta (2006) also observed linear variation of the bond strength for cross-bond test soil-cement couplets.

3.3 Concluding Remarks

In this study, some results obtained on mortar joints in brick masonry under shear and compression, are compared with other similar results from the literature. At first, various experimental results are compared, on the basis of two major affecting parameters, namely confining pressure and mortar strength. From these comparisons the following conclusions can be drawn:

1) The shear capacity of the joints, for both solid and hollow bricks, will definitely rise with the increase of confining pressure acting normal to the joint. The resulting relationship shows a nonlinear tendency, something that is consistent with the Mohr-Coulomb failure envelop. Once cohesion is lost (or the shear stress reduces to the residual shear strength), the confining pressure plays a significant role also for the residual shear capacity.
2) The shear strength does increase with the increase of mortar strength, as the interface cohesion increases with the increase of mortar strength, but a definitive relationship cannot be established at this current stage of knowledge. Strong mortar with weak brick and weak

mortar with strong brick will behave differently, and as a result, the shear strength will be very much scattering in nature.

3) The shear stress-slip relationship can best be described as pre-peak and post-peak regime. In pre-peak stage the stiffness is somehow constant throughout the loading process, and shows little hardening phase near the peak shear stress. So, the pre-peak behavior can be said as elastoplastic. In post-peak regime, the damage is rather gradual and shear stress reach to a constant value after the loss of interface cohesion, this stage is called residual shear strength.
4) Brick types, its surface roughness and mortar texture definitely have an effect on interface friction. Until and unless some vigorous investigation is carried out to know these effects, an explicit correlation between friction coefficient and mortar strength cannot be established at this present study. Merely a variation of friction coefficient can be shown with respect to mortar strengths and the strength of bricks.
5) The so called dilatancy which causes an upward displacement of the brick units upon sliding has some marginal effect on the overall deformation of brick-mortar assemblages but this deformation can be neglected on the grounds that the deformation of the brick and mortar themselves are large enough in comparison with the dilatant deformation.
6) The interface tensile strength is quite inconsistent with the test procedure. So, while taking the results from a particular test method, care should be taken about the test parameter and their applicability.

References

Abdou, L., Saada, R. A., Meftah, F., and Mebarki, A. (2006). "Experimental investigations of the joint-mortar behavior." *ELSEVIER J. Mech. Research Communications* 33, 370–384.

Armaanidis, V. I. (1998). "A model for the shear strength of rough rock discontinuities under low normal stress." Ms.C. dissertation, School of Civil Eng. and Geosciences, Univ. of Newcastle Upon Tyne, U.K.

ASCE 31-02. "Handbook for the seismic evaluation of buildings" *Building Seismic Safety Council for Federal Emergency Management Agency, Washington D.C.*

ASTM C 270. (2007). Standard Specification for Mortar for Unit Masonry.

ASTM C 1437. (2007). Standard Test Method for Flow of Hydraulic Cement Mortar.

Atkinson, R. H., Amadei, B. P., Saeb, S., and Sture, S. (1989). "Response of masonry bed joints in direct shear." *J. Struct. Eng.,* 115(9), 2276–2296.

Calvi, B. M., Macchi, G., and Zanon, P. (1985). "Random cyclic behavior of reinforced masonry under shear action." *Proc, 7th Int. Brick Masonry Conf.,* Melbourne, Australia.

Chaimoon, K. and Attard, M. M. (2009). "Experimental and numerical investigation of masonry under three-point bending (in-plane)." *ELSEVIER J. Eng. Struct*. 31,103–112.

Copleland, R. E., and Saxer, E. D. (1964) “Tests of structural bond of masonry mortars to concrete block.” *ACI Journal*, Title No. 61-70, 1964,1411–1452.

Cundall, P. A. (1971). "A computer model for simulating progressive large-scale movements in block rock systems." *Proc., Int. Symp. Rock Fracture,* Nancy, France, II-8.

El-Sakhawy, N. R., Raof, H. A., and Gouhar, A. (2002). “Shearing behavior of joints in load-bearing masonry wall” *J. Mat. in Civil Eng.,* 14(2), 145–150.

EN 1052-4, 2000, “Determination of shear strength including damp proof course.” European norm for method of test for masonry Units- Part 4.

Gabor, A., Ferrier,E., Jacquelin, E., Hamelin, P. (2006). “Analysis and modelling of the in-plane shear behavior of hollow brick masonry panels.” *ELSEVIER J. Const. Bldg. Mat.,* 20, 308–321.

Goodman, R. E. (1976). "Methods of geological engineering in discontinuous rocks." *West Publishing Company, St Paul.*

Gottfredsen, F. R. (1997). “Laterally loaded masonry.” Ph.D-Thesis, *SBI–Report 289*, Danish Building Research Institute, Hørsholm, Denmark.

Hamid, A. A., and Drysdale, R. G. (1980). "Behavior of brick masonry under combined shear and compression loading." *Proc. 2nd Canadian Masonry Symp.,* Ottawa, Canada.

Hansen, K. F. (1999). “Bending and shear test with masonry.” *SBI bulletin 123*, Danish Building research Institute , Hørsholm, Denmark.

Lourenço, P. B., Rots, J. G., and Blaauwendraad, J. (1998). “Continuum model for masonry: parameter estimation and validation.” *J. Eng. Mech.*, 124(6), 642–652.

Lourenço, P. B., Barros, J. O., and Oliveira, J. T. (2004). “Shear testing of stack bonded masonry.” *ELSEVIER J. Const. Bldg. Mat.*18. 125–132.

Lotfi, H. R., and Shing, P. B. (1991). "An appraisal of smeared crack models for masonry shear wall analysis." *J.Computers and Struct.,* 41(3), 413-425.

Meli, R. (1973). "Behavior of masonry walls under lateral loads." *Proc, 5th World Congress on Earthquake Eng.,* Rome, Italy, 853–862.

Nuss, L. K., Noland, J. L., and Chinn, J. (1978). "The parameters influencing shear strength between clay masonry units & mortar." *Proc., North Amer. Masonry Conf.,* Boulder, Colo.

Van Zijl, G. P. A. G. (2004). “Modeling masonry shear-compression: role of dilatancy highlighted.” *J. Eng. Mech.,* 130(11), 1289–1296.

Van der Pluijm, R. (1993). “Shear behavior of bed joints.” *Proc. 6th North Amer. Masonry Conf.,* Philadelphia, Pennsylvania, 125–136.

Yokel, F. Y., and Fattal, S. G. (1975). "A failure hypothesis for masonry shear walls." *Rept. No. NBSIR 75-703,* Nat. Bureau of Standards, Washington, D.C.

Chapter 4

Numerical Modeling for Brick Interface

4.1 Modeling Background

An important aspect of existing masonry structures under new loading conditions is safety, with an emphasis in the preservation of historical structures. Reliable numerical models are necessary to assess and strengthen existing masonry structures. The failure analysis of masonry structures has been based on modeling techniques developed in modern concrete mechanics. Unreinforced masonry is a composite material made by assembling blocks or bricks with mortar joints. The overall performance of this composite is influenced by several factors. These include the unit rate of suction, the surface roughness of the masonry units, the particle size distribution of sand, and the moisture content of mortar, brick and mortar properties, brick size and its aspect ratio, joint thickness, joint orientation, relative position of head and bed joints, properties of the unit/mortar bond and workmanship. The bond between brick and mortar is derived from penetration of the mortar and hydration products, such as calcium silicate hydrates, into the brick surface voids and pores (Lawrence and Cao 1987; Grandet 1975).The failure of the masonry structures may occur in the bricks, in the mortar or in their interface. Cracking and crushing may occur in the brick and/or in the mortar. As it was stated in the previous chapter that, in the brick/mortar interface, two failure modes are possible; namely, tensile failure and shear failure. The first leads to joint opening and the latter to joint sliding with friction.

For fully grouted reinforced masonry, where the influence of mortar joints is marginal, the smeared crack approach can be applied to the analysis of such masonry structures (Lotfi & Shing 1991). On the other hand, the behavior of unreinforced masonry may not be modeled accurately by the smeared crack approach as unreinforced concrete behavior cannot. Although intact brick units may be assumed homogeneous and isotropic, the presence of mortar joints makes unreinforced masonry composite, both heterogeneous and anisotropic and shows distinctive directional properties at the time of load-dispalcement interaction.

Considerable effort has been devoted in recent years to advance the numerical models of brick-mortar interface for accurate simulation of masonry structures. The main obstacles to this modeling are related to the localization process associated with the creation of macro cracks where damage and inelastic strain concentrate. In the finite-element analysis of unreinforced

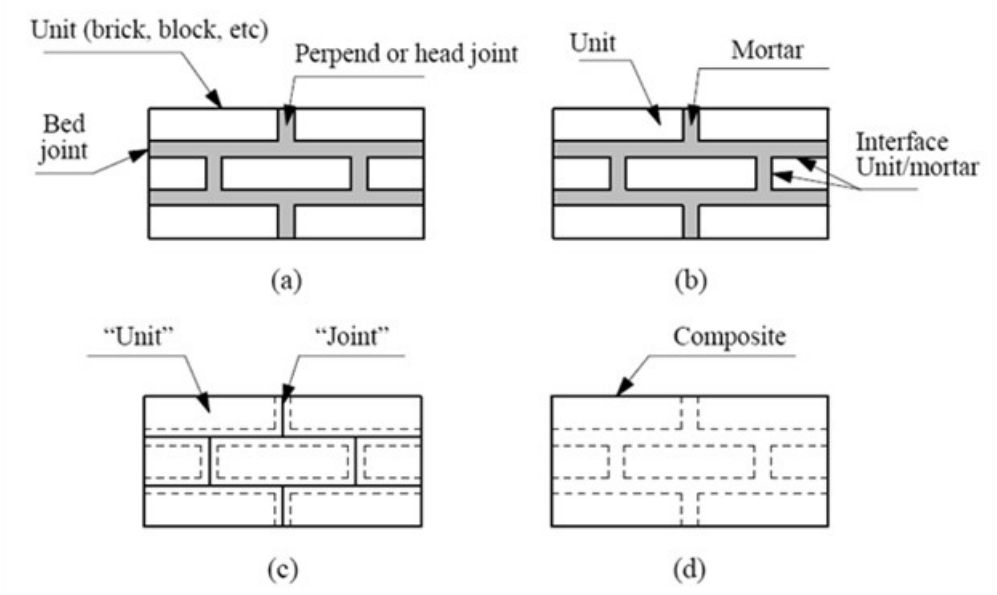

Fig. 4.1. *Modeling strategies for masonry structure: (a) masonry sample; (b) detailed micro-modeling; (c) simplified micro-modeling; and (d) macro-modeling*

masonry structures, the effect of mortar joints as the major source of weakness and material nonlinearity has been accounted for with different levels of refinement. In general, the approach towards its numerical representation can focus on the micro-modeling of the individual components, viz. unit (brick, block, etc.) and mortar, or the macro-modeling of masonry as a composite (Rots 1991). Depending on the level of accuracy and the simplicity desired, modeling technique can be categorized into three possible ways, (Fig. 4.1):

1. ***Detailed micro-modeling*** **–** units and mortar in the joints are represented by continuum elements whereas the unit-mortar interface is represented by interface elements;

2. Simplified micro-modeling **–** expanded units are represented by continuum elements whereas the behavior of the mortar joints and unit-mortar interface is lumped into interface elements;

3. Macro-modeling **–** units, mortar and the unit-mortar interface are smeared out in the continuum elements. In the macro analysis, masonry is considered as a single material (also known as a homogenized material), which inherently includes the effect of mortar joints.

In the first approach, Young's modulus, Poisson's ratio and, optionally, inelastic properties of both unit and mortar are taken into account. The interface represents a potential crack/slip plane with initial dummy stiffness to avoid interpenetration of the continuum.

In the simplified micro-modeling approach, masonry units are modeled with continuum elements, while mortar joints are modeled by means of interface elements. Each joint, consisting of mortar and the two unit-mortar interfaces, is lumped into an "average" interface while the units are expanded in order to keep the geometry unchanged. Masonry is thus considered as a set of elastic

blocks bonded by potential fracture/slip lines at the joints. Accuracy is lost since Poisson's effect of the mortar is not included. Early attempts with this approach were made by Arya & Hegemier (1978), Page (1978) and more recently Rots (1991). Obviously, the approach with this level of refinement is computationally intensive for the analysis of large masonry structures, but it is certainly a valuable research tool and also a viable alternative to the costly and often time-consuming laboratory experiments. From a modeling point of view the aforementioned approach is similar to the discrete element method, which was originally proposed by Cundall (1971) in the area of rock mechanics.

The third approach does not make a distinction between individual units and joints but treats masonry as a homogeneous anisotropic continuum. One modeling strategy cannot be preferred over the other because different application fields exist for micro- and macro-models. Micro-modeling studies are necessary to give a better understanding about the local behavior of masonry structures. Macro-models are applicable when the structure is composed of solid walls with sufficiently large dimensions so that the stresses across or along a macro-length will be essentially uniform. Clearly, macro-modeling is more practice oriented due to the reduced time and memory requirements as well as a user-friendly mesh generation. This type of modeling is most valuable when a compromise between accuracy and efficiency is needed.

In this current study, the simplified micro-modeling approach is adopted for simulating the behavior and failure mechanisms of masonry assemblages based on the behavior of the basic constituents. A simple but general model for shear cracking in masonry interface is proposed. It is defined in term of shear stress on the average plane of the crack and the corresponding shear relative displacement. In the following sections, the formulation of the interface model is explained, and the applicability of the interface model to mortar joints is validated by experimental results. The proposed model can be implemented directly as the constitutive law of the interface element in the context of discrete crack analysis.

4.2 Numerical Modeling Strategy

A simplified mechanical models for both brick-mortar and brick-FRP interface in masonry wall are proposed in this chapter. Those model equations were derived from phenomenological concept of load-reaction for masonry shear wall that can fully capture both the pre-peak and post-peak behavior with loading unloading and reloading process of masonry wall. In this study, simplified mechanical model is used wherein the two masonry components, namely the brick and mortar joint are modeled separately. The mortar joint is modeled through 16-nodes interface of zero thickness. Similarly the FRP is modeled as 8-nodes shell element and interface between FRP and brick unit is the same 16-nodes interface element of zero thickness with different

constitutive relationship. The proposed models have been verified for shear-compression only but for wider acceptability and versatile application the proposed models need to be installed in a 3D FEA program and verify for some of the experimental results.

4.3 Modeling for Brick-Mortar Interface

A simplified modeling approach is proposed here to model masonry. The mortar thickness and the brick–mortar interfaces are lumped into a zero-thickness 16 nodes interface plane elements while the dimensions of the brick units are expanded to keep the geometry of a masonry structure unchanged. Masonry components are thus modeled as a set of 20 nodes brick element, 8 nodes FRP element and 16 nodes interface element, as shown in Fig. 4.2(a). Each masonry unit is further subdivided into two interior brick elements which have boundaries either representing the mortar interfaces or monolithic to the next brick surface and thus perfectly simulate the alternate vertical bonds in single leaf masonry wall. Stresses were calculated at 8 Gauss integration points for solid element and 4 points for interface element. Possible failure is captured through a constitutive softening-fracture law at the interface nodes. Fracture is restricted to the horizontal and/or vertical mortar interface as shown in fig. 4.2(c) to Fig. 4.2(e) by either interface crack opening or interface slip. At high compression zone the crushing of mortar is formulated and is shown in subsequent sections. It was previously mentioned that the brick-mortar interface was modeled as zero thickness plane elements of 16 nodes and 4 Gauss points. This element are then inserted either in the horizontal plane between two adjacent units or in the vertical plane. This element is modeled in such a way that it can capture all the three modes of failure i.e. Mode I, II and III as depicted in Fig. 4.2. At any instant, there are two stresses components acting on each Gauss point [Fig. 4.2(b)]. Among these two stresses, one is normal to the interface, σ_n and the other one is shear stress τ acts along the plane of interface. To model bond between FRP and brick, same interface element is used with different constitutive laws and will be discussed later. In the next section, all the model equations are discussed in detail for different interaction of normal and shear stresses at mortar interface.

4.3.1 Case I: Tension Model

Crack does not appear until the strain generated at a point meets the cracking strain criteria (Okamura et al. 2003). Experimental result carried out by Reinhardt et al. (1986) depicts slightly nonlinear tendency of tensile stress before it reaches the peak tensile strength. In our own experiments (Fig. 3.14 and Fig. 3.16) no significant plasticity prior to crack opening was noticed and thus the plastic behavior of this tensile strain is ignored and a linear stress-strain relationship

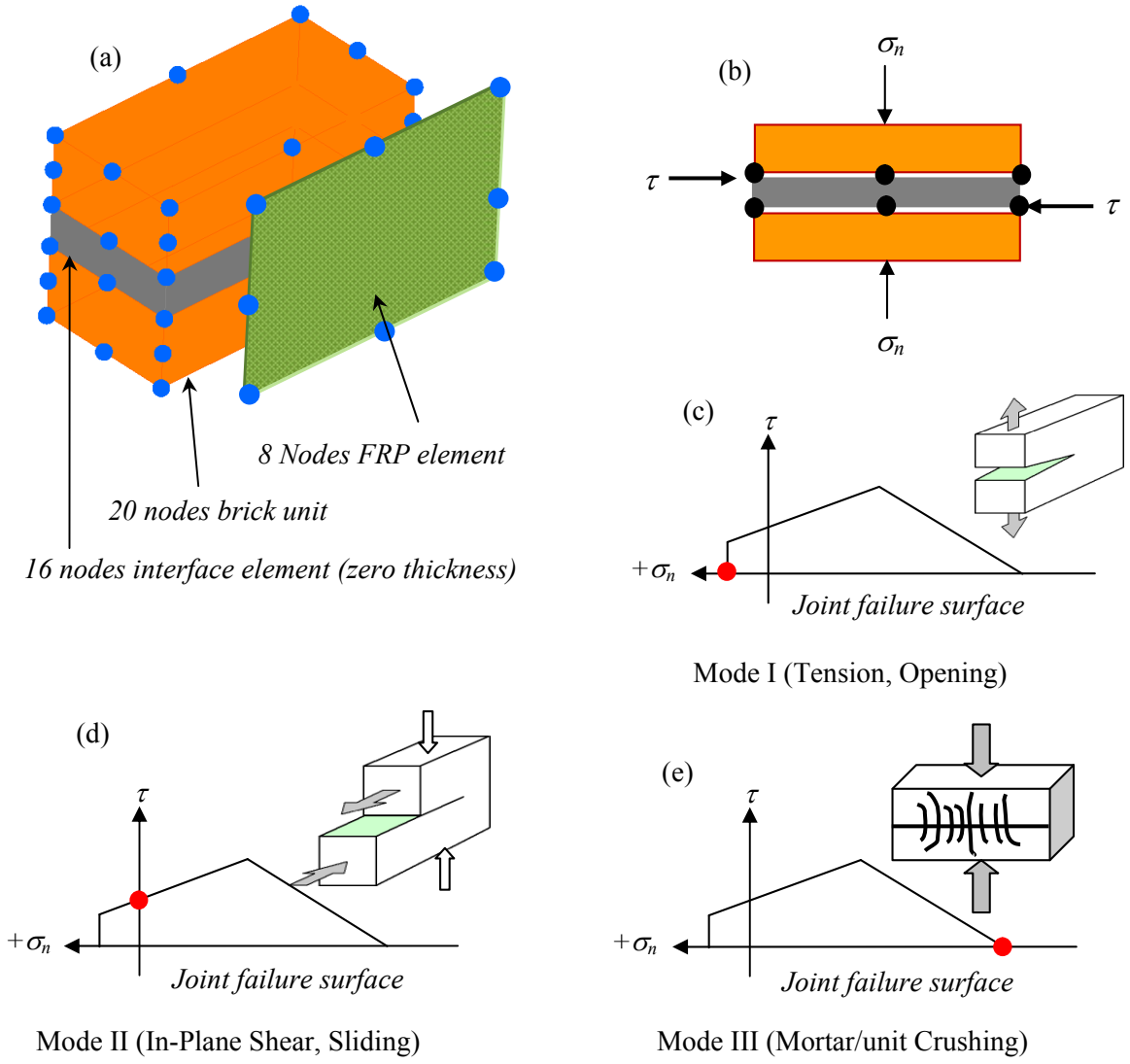

Fig. 4.2. *a) Brick, FRP and joint elements for FEA b) Component of stresses on an interface c) Interface failure in tension d) in shear and e) in compression*

is formulated instead that followed by a nonlinear tension softening, until it meets the maximum limit stain criterion of ε_{tmax} as shown in Fig. 4.3 that simulates the full crack opening.

It is well established fact (Lourenco et. al. 1998; and Chaimoon et. al. 2007) that the elastic tensile stiffness of masonry interface is not the individual stiffness of either brick or mortar but the combined action of these two and much less than that of the both. As a consequence the interface bond strength depends on the individual tensile strength of either brick or mortar. Eq. (4.1) calculates the interface bond strength f_{ti} from the splitting tensile strength of either mortar or brick, whichever is less. Also the corresponding strain ε_{t0} can be given by Eq. (4.2). Eq. (4.3) gives the strain correspond to maximum COD.

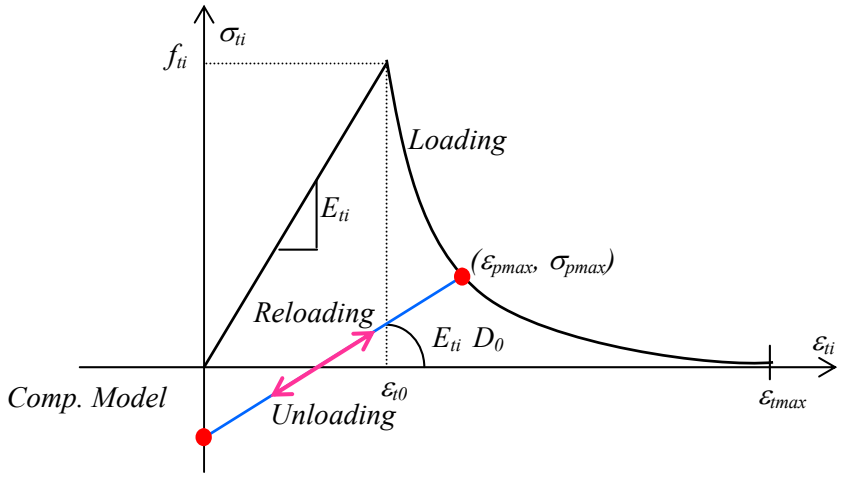

Fig. 4.3. *Model for interface intension*

$$f_{ti} = 0.254 + \frac{1}{22.2}\left(f_{spt}\right)^2 \ln\left(f_{spt}\right) \tag{4.1}$$

$$\varepsilon_{t0} = 0.0000724\, f_{ti}^{(0.216/f_{ti})} \tag{4.2}$$

$$\varepsilon_{t\max} = 25\varepsilon_{t0} \text{ and } \le 0.0015 \tag{4.3}$$

Thus the reduced elastic modulus for the interface can be calculated simply by Eq. (4.4).

$$E_{ti} = \frac{f_{ti}}{\varepsilon_{t0}} \tag{4.4}$$

A suitable softening equation [Eq. (4.5)] was installed in this FEA program and that was introduced by Okamura et.al (2003). A linear unloading a reloading is incorporated by Eq. (4.6) to Eq. (4.9).

$$\sigma_{ti} = f_{ti}\left(\frac{\varepsilon_{t0}}{\varepsilon_{ti}}\right)^{0.6} \tag{4.5}$$

Unloading: $\varepsilon_{ti} < \varepsilon_{p\max}$ and $\varepsilon_{ti} < \varepsilon_{last}$

$$D_0 = \exp\left[-2.8\frac{\varepsilon_{p\max} - \varepsilon_{t0}}{\varepsilon_{t\max}}\left\{1 - \exp\left(-2.5\frac{\varepsilon_{p\max} - \varepsilon_{t0}}{\varepsilon_{t\max}}\right)\right\}\right] \tag{4.6}$$

$$\varepsilon_p = \left\{\varepsilon_{p\max} - \left(\frac{\sigma_{p\max}}{E_{ti}D_0}\right)\right\} \tag{4.7}$$

$$\sigma_{ti} = E_{ti}D_0(\varepsilon_t - \varepsilon_p) \tag{4.8}$$

Relaoding: $\varepsilon_{ti} < \varepsilon_{p\max}$ and $\varepsilon_{ti} \ge \varepsilon_{\text{last}}$

$$\sigma_{ti} = \left[\sigma_{p\max} - (\sigma_{p\max} - \sigma_{last})\frac{\varepsilon_{p\max} - \varepsilon_{ti}}{\varepsilon_{p\max} - \varepsilon_{last}}\right] \tag{4.9}$$

Where, f_{ti}=tensile strength of the interface; f_{spt}=splitting tensile strength of brick(or mortar); ε_{t0}= tensile strain for f_{ti}; ε_{tmax}= max. limit of tensile strain in softening; E_{ti}=elastic modulus at interface; ε_{ti}=instantaneous strain at current load, σ_{ti}=stress corresponding to ε_{ti}; D_0= damage parameter ≤ 1.0; ε_{pmax} = max. strain throughout the loading history; σ_{pmax}= stress corresponding to ε_{pmax}; ε_{last} = stain at previous step; ε_p = plastic strain; σ_{last} = stress corresponding to ε_{last} .

4.3.2 Case II: Shear-Tension Model

The shear stiffness at interface should be lower than that of brick or mortar, and from experimental evidence it was found that this stiffness can be safely given by Eq. (4.10). Also the shear strength with the presence of tensile stress can be estimated by Rankine criterion as in Eq. (4.11), otherwise it is simply in the order of initial cohesion c_0. If c_0 is not readily available it can be calculated as a function of compressive strength of mortar [Eq. (4.12)] which was proved by experimental result on masonry prism. Shear stress along the crack plane before reaching the ultimate shear strength τ_u can be treated as linear (see Fig. 4.4) provided the tensile strain remains within the range of cracking strain ε_{t0}, otherwise a reduction in shear strength is expected and is given by Eq. (4.11). The unloading and reloading are of same nature of tension model [see Eq. (4.6) to (4.9)] and for brevity will not be repeated. The shear softening is of the same nature as given by Eq. (4.13). The maximum shear strain was taken 5.25 times that of γ_u(Okamura et al. 2003).

$$G_i = \frac{1}{0.0403 - 0.00475\ln\left(G_{me}\right)} \tag{4.10}$$

Here,

$$G_{me} = \frac{E_{me}}{\left(2+\nu_b+\nu_m\right)} \quad ; \quad E_{me} = \frac{E_b E_m}{E_b + E_m}; E_b = 2450\sqrt{f_c^b} \text{ and } E_m = 4800\sqrt{f_c^m}$$

$$\tau_u = c_0\sqrt{1-\frac{\sigma_t}{f_t}} \tag{4.11}$$

$$\gamma_u = \frac{\tau_u}{G_i} \text{ and } \gamma_{\max} = 5.25\gamma_u$$

$$c_0 = 1.456 + \frac{\exp\left(f_c^m\right)}{2.275\times10^{12}} - \frac{35.4\ln\left(f_c^m\right)}{\left(f_c^m\right)^2} \tag{4.12}$$

$$\tau = \tau_u\left(\frac{\gamma_u}{\gamma}\right)^{0.9} \tag{4.13}$$

Where, G_{me}, E_{me} = shear modulus and Young's modulus of masonry; G_i = shear modulus of interface; f_c^m, f_c^b = compressive strength of mortar and brick. All other notations have their usual meaning.

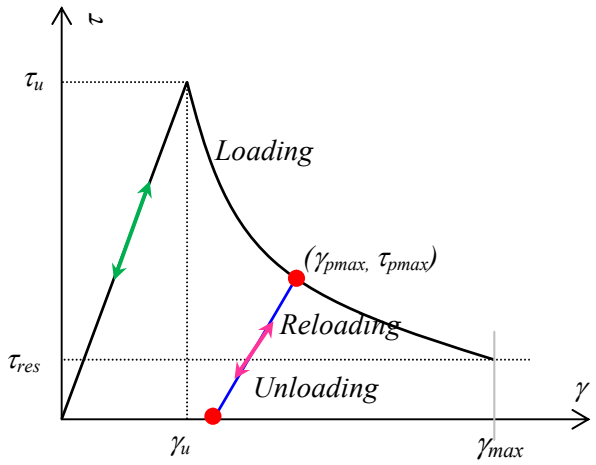

Fig. 4.4. *Interface shear-tension model*

4.3.3 Case III: Compression Model

The compressive strength of the masonry is a combined strength of both brick and mortar and is given by Eq. (4.14) which was established after a series of prism test for different mortar strengths. The corresponding elastic strain and strain at ultimate strength is given by Eq. (4.15) originally proposed by Hemant B. et al (2007) and is verified by our own experimental results. The elasto-plastic and fracture criterion [Eq. (4.16) to Eq. (4.18)] originally given by Okamura et al. (2003) is directly used here as work hardening phenomenon followed by a nonlinear softening curve (Fig. 4.5). A residual stress of only 2% of masonry strength is considered for the fact that even after the crushing of the mortar the interface is still able to carry some compressive stress. The ε_{max} is assumed 5.75 times that of ε_u.

$$f_c^{masn} = \left(f_c^{b} - 3.257\right) + 0.754\sqrt{f_c^{m}} - \frac{12.44}{f_c^{m}} \tag{4.14}$$

$$\varepsilon_e = \frac{0.33 f_c^{masn}}{E_e^{masn}} \quad \text{and} \quad \varepsilon_u = \frac{0.27}{(f_c^{m})^{0.25}} \frac{f_c^{masn}}{\left(E_e^{masn}\right)^{0.825}} \tag{4.15}$$

EPF model:

$$K_0 = \exp\left\{-0.73\frac{\varepsilon_c}{\varepsilon_u}\left(1-\exp(-1.25\frac{\varepsilon_c}{\varepsilon_u}\right)\right\} \tag{4.16}$$

$$\varepsilon_p = \left[\frac{\varepsilon_c}{\varepsilon_u} - \frac{20}{7}\left\{1-\exp\left(-0.35\frac{\varepsilon_c}{\varepsilon_u}\right)\right\}\right]\varepsilon_u \tag{4.17}$$

Where, $\varepsilon_c = \varepsilon_e + \varepsilon_p$

$$\sigma_c = 2.95 K_0 E_e^{masn}(\varepsilon_c - \varepsilon_p) \tag{4.18}$$

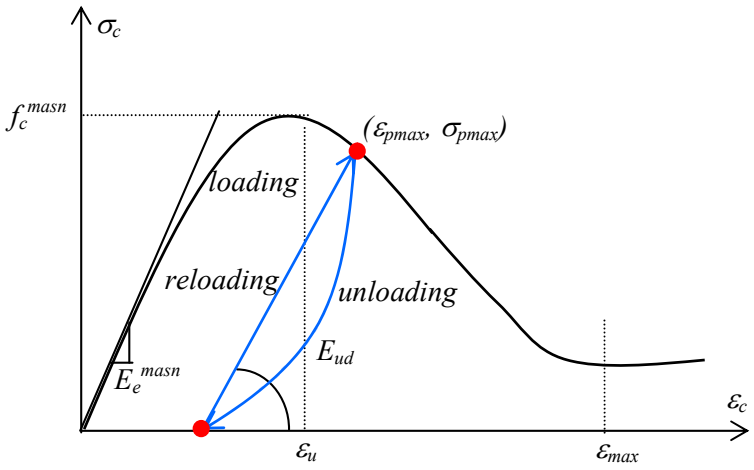

Fig. 4.5. *Compression model for the interface*

The unloading/reloading from the softening path will be the same nature of that of tension model. For the case of unloading from the hardening path a nonlinear unloading path is proposed which can trace all the way to the zero stress level until it reach the tension criterion. One the strain switch from compression to tension, the unloading reverse to tension loading which was clarified in the earlier section. In calculating the unloading stress, the scalar parameter α [see Eq. (4.19)] is calculated in addition to fracture parameter K_0 and plastic strain ε_p that are calculated before the initiation of unloading by the same Eq. (4.16) and Eq. (4.17). The reloading is just a linear relationship between the point of unloading and reloading as same as Eq. (4.9) above.

$$\alpha = K_0^{\,2} + \left(\frac{\sigma_{last}}{2.95 \times K_0 E_e^{masn} (\varepsilon_{last} - \varepsilon_p)} - K_0^{\,2} \right) \tag{4.19}$$

4.3.4 Case IV: Shear-Compression Model

In this model it was assumed that, at the level of the interface Gauss integration point, the inelastic failure surface is a function of the normal and interface shear stresses. Fig. 4.6 shows the adopted failure surface at each of the interface Gauss integration points for brick-mortar joints. The failure surface consists of a Mohr-Coulomb linear inelastic surface and a tension cut-off. The limit of the Mohr-Coulomb surface is assigned by adopting a compression cap line when the normal compression at the respective Gauss point goes beyond the compressive strength of masonry and high enough to crush the mortar or bricks, whichever is weaker in strength. The maximum shear capacity at the interface at a particular level of normal stress is given by the Mohr-Coulomb criterion in Eq. (4.20).

$$\tau_u = c + \sigma_n \tan\phi \tag{4.20}$$

The local bond stress-slip (τ-δ) relation up to the peak can be given by Eq. (4.21) (see Fig. 4.7) (Dai et al. 2005)

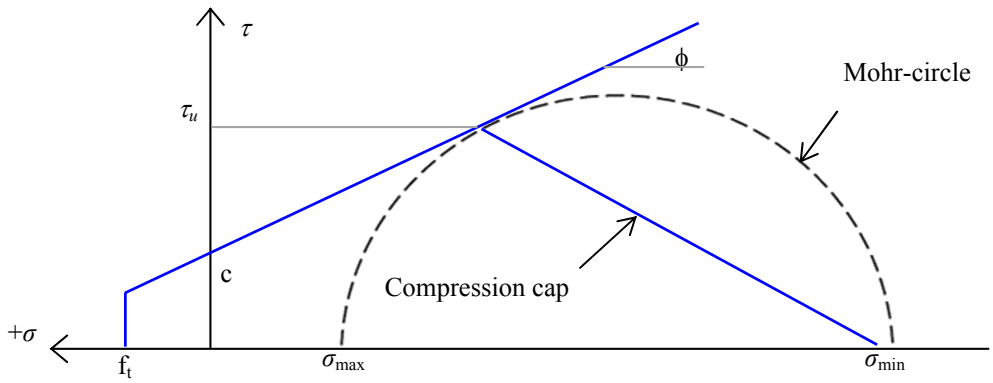

Fig. 4.6. *Failure surface of masonry joint with compression cap proposed by Chaimoon & Attard (2007)*

$$\tau = 2BG_f\left(\exp\left(-B\delta\right)-\exp\left(-2B\delta\right)\right) \tag{4.21}$$

In this equation only two parameters, interface fracture energy G_f and interface initial shear stiffness B are needed to define the bond stress-slip relationship. The interface initial shear stiffness B is a function of mortar thickness t_m, Young's modulus of brick and mortar E_b, E_m, normal pre-compression σ_n and mortar compressive strength f'_{cm}. In Eq. (4.22), B reads as,

$$B = 2.75\frac{\log\left(E_bE_mt_m\right)}{\exp\left[4.039\exp\left(-0.155f'_{cm}\right)\sigma_n^{0.525}\right]} \tag{4.22}$$

The fracture energy parameter G_f can be given by Eq. (4.23) once the peak shear stress τ_u and shear stiffness B are known, which reads as,

$$G_f = \tau_u / 0.5B \tag{4.23}$$

$$\delta_u = \ln\left(\frac{2}{B}\right) = 0.693/B \tag{4.24}$$

Here δ_u is the shear deformation corresponding to peak shear stress τ_u. The post-peak regime of the bond stress-slip (τ-δ) relationship in Fig. 4.7 can be given by the following equation:

$$\tau = \tau_u\left(\frac{\delta_u}{\delta}\right)^n \tag{4.25}$$

Where n is a function of fracture energy G_f and can be given by Eq. (4.26).

$$n = 1.01\exp\left(-2.288G_f\right) \tag{4.26}$$

After the complete loss of cohesion and permanent deformation at the interface, only a fraction of shear stress can be transferred through the joint which is residual shear stress τ_{res}. Eq. (4.27) gives the magnitude of this residual shear stress which depends on the level of available compression pressure and the tangent of the residual friction angle ϕ_{res}. A maximum slip δ_{max}

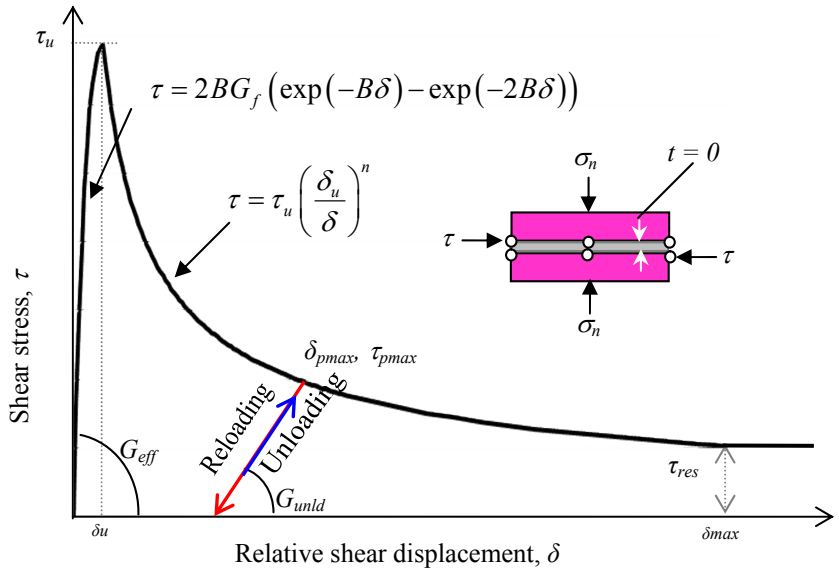

Fig. 4.7. *Shear stress-slip model for the interface*

corresponds to the point on the curve where shear stress τ is equal to the residual shear stress τ_{res} in Eq. (4.25) (Fig. 4.7).

$$\tau_{res} = \sigma_{res} \tan \phi_{res} \tag{4.27}$$

The relaxation of shear stress can happen at any stage of loading and at any location, which causes an unloading at a particular Gauss point during the evolution of loading. For compatibility and completeness of the constitutive relationship, it is necessary to introduce an unloading and reloading path along which the unloading and reloading can take place. In this model a suitable unloading and reloading path is introduced for pre-peak and post-peak regimes. Abdou et al. (2006) and Chaimoon & Attard (2009) observed quite similar loading and unloading path during their experimental procedure for the shear test (see Fig. 4.8). The unloading stiffness is less than the initial tangent stiffness G_{eff} because of the partial loss of interface cohesion especially at the pre-peak regime. In the post-peak regime the cohesion is completely lost and the overwhelming damage occurs on aggregate interlocking between brick and mortar grains. Once, the shear force due to aggregate interlocking is lost, the remaining shear resistance comes only from the interface friction in the order of residual stress where a state of complete damage prevails. Subsequent equations for unloading and reloading are postulated considering this phenomenological observation from the shear test on the brick-mortar couplet assemblage.

Loading: $\delta > \delta_{p\max}$

For pre-peak regime: $\delta \le \delta_u$

$$\tau = 2BG_f\left(\exp(-B\delta)-\exp(-2B\delta)\right) \tag{4.28}$$

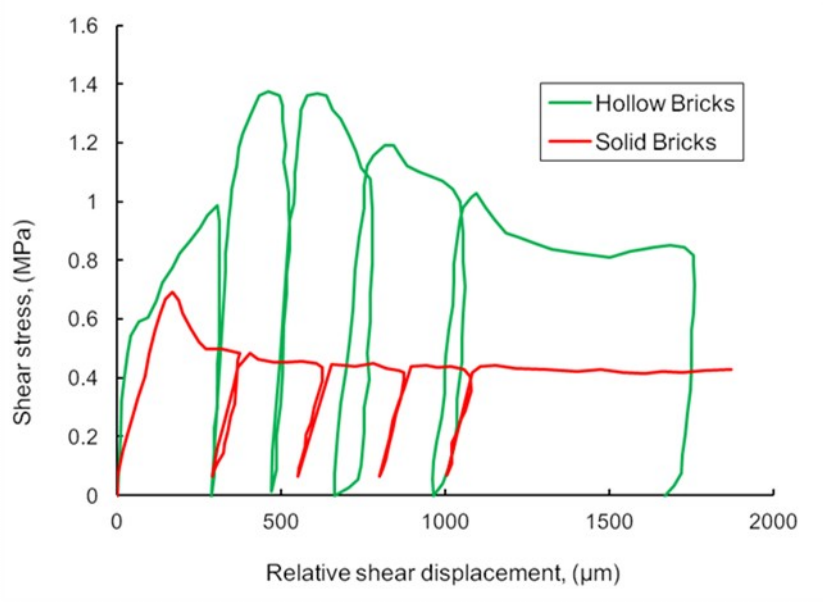

Fig. 4.8. *Typical unloading-reloading behavior of brick-mortar interfaces*

For post-peak regime 1: $\delta_u < \delta \le \delta_{\max}$

$$\tau = \tau_u \left(\frac{\delta_u}{\delta} \right)^n \tag{4.29}$$

For post-peak regime 2: $\delta_{\max} < \delta$

$$\tau_{res} = \sigma_{res} \tan \phi_{res} \tag{4.30}$$

Where, δ = instantaneous deformation; $\delta_{p\max}$ = max. slip during the loading history; δ_{last} = slip in the previous loading step; δ_u = slip for the peak shear strength; δ_{max} = slip at which shear stress turn to residual.

Unloading: $\delta < \delta_{last}$

For pre-peak regime: $\delta \le \delta_u$

$$\tau = \frac{1}{t_m} 2\alpha K_0 G_{eff} \delta_e \tag{4.31}$$

$$\delta_e = \delta - \delta_p \tag{4.32}$$

$$\delta_p = \left[\frac{\delta_{p\max}}{\delta_u} - \frac{20}{7} \left\{ 1 - \exp\left(-0.35 \frac{\delta_{p\max}}{\delta_u} \right) \right\} \right] \delta_u \tag{4.33}$$

$$\alpha = K_0^{\,2} + \left(\frac{\delta_{last}}{2K_0 G_{eff} (\delta_{last} - \delta_p)} - K_0^{\,2} \right) \left(\frac{\delta - \delta_p}{\delta_{last} - \delta_p} \right)^2 \tag{4.34}$$

$$K_0 = \exp\left\{ -0.73 \frac{\delta_{p\max}}{\delta_u} \left(1 - \exp(-1.25 \frac{\delta_{p\max}}{\delta_u} \right) \right\} \tag{4.35}$$

$$G_{eff} = G_i (1 + 0.784 \sigma_n) \tag{4.36}$$

$$G_i = \frac{0.85\exp\left[4.25+1.325\ln\left(f_t^m\right)-0.275\ln\left(f_t^m\right)^2\right]}{\exp\left(1/t_m\right)} \quad ; \text{if } f_t^m < f_t^b \tag{4.37}$$

$$G_i = \frac{0.85\exp\left[4.5+1.5\ln\left(f_t^b\right)-0.125\ln\left(f_t^b\right)^2\right]}{\exp\left(1/t_m\right)} \quad ; \text{ if } f_t^m > f_t^b \tag{4.38}$$

Here, K_0 = fracture parameter; α = stress reduction factor; δ_p = plastic deformation; δ_e = elastic deformation; G_i = Initial shear modulus of the interface at zero pre-compression, G_{eff} = Effective shear modulus at any level of pre-compression.

For post-peak regime1 and 2: $\delta > \delta_u$

$$\tau = \frac{1}{t_m} G_{unld}(\delta - \delta_p) \tag{4.39}$$

$$G_{unld} = G_{eff} \times D_0 \tag{4.40}$$

$$D_0 = \exp\left\{-2.8\frac{\delta_{p\max}-\delta_u}{\delta_{\max}}\left(1-\exp(-2.5\frac{\delta_{p\max}-\delta_u}{\delta_{\max}}\right)\right\} \tag{4.41}$$

$$\delta_p = \left\{\delta_{p\max} - \left(\frac{\tau_{p\max}}{G_{eff}D_0}\right)\right\} \tag{4.42}$$

Reloading: $\delta_{last} < \delta < \delta_{p\max}$

For pre-peak regime: $\delta \le \delta_u$

$$\tau = \left[\tau_{p\max} - (\tau_{p\max} - \tau_{last})\frac{\delta_{p\max}-\delta}{\delta_{p\max}-\delta_{last}}\right] \tag{4.43}$$

For post-peak regime 1 and 2: $\delta > \delta_u$

Same as Eq. (4.43)

Here, G_{unld} = unloading shear modulus; $\tau_{p\max}$ = stress corresponds to $\delta_{p\max}$; D_0 = damage parameter.

4.3.5 Model Implementation and Validation

The proposed analytical model needs only the Young's modulus of both brick and mortar E_b and E_m, the thickness of the mortar t_m and the overburden pressure σ_n. In most cases, experimental results given in Table 3.1 show good agreement with that of the analytical curves (Fig. 4.9). In some cases, the pre-peak stiffness and the peak shear stress were simulated quite closely where as in few cases the post-peak regimes show a little difference with the experimental one. This can partly be explained because of the experimental shear stress gives an average stress over the entire interface under investigation where a single softening constitutive law is not valid because of the variation of interface properties and cohesion over the sliding surface due to the lack of

uniformity at the time of specimen fabrication involving human error, whereas in numerical models all of this variability is ignored and a single branch softening constitutive law is provided, hence the softening behavior appears to be of the same nature for all cases. Moreover in experimental procedure the damage is gradual and the location where a complete state of interface damage prevails is rather difficult to locate, hence the exact point from where the residual stress is going to initiate is also difficult to determine. For numerical models it is done when the softening shear stress meets the residual shear stress criterion, so the junction of this two is not smooth but an abrupt change in direction and slope that is evident in some experimental results also. In addition, the post-peak behavior during the testing procedure is so delicate and abrupt that it is quite impossible to obtain solicited data from the test unless one has very sophisticated and well controlled experimental facilities. In this experimental procedure we did not have that level of control over the post-peak regime and that is the reason for the straight line softening and inconsistent variation in the post-peak regime for most of the cases. This may also be true for other experimental results such as Lourenço et al. (2004) in Fig. 3.2(e). Nevertheless, the model curve can predict the ultimate shear strength and residual shear stress quite correctly, and this is the merit of this model over few others limitations. If an accurate estimation of the empirical parameter B is ensured, the initial stiffness and shear displacement at peak shear stress will be very close to that of the experimental results.

If the modulus of Mortar is not readily available, Eq. (4.44) is recommended by Euro Code 6 for normal weight Concrete and can be used for mortar as well.

$$E_m = 22,000\left(\frac{f_c^m}{10}\right)^{1/3} \tag{4.44}$$

The interface cohesion c and the initial friction angle ϕ are the two inherent properties of mortar and brick, the materials used in this experiment. One is independent of stress and other is stress-dependent parameter. For numerical analysis of masonry wall for shear any reasonable value for these two will produce consistent result. However, for normal strength mortar and brick a range between 0.15 to 0.25 for c and 50° to 65° for ϕ will yield a good approximation of experimental results. For residual friction angle τ_{res}, a reasonable approximate value between 45° to 55° can be used safely for model implementation.

4.4 Brick-FRP Interface

The Shear transfer mechanism between brick and FRP through the epoxy bond is well clarified by numerous authors and can be found elsewhere in the bulk volume of FRP literatures. In this

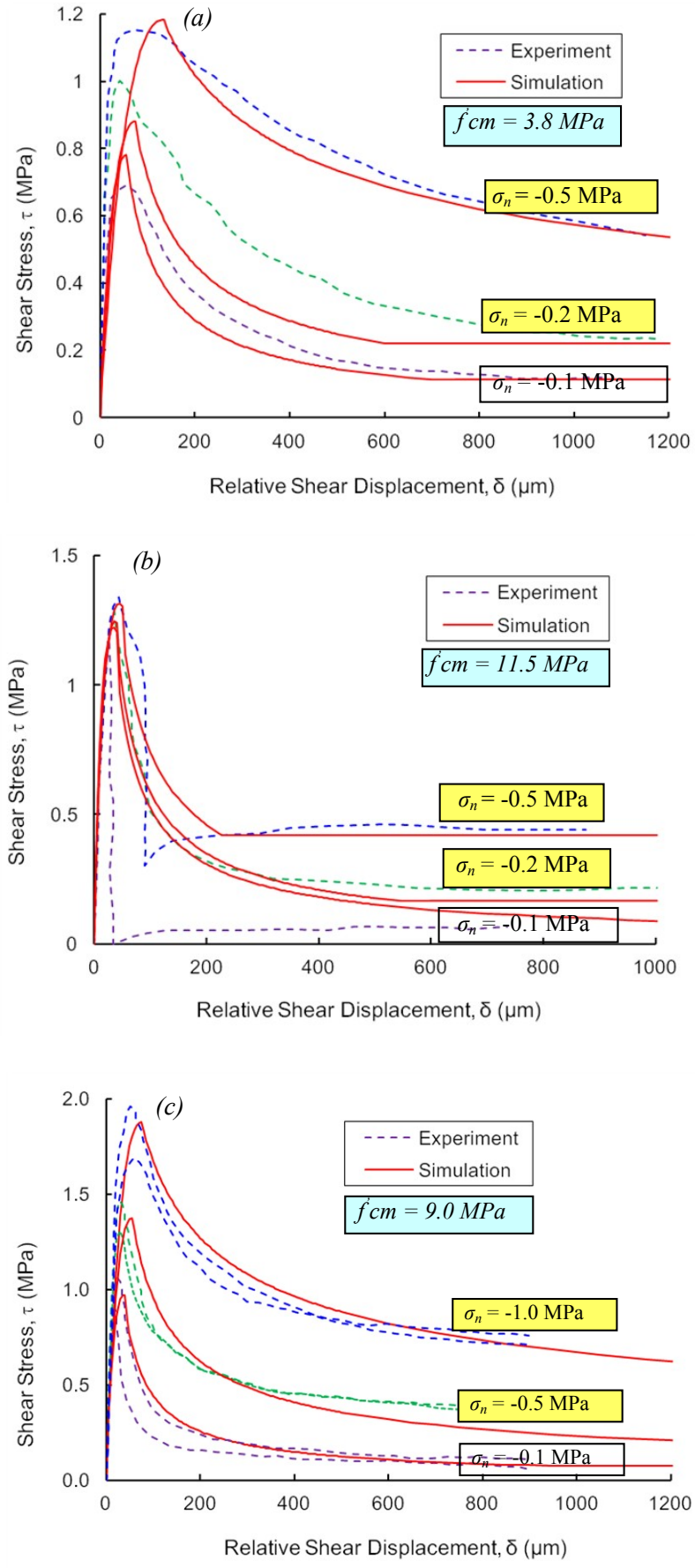

Fig. 4.9. *Comparison of simulation with experimental results of (a) & (b) Hansen (1999); (c) Van der Pluijm (1993)*

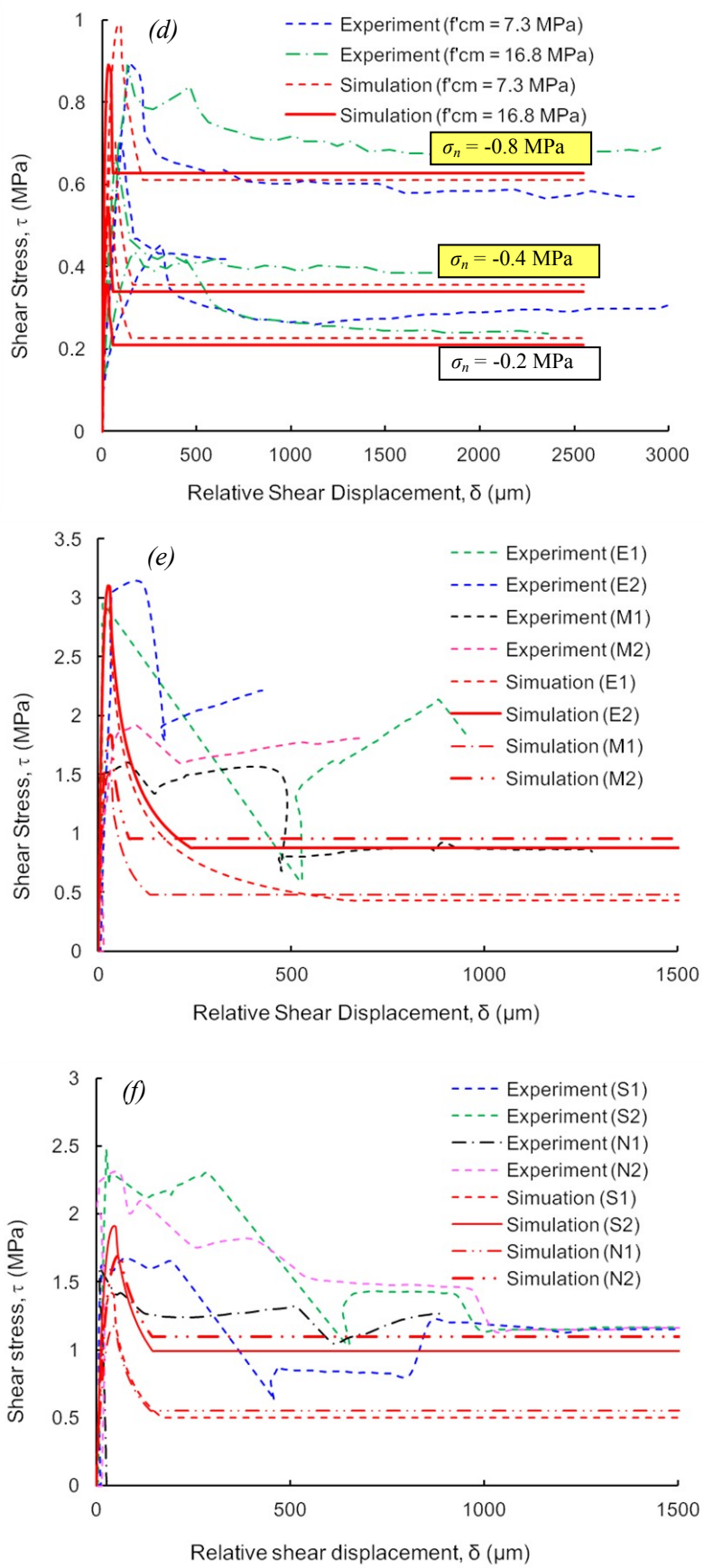

Fig. 4.9. *Comparison of simulation with experimental results of (d) Chaimoon (2007); (e) and (f) from this study*

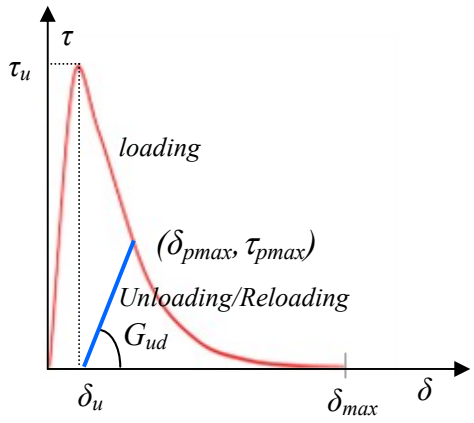

Fig. 4.10. *Bond Stress-slip model for FRP*

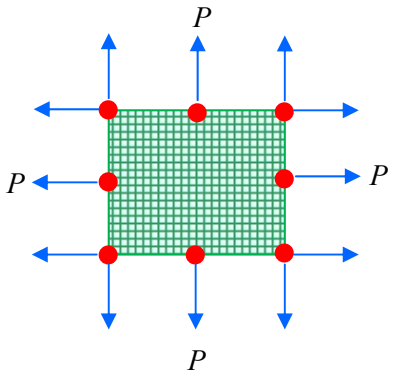

Fig. 4.11. *8 nodes FRP element with nodal force vector*

study a mechanical model with very good approximation proposed by Dai et al.(2005) is used (Fig. 4.10). They proposed the following equations [Eq. (4.45) to Eq. (4.47)] after a good number of pullout tests on FRP bonded with concrete. It is our understating from the beginning that the behavior of brick and concrete is quite similar under tension and compression and that is why some of the models originally developed for concrete can safely be used for brick as long as the mechanical properties of these two remain in close proximity of each other. The Shear stiffness of the adhesive layer reads,

$$\frac{G_a}{t_a} = \frac{G_p G_{ad}}{G_p t_{ad} + G_{ad} t_p} \tag{4.45}$$

$$\text{Where, } G_p = \frac{E_p}{2(1+\nu_p)}; \text{ and } G_{ad} = \frac{E_{ad}}{2(1+\nu_{qd})}$$

The fracture enegy of the interface slip is given by,

$$G_f = 0.446\left(G_a / t_a\right)^{-0.352}\left(f_c^b\right)^{0.236}\left(E_f t_f\right)^{0.023} \tag{4.46}$$

After getting the stiffness and fracture energy the shear-slip relation can be established as,

$$\tau = 2BG_f \exp\left(-B\delta\right)\left(1-\exp\left(-2B\delta\right)\right) \tag{4.47}$$

$$\text{Here, } B = 6.846\left(E_f t_f\right)^{0.108}\left(G_a / t_a\right)^{0.833}$$

$\delta_u = \ln 2 / B = 0.693 / B$ and $\tau_{\max} = 0.5BG_f$

Where, G_a= shear modulus of the adhesive layer; t_a=thickness of the adhesive layer; E_p, E_{ad}, t_p, t_{ad}, ν_p, and ν_{ad} = elastic modulii, thicknesses and Poission ratios of primer and adhesive layer respectively; E_f, t_f= Elastic modulus and thickness of fiber; B=interface ductility index.

A nonlinear unloading in the stress hardening part was incorporated into the model in the same way that was modeled for the compression model (see CaseIII). And for the softening part a linear model is used. Reloading for both hardening and softening is just a linear relationship

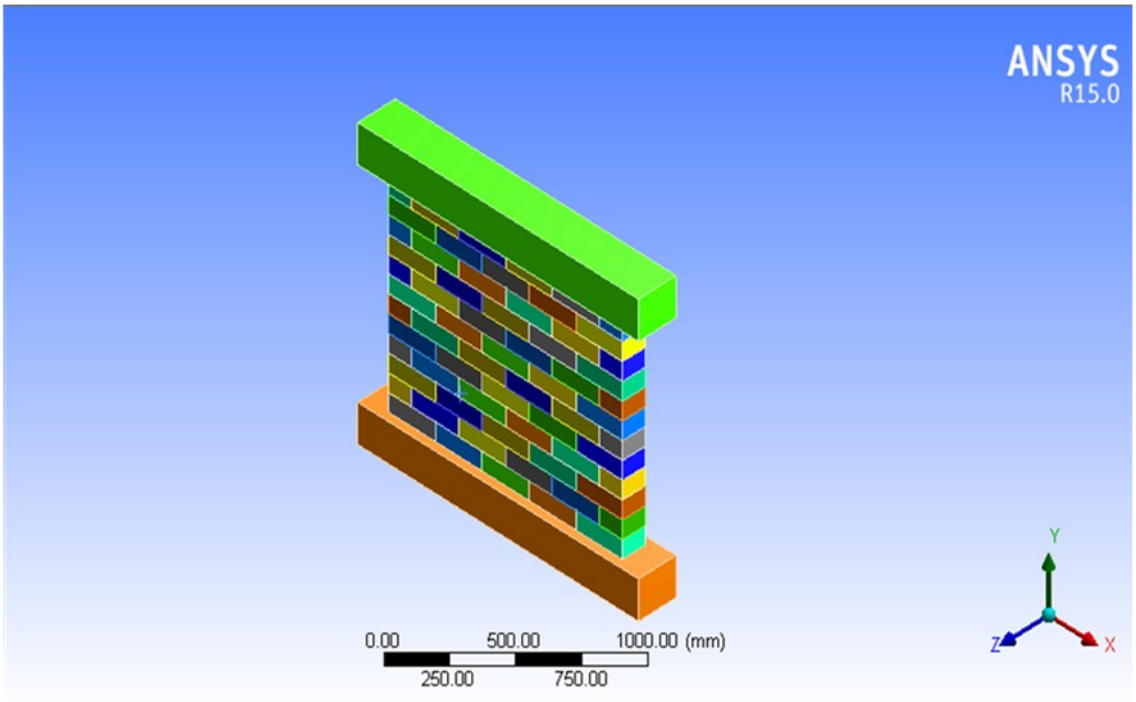

Fig. 4.12. *Finite Element modeling of experimental shear wall RWS*

between last loading point from where the unloading started and the point of reloading [Eq. (4.43)]. Concerning the normal stress on the interface between FRP and brick, a suitable stress-stain model that is similar to that of tension (CaseI) and compression (CaseIII) models are used and will not be mentioned explicitly. The FRP element was modeled as simply a 8-nodes elastic shell element where only the tensile forces along the fiber directions are considered (Fig. 4.11).

4.5 Model Implementation Strategy

The proposed models mentioned in the foregoing sections have been verified for element level but for member level such as unreinforced masonry and masonry with FRP strengthening has not yet been verified in full scale. Only one wall specimen (RWS) was modeled using a general purpose commercial software **AN**SYS™ which is capable of numerical simulation of a variety of physical problems. The finite element model, simulation result and the numerical fracture pattern obtained after analysis are given in Fig. 4.12 and 4.13(a, b).

4.6 Concluding Remarks

Considering the models proposed in this chapter, the following conclusions can be drawn:

1) The proposed model equations have uniqueness in their simplicity and can predict the peak shear stress as well as the initial stiffness and the softening behavior of the interface quite well for the experimental results examined in this research. The necessary information for the

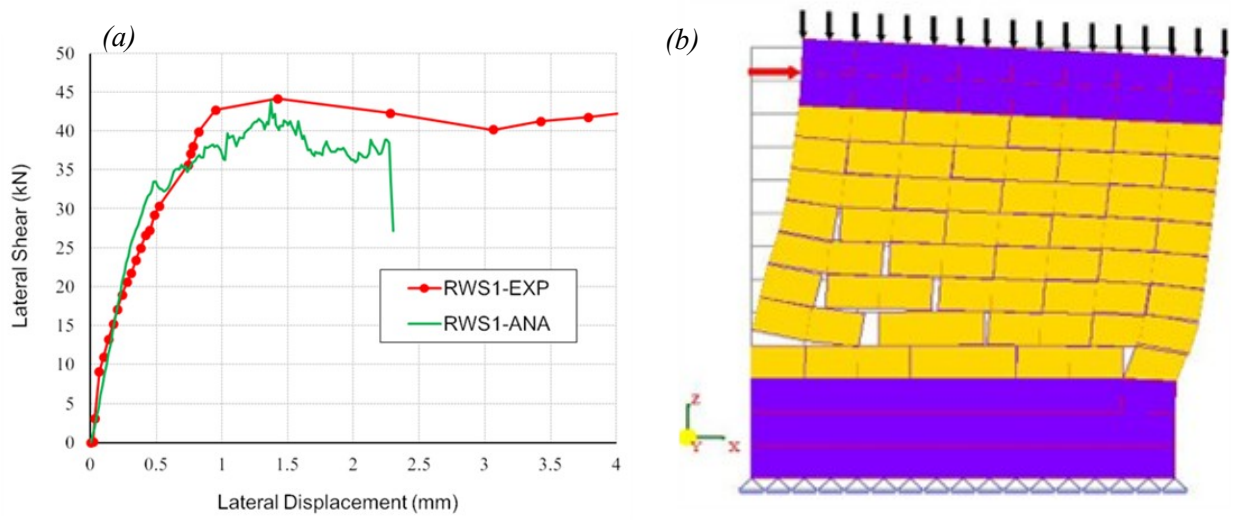

Fig. 4.13. *a)Comparison between experimental and numerical results of load-displacement response of URM wall; b) Simulated fracture pattern in the wall*

proposed model is only the Young's modulus of brick and mortar, the mortar thickness and the normal compressive stress acting on the interface. Proposed value for c and ϕ can give good numerical approximation.

2) A comprehensive numerical strategy is needed to verify these proposed numerical models for full scale walls. General purpose commercial Finite Element program such as ANSYS, DIANA or MATLAB can be the best option for this numerical work. Sufficient care should be taken at the time of implementing these proposed models into the user-defined subroutine of these FEA software, so that the units and parameters are consistent with the core program.

References

Abdou, L., Saada, R. A., Meftah, F., and Mebarki, A. (2006). "Experimental investigations of the joint-mortar behavior." *ELSEVIER J. Mech. Research Communications* 33, 370–384.

Armaanidis, V. I. (1998). "A model for the shear strength of rough rock discontinuities under low normal stress." Ms.C. dissertation, School of Civil Eng. and Geosciences, Univ. of Newcastle Upon Tyne, U.K.

Arya, S. K., and Hegemier, G. A. (1978). "On nonlinear response prediction of concrete masonry assemblies." *Proc., North Amer. Masonry Conf.,* Masonry Society, Boulder, Colo., 19.1–19.24.

ASCE 31-02. "Handbook for the seismic evaluation of buildings" *Building Seismic Safety Council for Federal Emergency Management Agency, Washington D.C.*

ASTM C 270. (2007). Standard Specification for Mortar for Unit Masonry.

ASTM C 1437. (2007). Standard Test Method for Flow of Hydraulic Cement Mortar.

Atkinson, R. H., Amadei, B. P., Saeb, S., and Sture, S. (1989). "Response of masonry bed joints in direct shear." *J. Struct. Eng.,* 115(9), 2276–2296.

Calvi, B. M., Macchi, G., and Zanon, P. (1985). "Random cyclic behavior of reinforced masonry under shear action." *Proc, 7th Int. Brick Masonry Conf.,* Melbourne, Australia.

Chaimoon, K. and Attard, M. M. (2009). "Experimental and numerical investigation of masonry under three-point bending (in-plane)." *ELSEVIER J. Eng. Struct*. 31,103–112.

Copleland, R. E., and Saxer, E. D. (1964) "Tests of structural bond of masonry mortars to concrete block." *ACI Journal*, Title No. 61-70, 1964,1411–1452.

Cundall, P. A. (1971). "A computer model for simulating progressive large-scale movements in block rock systems." *Proc., Int. Symp. Rock Fracture,* Nancy, France, II-8.

El-Sakhawy, N. R., Raof, H. A., and Gouhar, A. (2002). "Shearing behavior of joints in load-bearing masonry wall" *J. Mat. in Civil Eng.,* 14(2), 145–150.

EN 1052-4, 2000, "Determination of shear strength including damp proof course." European norm for method of test for masonry Units- Part 4.

Gabor, A., Ferrier,E., Jacquelin, E., Hamelin, P. (2006). "Analysis and modelling of the in-plane shear behavior of hollow brick masonry panels." *ELSEVIER J. Const. Bldg. Mat.,* 20, 308–321.

Goodman, R. E. (1976). "Methods of geological engineering in discontinuous rocks." *West Publishing Company, St Paul.*

Gottfredsen, F. R. (1997). "Laterally loaded masonry." Ph.D-Thesis, *SBI–Report 289*, Danish Building Research Institute, Hørsholm, Denmark.

Hamid, A. A., and Drysdale, R. G. (1980). "Behavior of brick masonry under combined shear and compression loading." *Proc. 2nd Canadian Masonry Symp.,* Ottawa, Canada.

Hansen, K. F. (1999). "Bending and shear test with masonry." *SBI bulletin 123*, Danish Building research Institute , Hørsholm, Denmark.

Lourenço, P. B., Rots, J. G., and Blaauwendraad, J. (1998). "Continuum model for masonry: parameter estimation and validation." *J. Eng. Mech.*, 124(6), 642–652.

Lourenço, P. B., Barros, J. O., and Oliveira, J. T. (2004). "Shear testing of stack bonded masonry." *ELSEVIER J. Const. Bldg. Mat.*18. 125–132.

Lotfi, H. R., and Shing, P. B. (1991). "An appraisal of smeared crack models for masonry shear wall analysis." *J.Computers and Struct.,* 41(3), 413-425.

Meli, R. (1973). "Behavior of masonry walls under lateral loads." *Proc, 5th World Congress on Earthquake Eng.,* Rome, Italy, 853–862.

Nuss, L. K., Noland, J. L., and Chinn, J. (1978). "The parameters influencing shear strength between clay masonry units & mortar." *Proc., North Amer. Masonry Conf.,* Boulder, Colo.

Page, A. W. (1978). "Finite element model for masonry." *J. Struct. Div. ASCE*, 104(8), 1267–1285.

Rots, J. G. (199l). "Numerical simulation of cracking in structural masonry." *HERON,*36(2), 49-63.

Saeb, S., and Amadei, B. (1990). "Modeling joint response under constant or variable normal stiffness boundary conditions." *Int. J. Rock Mech. and Mining Science.* 27(3), 213-217.

Saeb, S., and Amadei, B. (1990). "Modeling joint response under constant or variable normal stiffness boundary conditions." *Int. J. Rock Mech. and Mining Science.* 27(3), 213-217.

Van Zijl, G. P. A. G. (2004). “Modeling masonry shear-compression: role of dilatancy highlighted.” *J. Eng. Mech.,* 130(11), 1289–1296.

Van der Pluijm, R. (1993). “Shear behavior of bed joints.” *Proc. 6th North Amer. Masonry Conf.,* Philadelphia, Pennsylvania, 125–136.

Yokel, F. Y., and Fattal, S. G. (1975). "A failure hypothesis for masonry shear walls." *Rept. No. NBSIR 75-703,* Nat. Bureau of Standards, Washington, D.C.

PART-3

Chapter 5

In-Plane Shear Strength of Masonry Wall

5.1 Introduction

Recent earthquakes in Nepal and elsewhere in the world have caused an extensive damage in large number of existing unreinforced masonry (URM) buildings. The majority of those URM buildings have been constructed with little or no attention to seismic considerations. This has resulted in a large inventory of buildings that lack ability to withstand strong seismic jolts. Therefore, there is an urgent need to improve the performance of URM structures by retrofitting and strengthening them to resist potential earthquake damage.

Depending on the direction of the earthquake loads, two types of failures are commonly seen in load bearing URM walls subjected to seismic loading. These are in-plane failure, characterized by either flexural bending or shear, and out-of-plane failure (Tan and Patoary 2004; Albert et al. 2001), where flexural behavior dominates. Common damage patterns for URM construction observed following earthquakes can be reduced to the following four categories (Abrams 2004);

Damage or collapse of out-of-plane walls

Shear or flexural cracking of in-plane walls

Loss of anchorage of walls to floor or roof diaphragms

Damage or collapse of corners

Seismic performance of masonry structures largely dependents on the strength and behavior under in-plane loading. However, the behavior of masonry walls under in-plane loading can generally be divided into two categories, shear, and flexure. Whether a wall is dominated by shear or flexure is largely dependent on the aspect ratio (*L/H*) and vertical compression on the masonry (σ_n). For slender walls (*L/H* less than 1.0) with relatively light axial stress, behavior is usually dominated by flexure and the strength is limited by either rocking or toe-crushing preceded by a flexural cracking. For stocky walls (*L/H* greater than 1.5) with moderate to heavy axial stress, shear usually dominates through bed joint sliding or diagonal tension modes of failure (Magenes and Calvi 1997, Zhuge 2010, Tomaževič and Gams 2009). Among these four

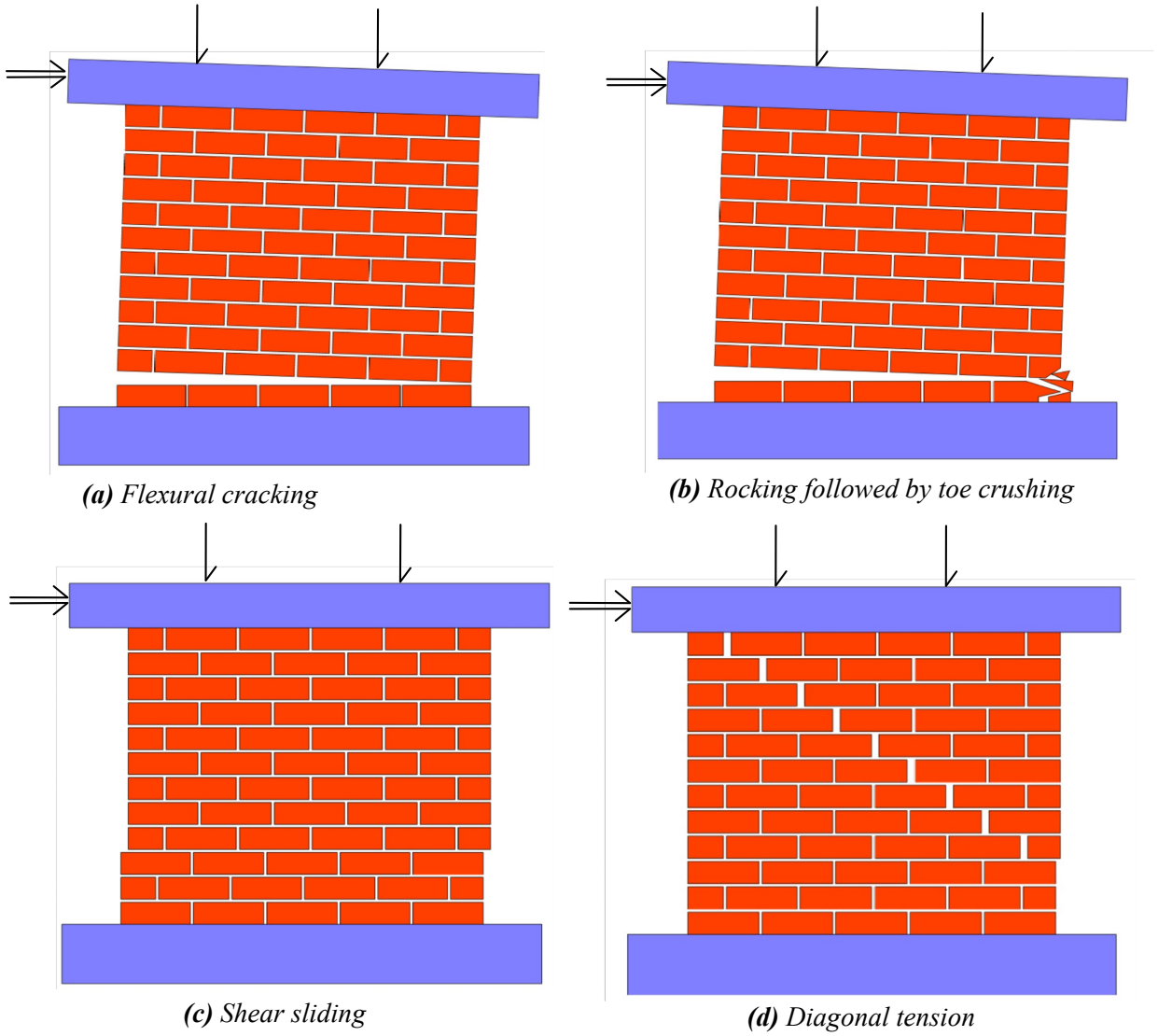

Fig. 5.1. *Different Failure modes of URM*

inelastic failure modes (Fig. 5.1), rocking and sliding shear are classified as deformation controlled phenomena because large lateral deformation of walls and piers is possible without a significant loss in strength (Foraboschi 2009). In contrast, diagonal tension and toe crushing behavior modes are known as force controlled phenomena because the ultimate failure can be abrupt with little or no subsequent deformation. Stair-stepped diagonal cracking can also be considered as a deformation controlled action because frictional forces along bed joints are conserved with vertical compressive forces. However, diagonal tension cracking must be classified as a force-controlled action unless stair-stepped cracking can be distinguished from diagonal cracking through units (FEMA 274, 1997). It should be noted that not all these failure modes will involve collapsing of the masonry shear wall, and the final failure may be a combination of several failure modes.

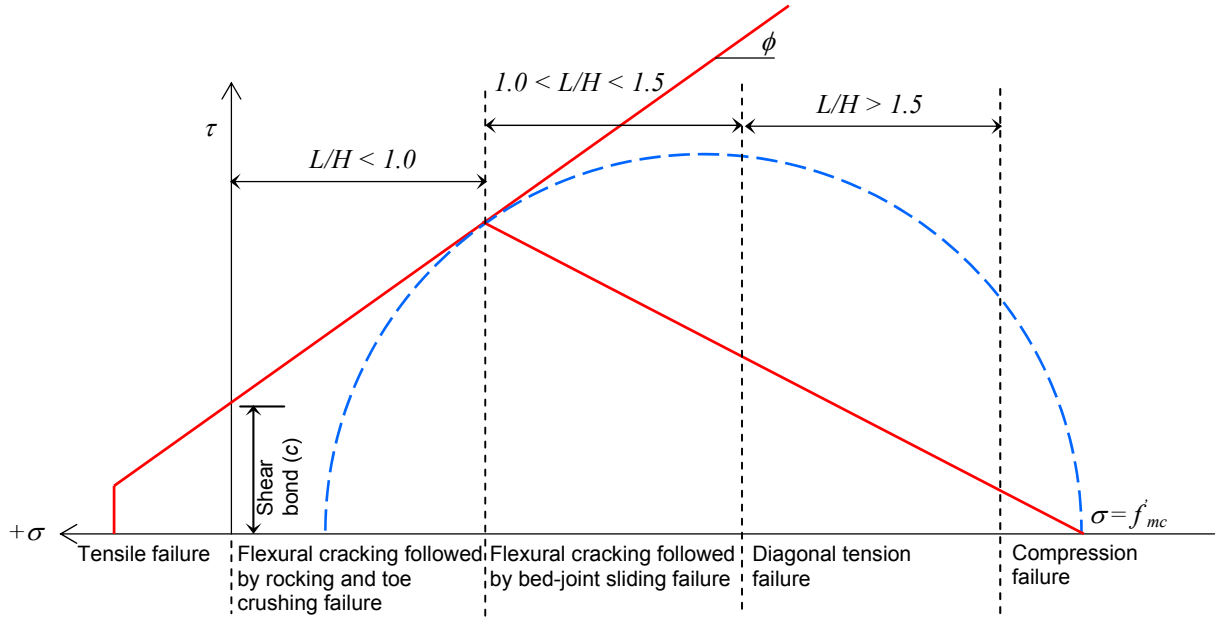

Fig. 5.2. *Generalized behavior of URM under combined shear and normal stress*

A more general way of representing the various failure modes of masonry shear wall is shown in Fig. 5.2, where the interactions between normal and shear stresses on the masonry bed joints are shown. It is evident in Fig. 5.2 that the failure modes in masonry shear walls are generally dictated by the magnitude of vertical compression force applied over the wall. However, a rationally developed failure criteria should be able to predict the tensile, compressive and shear types of failure.

FEMA 356 (2000) provides most up-to-date guideline for analysis of masonry structures considering performance-based design. Three performance levels are defined and used as discrete points to guide a rehabilitation design based on the expected performance of a building. Performance levels are based on the amount of damage to both the structural and non-structural elements. The three defined levels for primary structural elements are Immediate Occupancy (IO), Life Safety (LS) and Collapse Prevention (CP). The guideline states two procedures for determining the acceptability of URM walls as a function of these performance levels, they are Linear Static Procedure (LSP) and Nonlinear Static Procedure (NSP). For any of the procedures, a load-deformation backbone curve is required to determine the strength and expected level of performance of the component. Detail description of these procedures can be found in Chapter 3 and 7 of FEMA 356. However, design guidelines based on component performance for FRP retrofitted masonry wall are still lagging and this study aims to spot light on this backdrop to some extent.

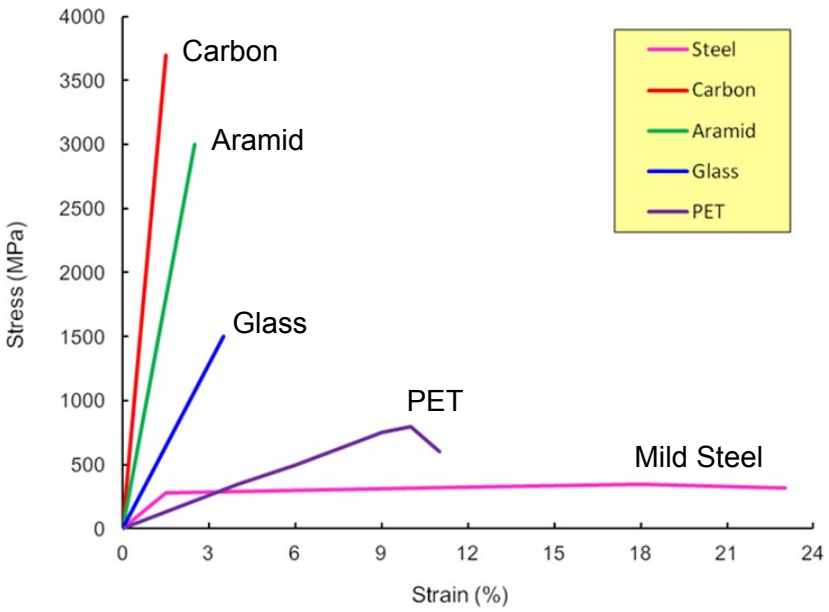

Fig. 5.3. *Tensile strength of different FRPs*

Various techniques e.g., ferrocement, shotcreting overlay, grout injection, FRP external bonding, posttensioning with external cable, etc. are available and getting popular for retrofitting of existing masonry structures. The benefit of using FRPs as potential strengthening material comes from the reduction in handling costs; despite additional material costs, and they are easy to install due to light weight (Burgoyne and Balafas 2007).

The aim of seismic retrofitting is to upgrade the ultimate strength/deformation of the structure by improving the structure's ability to undergo inelastic deformation without fully collapsing during an earthquake. Fiber reinforced polymer (FRP), which is a composite material consisting of a polymer matrix imbedded with high-strength fibers, such as Glass, Aramid, Carbon, etc (Fig. 5.3) to achieve certain properties better than either of the base materials, is getting popular for retrofitting of the existing masonry structures. The benefit of using FRPs as potential strengthening material comes from the reduction in handling costs; despite additional material costs, and they are easy to install due to light weight (Burgoyne and Balafas 2007).

There is enough potential for agro based product as an additives / reinforcement materials. Natural fibers offer many technical and ecological benefits for their use in reinforcing composites. In addition to that natural fibers are biodegradable or recyclable depending on the selected matrix (NGCC 2008). Many types of natural fibers have been investigated for use in plastics including cotton, jute, kenaf, sisal, coir, flax etc (Beckwith 2003). These materials are predominantly used as a replacement for conventional synthetic and petroleum based fibers. Though the strength of bio-fibers is not as great as conventional fibers, the specific properties are comparable and they are compatible with conventional resins.

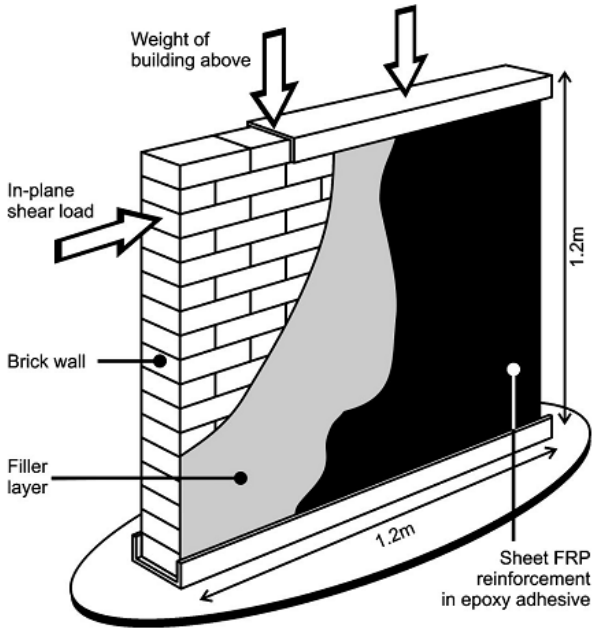

Fig. 5.4. *Experimental shear wall set-up of Stratford et al. 2004*

Externally bonded PET-FRP with a large fracturing strain (more than 10%) is a retrofitting technique that has drawn significant attention as a unique alternative to CFRP or GFRP. High fracturing strain in PET-FRP yields substantial inelastic deformation in masonry which compensates the inherent brittleness of these structures, without compromising the other advantages of FRP. In Japan, the use of PET-FRP has emerged as an alternative to traditional FRPs, such as carbon and glass FRP, where ductility is a major concern than strength (Anggawidjaja et al. 2006).

Various approaches have previously been undertaken to investigate masonry strengthened with FRPs. There is no harmonized test method available to determine the shear performance of masonry elements under lateral loading (Bosiljkov et al. 2008, Tomaževič and Gams 2009). A TNO report (TNO 2004) gives an exhaustive discussion and literature review of various methods for testing of masonry shear wall, that have been undertaken by different researchers. None of them simulate real-time behavior, but have been chosen because they reproduce static or kinematic boundary conditions, which can be easily interpreted with a perceived analytical model. Stratford et al. 2004 tested masonry wall strengthening by GFRP sheet (Fig. 5.4), which shows quite ductile behavior prior to failure and a significant increase (65%) of shear capacity, whereas the failure was primarily attributed to debonding of the GFRP sheet. Alcaino and Santa-Maria (2008) applied CFRP strips in two different configurations over 16 masonry panels of 1975 × 2000 × 140 mm in size and tested them in according to Fig. 5.5. Another technique for strengthening is the mounting of the FRP rod inside the horizontal mortar joint, embedded near the surface as shown in Fig. 5.6(a) (Petersen et al. 2010). An alternative to this system is to

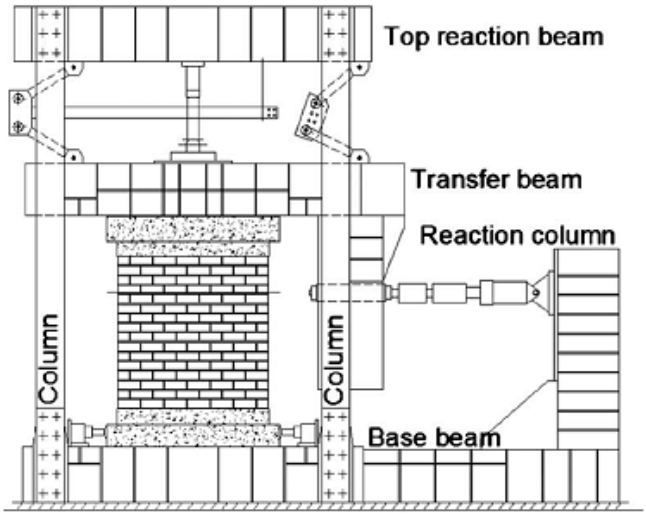

Fig. 5.5. *Experimental shear wall set-up of Alcaino and Santa-Maria 2008*

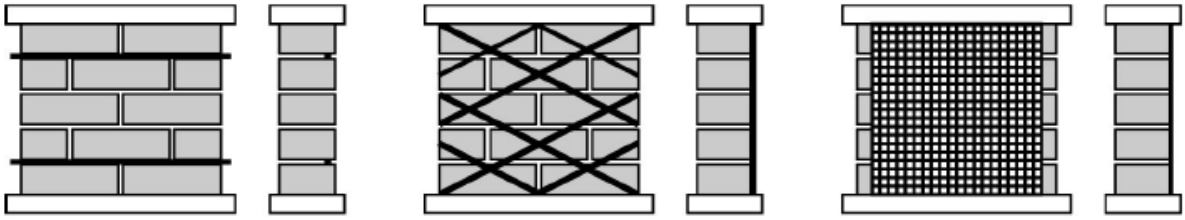

(a) Near surface mounted FRP *bars* (b) Strip FRP in diagonal fashion (c) Sheet FRP all over the wall

Fig. 5.6. *Different techniques of FRP installation on masonry wall (Stratford et al. 2004)*

attach the FRP strips over the surface of the wall in a diagonal fashion (Dizhur et al. 2013; Akin et al. 2014; Altin et al. 2007) or in a grid system (Benedetti and Steli 2006). The FRP strips here act as a truss made from unidirectional fibers [Fig. 5.6(b) and Fig. 5.6(c)].

When FRPs are bonded to the surface of the wall, diagonal tension failures or compressive crushing failures at wall toe are quite common (Hamid et al. 2005; Wang et al. 2006). Also, premature debonding of FRP, a brittle but unavoidable failure mode, was commonly observed during the test and, in general, FRP could not reach its ultimate strength (Ehsani et al. 1997; Stratford et al. 2004; ElGawady et al. 2005; Foraboschi and Vanin 2013). Experimental tests indicate that the failure patterns are affected by but not limited to the strength, orientation, amount and anchorage length of FRP (Alcaino and Santa-Maria 2008; Marcari et al. 2007). Long-term durability of FRP strengthening work is a great concern of modern-day researches. One new finding that affects both masonry and concrete members that are externally strengthened using FRP, is delayed debonding, which is a phenomenological development of critical crack throughout the life-time of the structure along the substrate-FRP interface that causes the external FRP to lose bond stress and eventually reduce the lifetime of strengthening work (Foraboschi 2015). Shrestha et al. (2014) pointed out that there is considerable influence

Fig. 5.7. *Typical diagonal tension failure in a squatting wall during Emiliana Earthquake in Italy, 2012 (EAI 2012)*

of moisture in deteriorating the bond property and reduce the durability of FRP retrofitted works. In general, the possible failure mode for masonry strengthened with FRP can be a combination of several mechanisms such as, excessive cracking due to tensile stresses in the wall, crushing of masonry in the compression zone, shear-slip of masonry, FRP debonding (instantaneous and delayed), and FRP rupture (CNR DT200 R1/2013).

In this study, CFRP have been used as conventional but expensive strengthening materials. On the other hand PET-FRP, Nylon-FRP, Jute-FRP and Cotton-FRP have been used as low cost strengthening materials. A comparison of these FRPs in term strength and deformation has been shown in this study. The strength of CFRP is higher than PET-FRP, whereas PET-FRP posses a relatively higher fracturing strain than CFRP (Fig. 5.3), which is an essential property of a strengthening material to be coherent with the brittle nature of masonry. On the contrary, natural fibers like Jute and Cotton are much weaker than these two, but are quite available at low cost and have significant elongation at failure. Similarly, Nylon-FRP has also a good ductile behavior. The purpose of this study is to show the difference in behavior of masonry shear wall strengthening with these distinct FRPs and the superiority of the one type of FRP over the others. Ultimate load bearing capacity, deformation at peak load, and mode of failure, are observed in this study for two different arrangements of the FRPs on the surface of the wall. At the end, a simplified model based on effective strain in FRP, for calculating in-plane shear strength of masonry wall is also proposed in Chapter 6.

Table 5.1 *FRP Configurations and Summary of Test Results for Masonry Specimens*

Wall ID	Peak Load (*kN*)	Def. at Peak Load (*mm*)	FRP configuration
RWS1	48	8.7	Reference wall
RWS2	30	5.4	
PSD1	114	8.9	PET cross diagonal
PSD2	101	24.7	
PSG1	129	10.0	PET in grid system
PSG2	88	9.7	
PSF	168	6.5	PET fully wrapped
CSD1	95	2.9	Carbon cross diagonal
CSD2	94	4.4	
CSG1	134	2.5	Carbon in grid system
CSG2	99	7.0	
CSF	107	2.7	Carbon fully wrapped
NSD	103	15.5	Nylon Diagonal
JTSF	104	21.4	Jute fully wrapped
CTSF	133	15.7	Cotton fully wrapped

Table 5.2 *Properties of fibers and adhesive*

Properties	FRP materials					Adhesive
	PET (*600*)	CARBON (*FTS-C1-20*)	JUTE	COTTON	NYLON	RESIN (*D-90 R*)
Tensile strength (*MPa*)	740	3400	250	175	515	45
Elastic modulus (*GPa*)	10	245	1.6	1.8	3.3	1.56
Elongation at fracture (*%*)	10±1	1.5	22.7	9.8	15.6	28
Thickness (*mm*)	0.841	0.111	1.304	1.298	2.345	-
Width (*mm*)	300	250	500	750	80	-

5.2 Experimental Program

5.2.1 Specimen Details

In this experimental study, a total of 12 masonry walls having a nominal dimensions of 1270 × 1020 × 120 mm, were fabricated. All of the walls were made with single layer running bond of bricks having a dimensions of 240×120×74 mm with an average compressive strength of 30 MPa. A 10 mm thick mortar joint with a compressive strength of 22 MPa was used throughout. Due to the anchorage at the wall top and bottom, the topmost and bottommost layers of the brick were ineffective in transferring the shear. So, the effective height (872 mm) of the wall comprised of the remaining ten courses of brick, offered an aspect ratio (*L/H*) of 1.45. Though the size of the masonry wall chosen for this experimental purpose does not necessarily reflect the nominal size of actual masonry structures, an aspect ratio of 1.45 does resemble that of the real time masonry shear wall as failure in this size of wall predominantly governed by either bed joint shear sliding or diagonal tension failure [Fig. 5.1(c) and Fig. 5.1(d)], which can be seen in many masonry failure during the past earthquakes (Fig. 5.7). Table 5.1 gives the details of the walls. In this table, RW stands for Reference Wall, P for wall strengthening with PET-FRP, C for wall strengthening with CFRP, JT for Jute-FRP, CT for Cotton-FRP, N for Nylon-FRP, D for Diagonal strip configuration, G for Grid system, F for Fully wrapped wall and S for Solid bricks.

5.2.2 Test of Fiber Sheet

Among the above mentioned five types of FRPs, CFRP and PET are being manufactured commercially for the purpose of structural strengthening and their mechanical properties are quite available in the vast literatures and model codes. However Nylon, Jute and Cotton are yet to come in construction industry, and some of their properties are not so available. In this study, uniaxial test was conducted for each of these three materials according to ASTM D 1777, ASTM D 2905 and ASTM C 1557 as shown in Fig. 5.8(a) and (b). For each case, three samples were tested and the average results of these three are posted in Table 5.2.

5.2.3 Specimen Preparation

PET-FRP and CFRP sheets both having unidirectional fibers, were applied using a wet layup procedure on wall specimens in three different configurations as shown in Fig. 5.9. At first, the wall specimens were cleaned by removing loose mortar and dirt with the help of a wire brush. Epoxy putty (filler) was used to fill the depression on the wall surface to provide a smooth plane surface ready for FRP laying. A thin layer of primer was then applied all over the wall to seal the pores in the masonry. Epoxy resin having the properties indicated in Table 5.2 was then applied

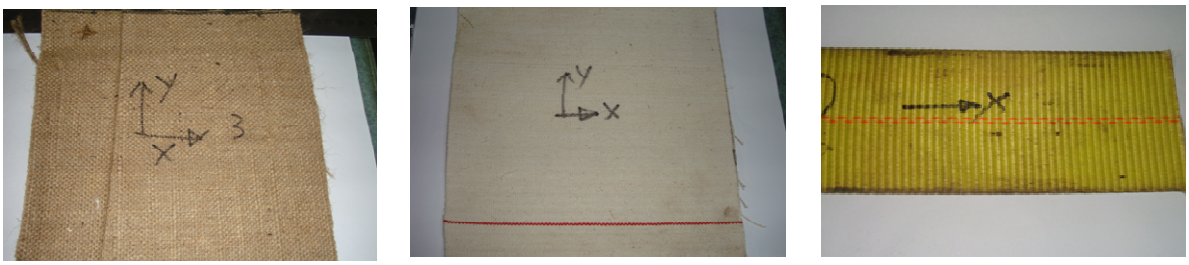

(i) *(ii)* *(iii)*

Fig. 5.8a. *Fiber sheet specimens for tension test, (i) Jute, (ii) Cotton and (iii) Nylon*

(i) *(ii)* *(iii)*

Fig. 5.8b. *Uniaxial tension test of fiber sheet, (i) Jute, (ii) Cotton and (iii) Nylon*

over the wall wherever necessary. Fiber sheets were cut to the width of 80 mm for diagonal strip and 70 mm for grid system. Resin was then applied with a roller brush all over the sheet strip so that it was fully saturated by the resin. As soon as the application of the resin was completed, the FRP strips were laid over the wall and wrapped tightly to keep them in place. For the diagonal strip, the wall corners were cut in the same dimension width (80 mm) as the strip [Fig. 5.9(b)] in order to avoid sharp edges and problem in wrapping. For fully wrapped walls [Fig. 5.9(d)], FRPs that have unidirectional fibers (CFRP and PET) were applied in horizontal and vertical wraps according to Fig. 5.10. FRPs with bidirectional fibers (Cotton and Jute) were applied in a single ply (only horizontal wrap).

5.2.4 FRP Anchorage

After the required curing period, the wall was transferred to the loading frame as shown in Fig. 5.11 and Fig. 5.12, specially designed for this experimental study. The wall top and bottom were anchored to the top and bottom channel beams, with the help of twenty four 22 mm bolts as

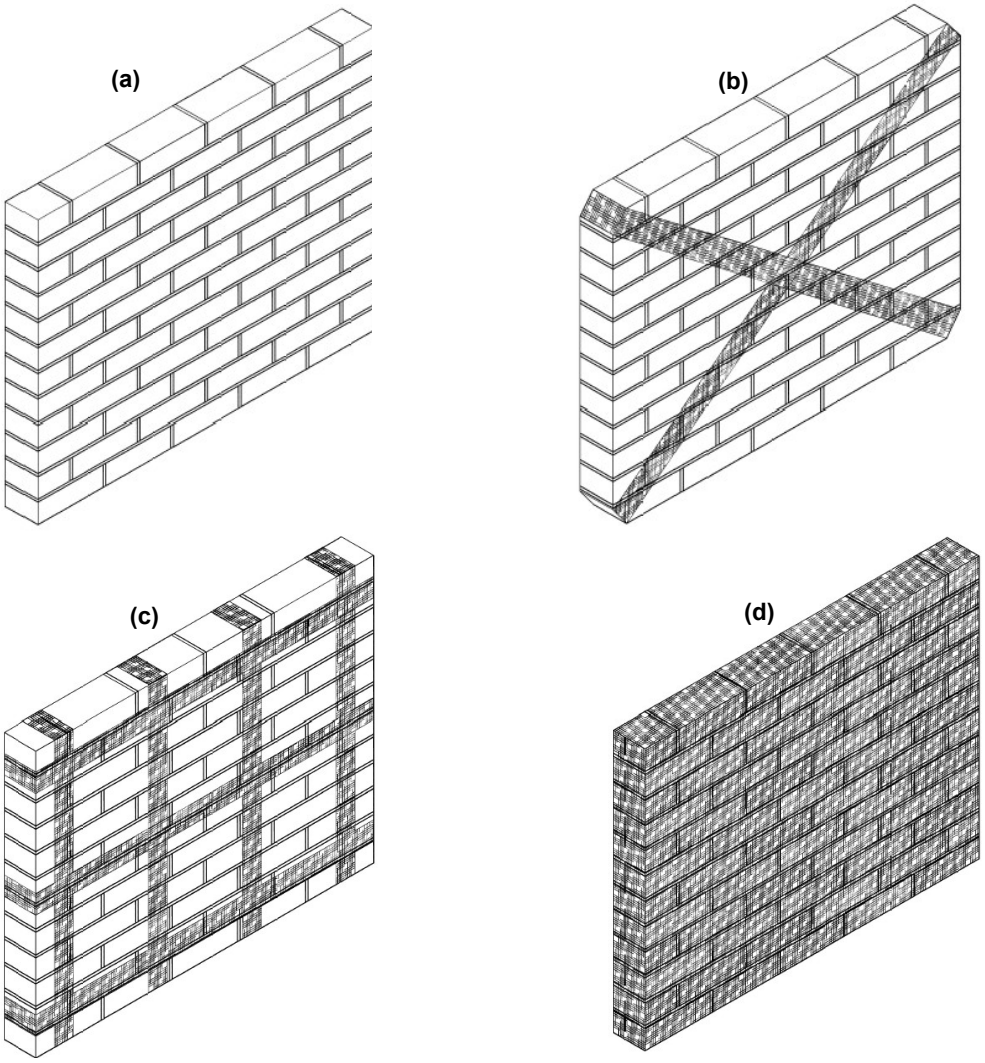

Fig. 5.9. *FRP reinforcement layout: (a) Control wall (RWS) (b) FRP cross diagonal bracings (CSD, PSD); (c) FRP strips in grid system (CSG, PSG); (d) Fully wrapped by FRP (CSF, PSF)*

shown in Fig. 5.11. Between the wall and the channel beam, a 16mm thick steel plate was inserted so that pressure could be applied on the wall by tightening the bolts. Gypsum plaster was used to fill the gap between the wall and the steel plate. For FRP strengthened walls, the FRP itself was wrapped in a U-shape anchorage, so there was almost no chance of slippage of the FRP during the experiment. Although this kind of anchorage system is not very much practical for the real structure, it has been chosen so for this experimentation to avoid premature anchorage failure of FRP prior to attaining full shear strength. For fully wrapped masonry walls, horizontal FRP sheets were installed on the wall in 360° wrapping (Fig. 5.10) and vertical sheets were anchored to the top and bottom channel beams with 22 mm bolts as shown in Fig. 5.13.

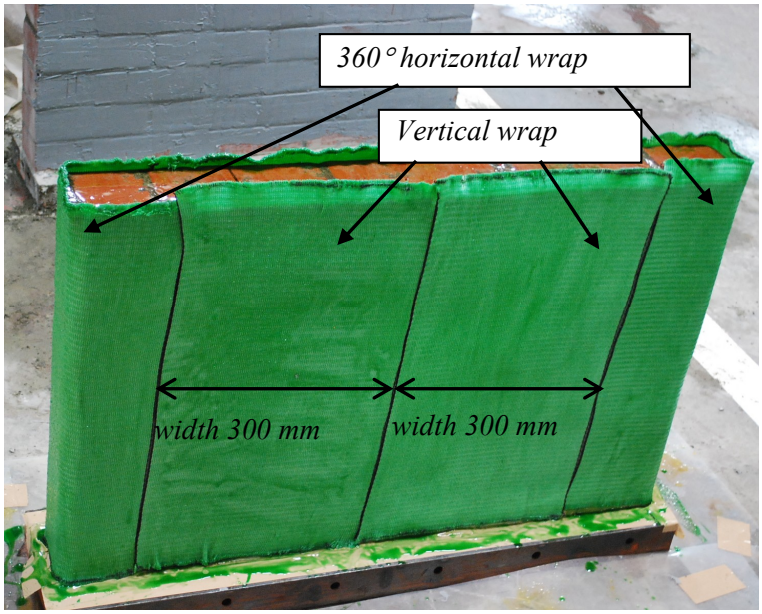

Fig. 5.10. *FRP installation in fully wrapped wall*

5.2.5 Application of Load

A pre-compression of 40 kN which is equivalent to a uniform pressure of 0.25 MPa, was applied on the top of the wall through two hydraulic jacks, prior to incrementally increasing lateral loading (Fig. 5.10 & Fig. 5.11). Lateral load was applied gradually, increasing at a constant rate of 5 kN/min until it reached at peak. In post-peak regime, a constant displacement of 2mm/min was applied until complete failure. The two vertical loads restricted the rotation of the top beam only to some extent, as the beam was not restrained against rotation during the evolution of lateral load. A fixed-free experimental condition was maintained throughout the loading process.

5.2.6 Instrumentation and Data Acquisition

Sufficient number of uniaxial, biaxial and rosette strain gages, LVDTs, and load cells (50 tons capacity) were used to record all the necessary information during the testing (Fig. 5.14). A lateral load was applied in a pull-out manner by a 50-ton capacity center-hole jack, with a remote pump, until the complete failure of the masonry wall. All of the data (displacement, strain, and load) were recorded through a digital data logger.

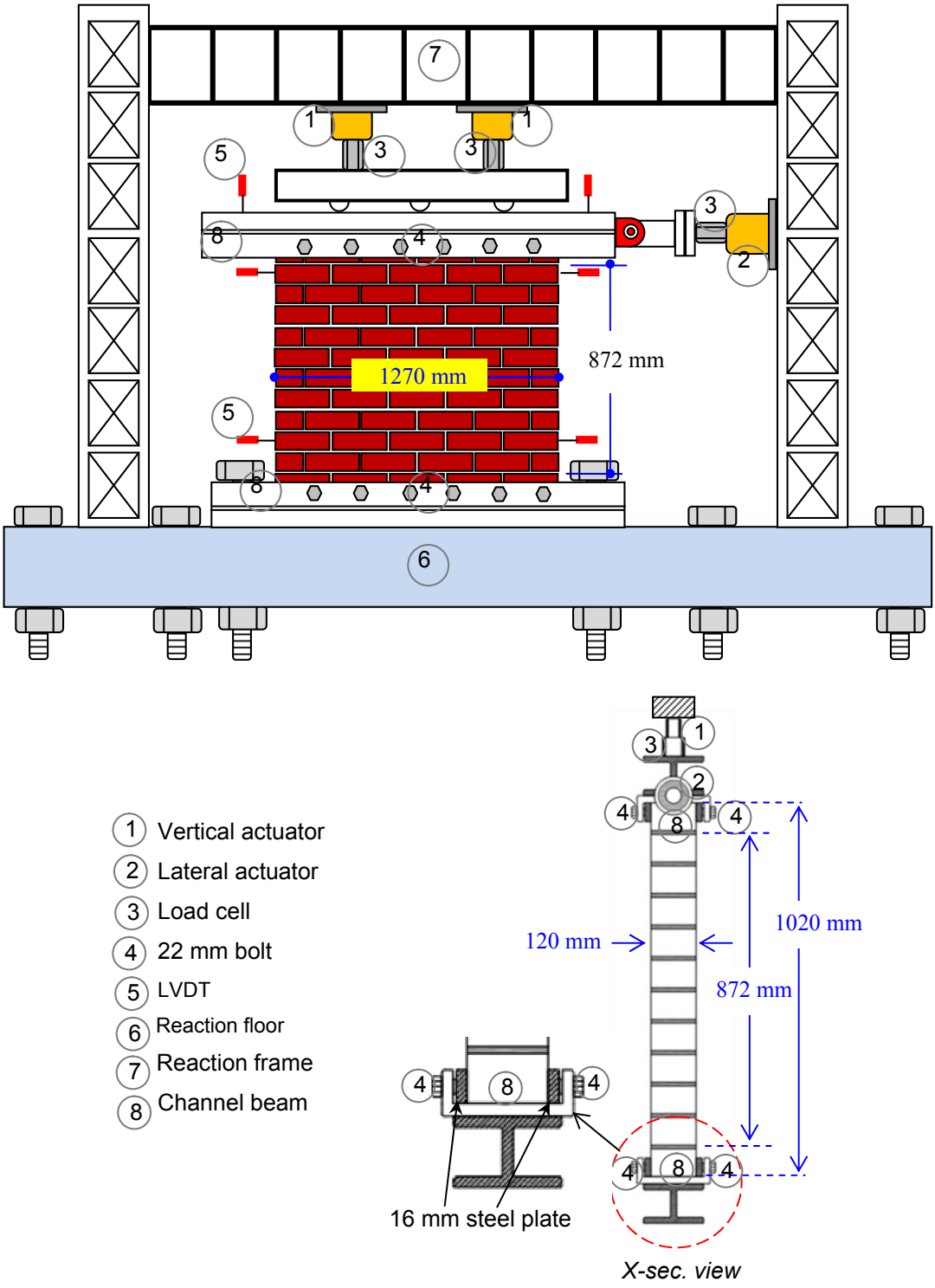

Fig. 5.11. *Schematic diagram of experimental setup of shear wall*

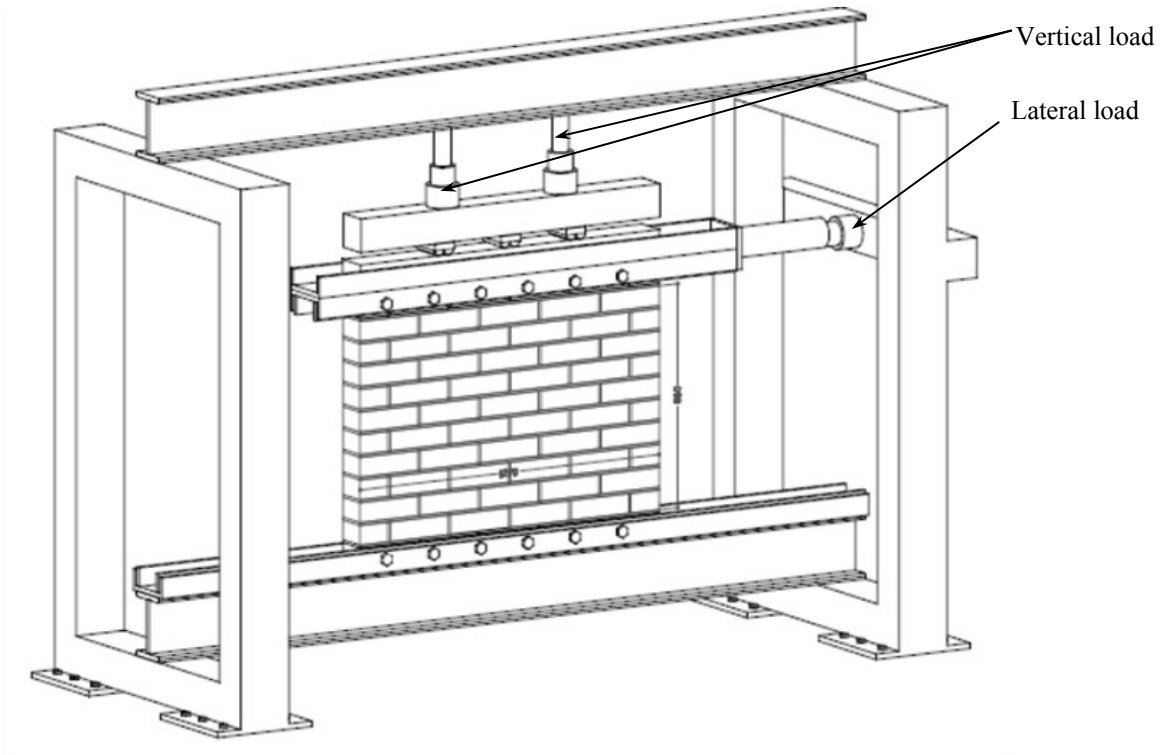

Fig. 5.12. *3D view of experimental setup of shear wall*

Fig. 5.13. *Experimental setup of FRP reinforced masonry*

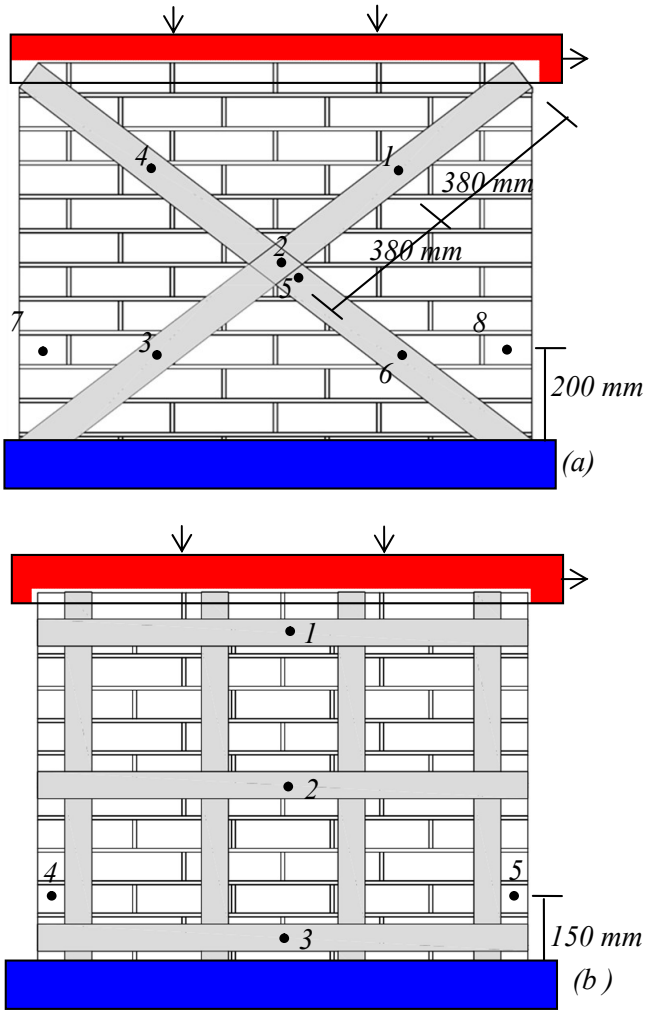

Fig. 5.14. *Strain gauges layout (a) cross diagonal layout (b) grid layout*

5.3 Experimental Observation

5.3.1 Failure of URM Walls (RWS1, RWS2)

These two reference specimens were tested under similar boundary conditions to make a comparison with rest of the walls mentioned in Table 5.1. No potential crack was observed in either of the walls until the load reached about 80% of the peak load. Only after that a flexural crack appeared at the heel of the wall, and propagated towards the toe as shown in Fig. 5.15(a) and Fig. 5.15(b), and the load dropped slightly. Lateral load was further increased to ultimate load, and the crack opening widened as the crack propagated all the way to the toe of each wall. After the applied load reached its peak, it did not decrease much with the increased displacement, which furthered the shear-slip along the crack plane for wall RWS1 [Fig. 5.15(a)]. In specimen RWS2 no shear-slip was observed rather the crack propagated in a stepped fashion and travelled all the way to the toe and a faster crushing at the wall toe was observed which caused a rapid

decrease in load. This kind of failure in URM wall under shear is reported in a number of papers (Stratford et al. 2004; Salmanpour et al. 2013; Bosiljkov et al. 2003; ElGawady et al. 2007 etc).

5.3.2 Failure of FRP Reinforced Walls

1) Diagonally Braced Walls (CSD, PSD)

These four walls were externally strengthened by two diagonal CFRP and PET-FRP strips each, of 80 mm in width in a fashion shown in Fig. 5.9(b). No noticeable crack appeared on either of the wall until the lateral load reached about 75% of the ultimate strength. In the case of the wall CSD1 two flexural cracks appeared at the wall top on the loading end and at the wall bottom on the far end [Fig. 5.15(c)] followed by some debonding of the CFRP tension diagonals. No rupture or damage of the CFRP was observed. For wall CSD2, some fine line cracks appeared at the top of the wall on far end and started to propagate downward in a stepped fashion. Almost simultaneously another crack, parallel and above to this one appeared and began to propagate downward in a same manner but with a lesser degree of crack opening displacement. Once the load increased to a maximum of 94 kN, a sudden rupture of the diagonal tension strip on the both sides of the wall took place and the load suddenly dropped to the half of the peak load. Accumulated compressive stress caused some crushing at wall toe just before the rupture of the CFRP strip which can be seen Fig. 5.15(d).

In the case of the walls reinforced with PET-FRP strips (PSD1 and PSD2), at a load of nearly 50% of the peak load, similar diagonal cracks were observed being appearing on these two walls along the bottom of the compression diagonal and traversed along the compression diagonal in a stepped fashion [Fig. 5.15(e) and Fig. 515(f)]. In PSD2, another crack appeared on the top of the compression diagonal and propagated all the way to the toe of the wall followed by some toe crushing. The peak loads of 114 kN and 101 kN respectively were not attenuated much with the applied displacement for quite a long time, and at that stage the experiment was ceased. Some debonding in tension diagonal PET strips was observed in both of these two walls.

2) Wall Strengthened by FRP Grid System (CSG, PSG)

These four walls were strengthened with CFRP and PET-FRP strips of having 70 mm width each in a grid system as shown in Fig. 5.9(c). In the case of the CFRP reinforced wall (CSG1), at a load, amounting to 70% of peak load, some fine-line diagonal cracks appeared at the central area of the wall. More cracks appeared across the tension diagonal with simultaneous debonding of the CFRP strips, while the load reached at a level of 130 kN [Fig. 5.16(a)]. Almost simultaneously, one of the horizontal CFRP strips ruptured with a loud explosive sound, and the load dropped to 109 kN. With further displacement, the crack width increased and, in some

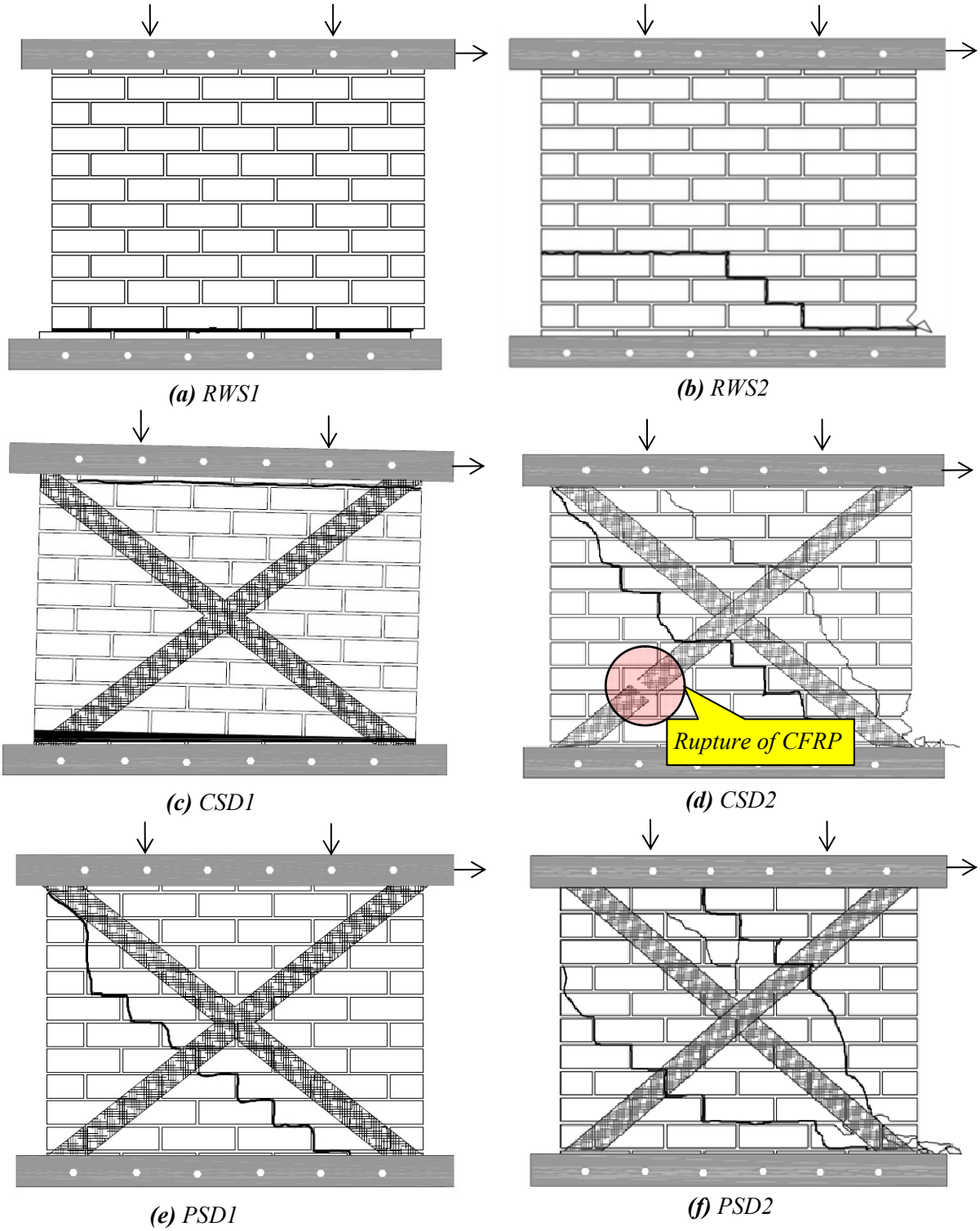

Fig. 5.15. *Schematic illustration of crack patterns in URM and diagonally strengthened masonry walls*

places, the CFRP totally separated from the wall. In CSG2, at a load equal to about 75% of the peak load, flexural crack along the bottom of the wall appeared and followed by another flexural crack at the mid-height of the wall and a web crack at the center [Fig. 5.16(b)]. With further displacement the peak load did not change from 99 kN, which only widened the crack opening. No rupture of CFRP was noticed, except some debonding in horizontal strips at few places.

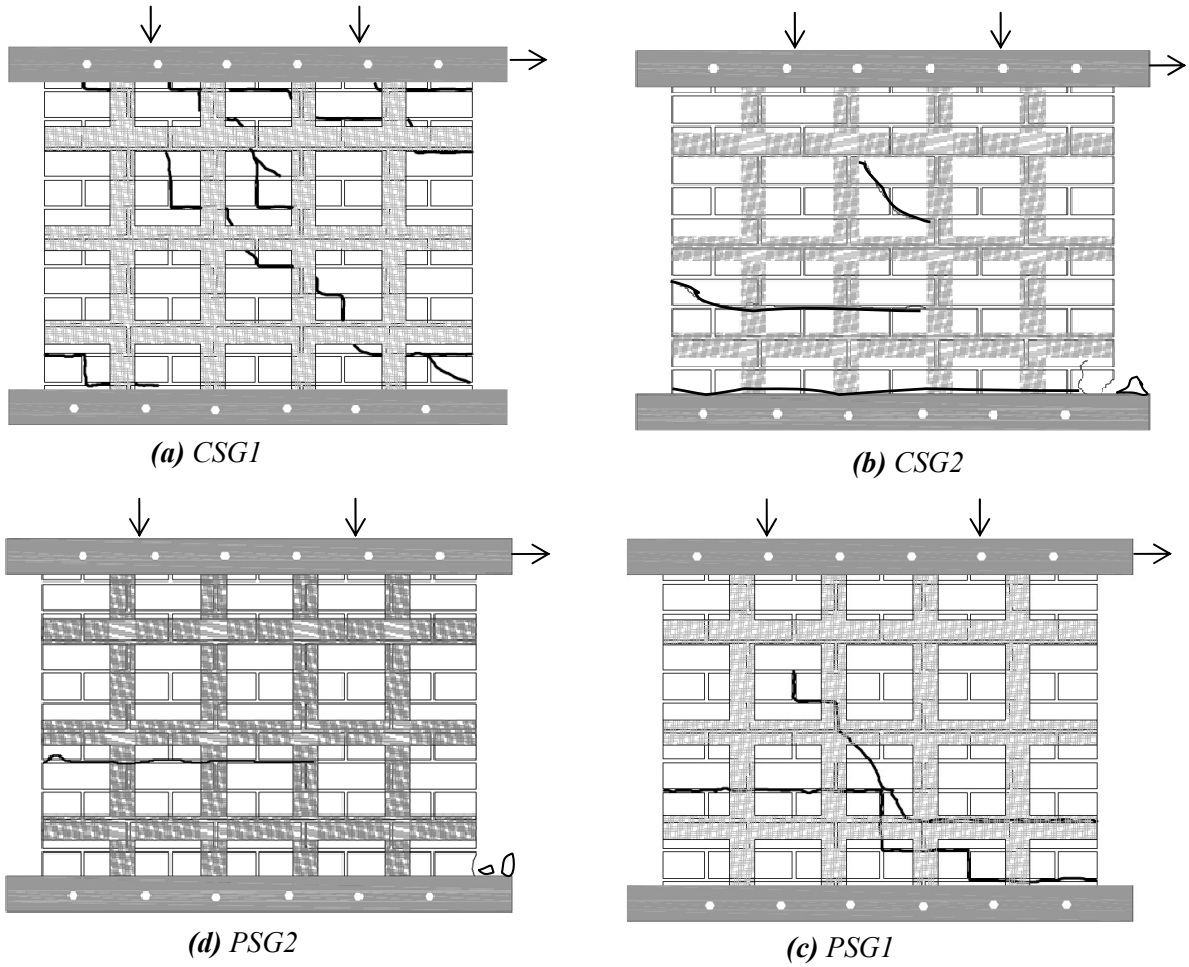

Fig. 5.16. *Schematic representation of crack patterns in wall strengthening with FRP grid system*

For PSG1, at a load of about 120 kN which is tantamount to 93% of the peak load, some debonding of the PET-FRP strip occurred along the tension diagonal. Almost simultaneously, a flexural cracking followed by some discontinuous diagonal cracking appeared at the lower half of the wall on the heel side, and travelled all the way to the wall toe in a stepped fashion as shown in Fig. 5.16(c). Similar but a single flexural crack was observed in the wall PSG2 at a load of 63 kN, as shown in Fig. 5.16(d). Minor crushing at wall toe was noticed as soon as the peak load reached at 88 kN.

3) Walls Fully Wrapped with FRPs (CSF, PSF)

These two walls were strengthened after fully wrapped with CFRP and PET-FRP sheets according to Fig. 5.10. For CSF, the stiffness as well as the lateral load capacity was so high that at a later stage the grip at the wall bottom prematurely failed before the wall attained its full strength [Fig. 5.17(a)]. Since the wall was fully wrapped by the CFRP sheets, damage, if any, could hardly be detected by visual observation. On the other hand, the wall PSF showed constant stiffness until it reached about 60% of its peak shear capacity. Only after that, did the stiffness show a reduction, but no damage or crack whatsoever was seen on the wall [Fig. 5.17(b)]. Once

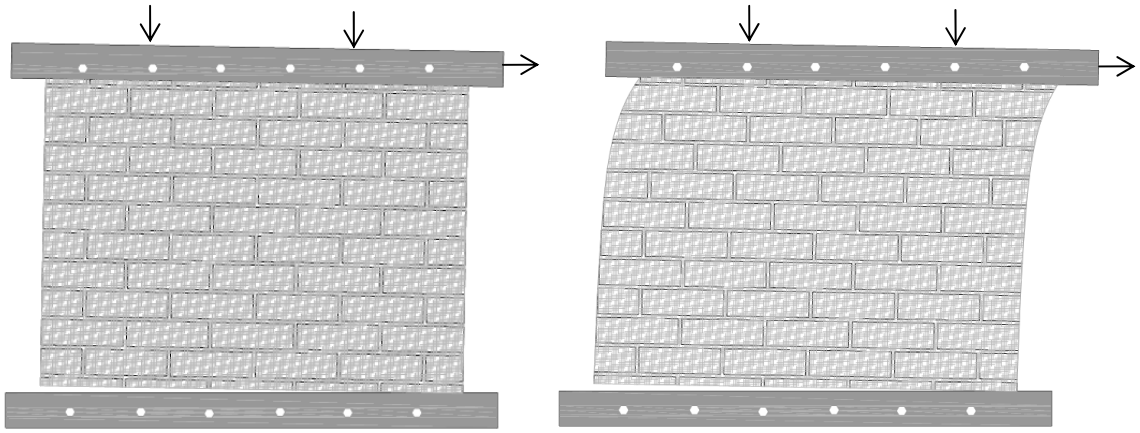

Fig. 5.17. *Schematic representation of crack patterns in fully wrapped walls*

it reached its full strength, further displacement only resulted in load reduction and the wall failed at its grip at the bottom similar to the wall CSF. It was quite clear from fully wrapped wall that higher the percent of FRP higher is the stiffness as well as some enhancement in shear strength of masonry wall. However, higher amount of FRP materials do compromise with the ductility of the wall and are not fitting well with the purpose of seismic strengthening.

4) Low Cost Strengthening System (NSD, JTSF, CTSF)

Three walls were tested after strengthening with low cost FRP materials, they were, Nylon-FRP, Cotton-FRP and Jute-FRP. For the case of Nylon-FRP diagonal strips (NSD), at a load of 62 kN a fine line crack developed at wall heel and propagated all the way to the wall toe with further loading. When the load reached to 100 kN, sound of debonding of the diagonal tension strips on both sides of the wall was heard and the load dropped by a little. Almost simultaneously a crack

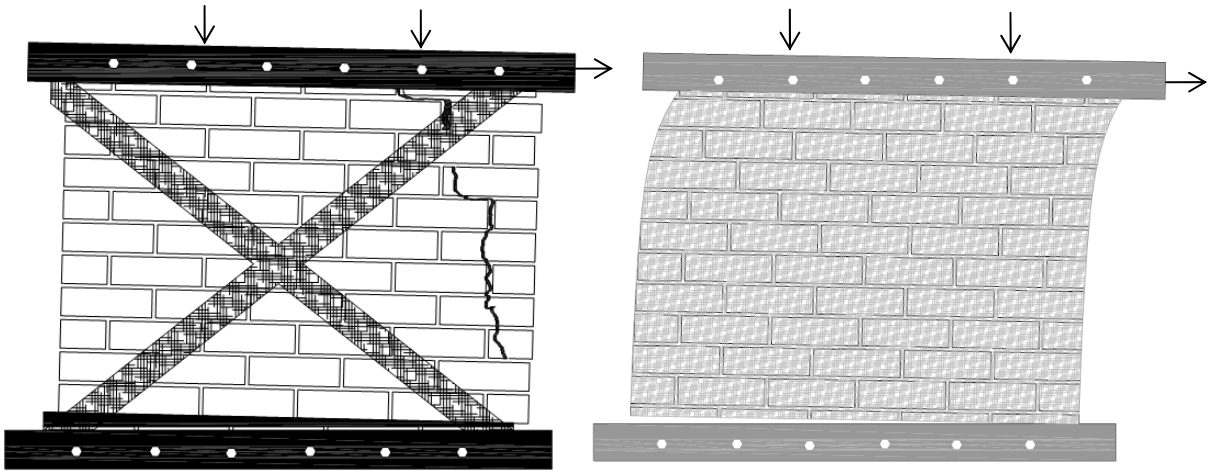

Fig. 5.18. *(a) Crack pattern in NSD wall; (b) Inelastic deformation and rotation at the wall bottom for fully wrapped wall with Jute-FRP*

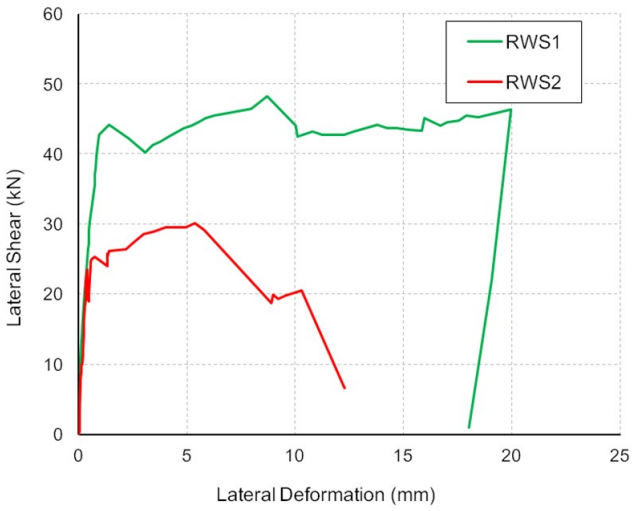

***Fig. 5.19**. Load-deformation responses of unreinforced Reference walls*

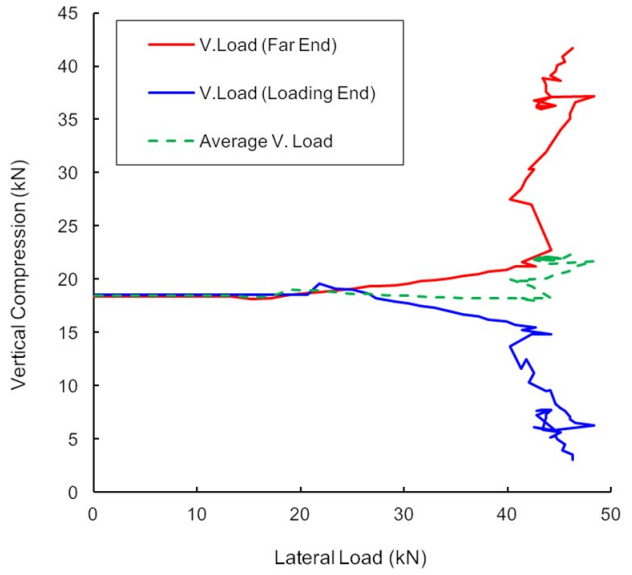

***Fig. 5.20.** Variation of vertical load with progressive shear*

developed at the wall top on the load end and travelled downward in a stepped fashion as shown in Fig. 5.18(a). With further displacement, load did not increase much but the crack opening only widened and at that point the specimen was unloaded.

In contrast to PET-FRP and CFRP, Jute and Cotton sheets, both having bi-directional fibers, were applied on the wall in a single ply. For wall strengthened by Jute-FRP, no significant crack or damage over the Jute-FRP was noticed throughout the loading history but a ductile deformation can be observed [Fig. 5.18(b)]. The initial stiffness was similar to URM and a softening tendency can be seen after the load reached to 50 kN. The load was increasing steadily to 100 kN and a crack was observed in the wall heel side and the crack opening only widened with the applied displacement. Subsequently the wall bottom on the heel side started to come out

of the anchorage gird, and the experiment was ceased at that stage. On the other hand wall (CTSF) reinforced with Cotton-FRP, also showed quite ductile load-deformation behavior. This wall also failed at a peak load of 133 kN in anchorage grip similar to JTSF. Since these walls were fully wrapped by the FRP sheets, damage, if any, could hardly be detected by visual observation.

5.3.3 Load-Deformation Response

1) Unreinforced Masonry Walls

The load-deformation characteristics of reference walls (RWS1 and RWS2) are depicted in Fig. 5.19**.** It is quite evident from the figure that, before appearance of any potential flexural crack, the load-deformation relationship is almost linear for both the two walls. It is interesting to note that RWS1 shows quite ductile behavior while maintaining a constant lateral strength due to shear slip at the wall bottom. On the other hand RWS2 shows a rapid reduction in lateral shear after a crushing took place at the wall toe.

Fig. 5.20 shows the variation of vertical pre-compression with the progress of lateral load. It is evident from Fig. 5.20 that the vertical load on the far-end increased with the progressive shear, while the vertical load went down on loaded-end. This is due to the fact that, with the increase of lateral load, the top beam on the wall underwent a small rotation, which exerted a vertical upward pressure on the far-end jack on the wall. However, the average vertical load (broken line in Fig. 5.20) did not change much from the initial stipulated value of 20 kN.

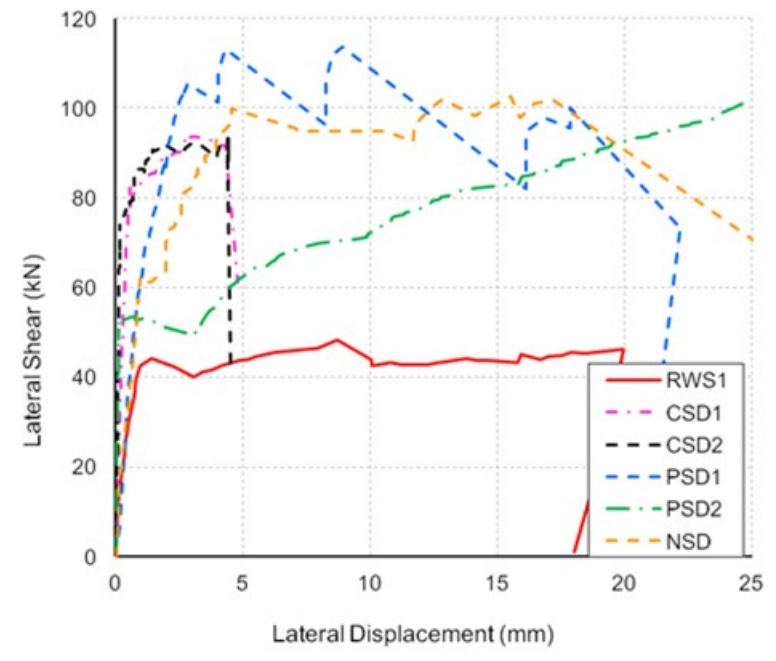

Fig. 5.21. *Load-deformation responses of with diagonal FRP*

2) Strengthened Masonry Walls

The load-deformation characteristics of diagonally braced walls (CSD, PSD and NSD) are plotted in Fig. 5.21. It is quite evident from the figure that, the lateral load capacity increased more than twice for all the four retrofitted walls. The lateral load increased quite linearly until a potential crack appeared in those walls. A reduction in stiffness can be seen there after which depicts the inelastic response of the strengthened masonry walls. One important characteristic here is that the wall diagonally braced with CFRP strips, shows a brittle type of failure where load reduction was quite abrupt with no softening at all. This was due to the crushing at wall toe immediately followed by a rupture of the tensile CFRP strips on the both side of the wall [Fig. 5.15(d)]. It is evident in Fig. 5.21 that walls strengthened by either PET-FRP or Nylon-FRP, show quite ductile nature of inelastic behavior, followed by a gradual softening regime, retaining some residual strength. The development of diagonal strain at the center of these two walls can be seen in Fig. 5.22. It is interesting to note that until the initiation of a potential diagonal cracking [Fig. 5.15(a), Fig. 15(e) and Fig. 5.15(f)] the development of strain in the diagonals strips are quite low. After the onset of cracks, the internal stresses transfer from masonry to FRP, and the internal strain in FRP rises quite significantly but remains less than its fracturing strain.

Fig. 5.23 portrays the load-deformation response of the walls that were strengthened with CFRP and PET-FRP in grid system. Initial stiffness was fairly linear at the beginning and maintained a constant stiffness up to the two-third of the peak load. Only after that a reduction in stiffness can be seen and a ductile nature of inelastic response continued for quite a long time. It is also interesting to note that the ductility is not compromised substantially when the walls are

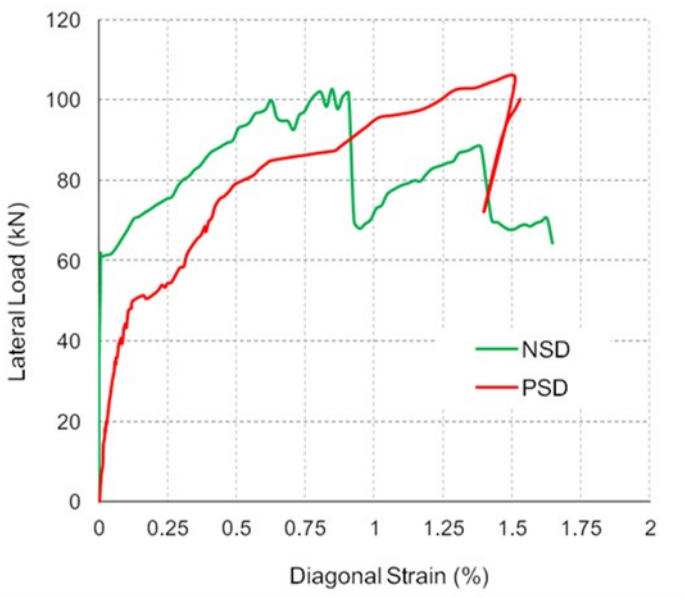

Fig. 5.22. *Load-FRP strain response of diagonally reinforced walls (NSD and PSD)*

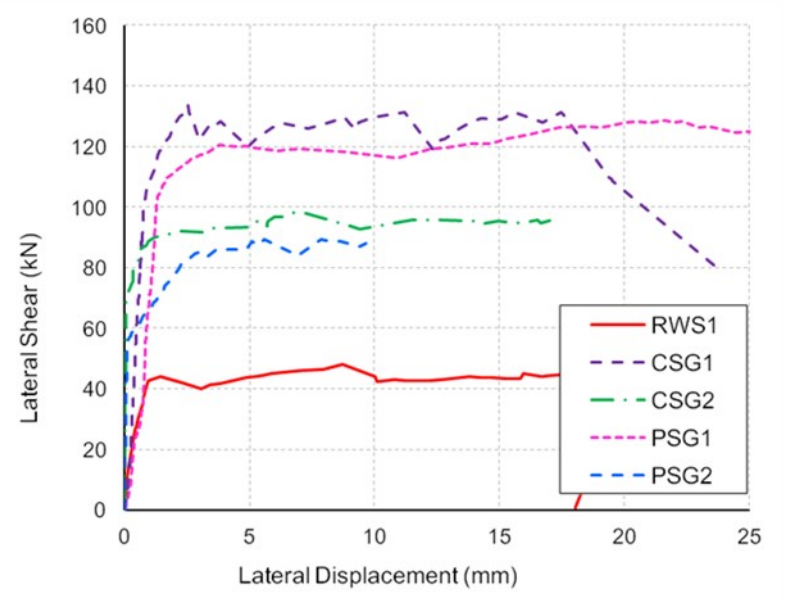

Fig. 5.23. *Load-deformation responses of walls CSG and PSG with FRP grid system*

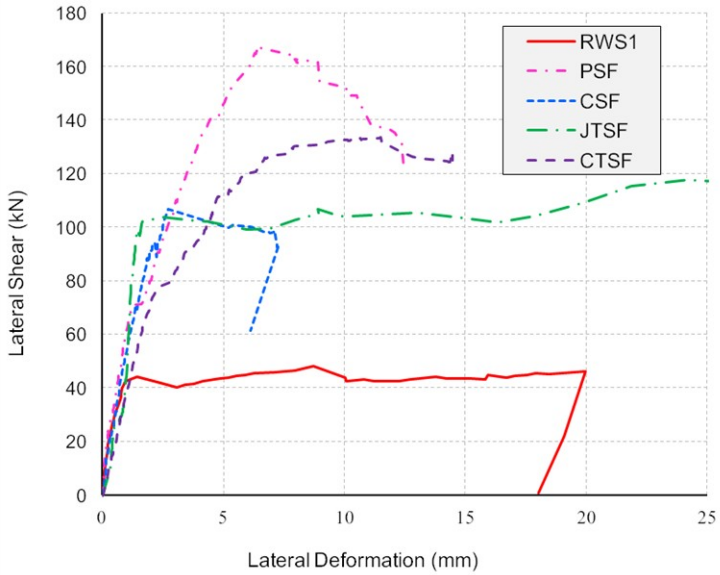

Fig. 5.24. *Load-deformation envelops for walls with fully wrapped FRP*

strengthened with higher amount of CFRP such as in grid system than the amount of CFRP in diagonal configuration. This phenomenon also holds true for PET-FRP walls (PSG1 and PSG2) as well.

On the other hand, Fig. 5.24 demonstrates the load-deformation response of the walls fully wrapped by FRPs. The shear capacity of those walls increased by more than three time of that of unreinforced walls. The deformation does not portray the real picture as it was stated earlier that these two walls underwent some rotation at their bottom and a premature failure at the grip followed. Even then, a lesser amount of deformability of these walls can be foreseen from their load-deformation characteristics. However, it can be predicted that wall strengthened with PET

sheet behave in a ductile manner than its counterpart CFRP wall and wall strengthened with PET-FRP can resist more lateral load than CFRP wall. Wall retrofitted by bio-FRP such as Jute-FRP and Cotton-FRP behave in a ductile manner than their counterpart CFRP wall. PET-FRP wall can resist more lateral load than any of them, where as the lateral shear resistance by Cotton-FRP wall is more than Jute-FRP wall.

5.4. Analysis and Discussion of Test Results

From the foregoing observation of the experimental results it was evident that the load carrying capacity of the masonry walls subjected to in-plane shear can be greatly increased by applying either of the synthetic (CFRP, PET-FRP, Nylon-FRP) or FRP from natural fibers (Jute-FRP and Cotton-FRP) sheet on their external surfaces. However, the ductility of those walls are substantially compromised, once they are bonded with CFRP sheet. It was also observed that the failure modes of the strengthened masonry walls are largely affected by the strength, orientation, and anchorage system of FRP. In the following section more in depth analysis of failure mechanism and in-plane shear resistance are discussed in light of the aforementioned experimental observation and existing knowledge on masonry.

5.4.1. Analysis of Unreinforced Masonry

The difference in failure modes for the reference specimens RWS1 and RWS2 can be attributed to the location where the first flexural cracks appeared in these two specimens and their line of propagation [Figs. 5.15(a) and (b)]. In RWS1, first flexural crack appeared at the very bottom course of the wall and propagated horizontally in a straight fashion towards the wall toe [Fig. 5.15(a)], which facilitated the wall to slip along the crack path. Once a crack forms at the wall heel, no tension force perpendicular to the crack can be transmitted across it, and the load drops by a little but as long as the crack is narrow, the wall can still transmit some shear forces in its own plane through friction of the surface roughness that can be characterized as elasto-plastic behavior. With further deformation and slip, the interlocking planes suffer substantial damage and are flattened to some extent after which the wall reaches in a state of kinematic equilibrium where only some residual frictional shear resistance prevails (Rahman and Ueda 2014), which does not diminish with the applied displacement as can be seen in Fig 5.19. In reference wall RWS2 first flexural crack appeared three courses above the bottom course on the wall heel side and propagated towards the wall toe in a stepped fashion [Fig. 5.15(b)]. This failure pattern prompted a rocking phenomenon in the wall instead of shear sliding and consequently a softening behavior was observed in the post-peak regime (Fig. 5.19) caused by a toe crushing in the wall. It is worth noting here that the location where the first flexural crack will appear is

somehow difficult to predict as was the case for these two reference walls. This is largely because of the non-homogeneous nature of masonry fabrication that creates several plane of weakness along the horizontal bed joints.

So, it can be said that an earlier flexural crack normally followed by either a toe crushing or a sliding shear type of failure. Stratford et al. (2004) observed similar failure mode in masonry walls. Moreover, it is quite evident in Fig. 5.16 that the shear strength for masonry sliding is higher than that of rocking and toe crushing because shear sliding endures a resistance along the entire crack plane where as toe crushing occurs due to accumulation of compression stress on a very small area at the crack tip on the wall toe. It is also observed that the existing equations [Eqs. (5.1) and (5.2)] proposed by FEMA 356 (2000) to calculate masonry in-plane shear strengths for different modes of failure can fairly approximate the experimental results (48 and 30 kN) and the predicted results were 47 and 27 kN for RWS1 and RWS2 respectively.

Shear strength for bed-joint sliding:

$$V_M = A_g \tau_{sld} = A_g \left(c + \sigma_n \tan \phi \right) \tag{5.1}$$

Shear strength for toe crushing:

$$V_M = \alpha_1 \sigma_n A_g \left(\frac{L}{H} \right) \left(1 - \frac{\sigma_n}{0.7 f'_{mc}} \right) \tag{5.2}$$

Some of the parameters used in these equations depend on test results. In absence of candid test results for masonry compressive strength and cohesion Eq. (5.3) (Eurocode 6, 2005) and Eq. (5.4) (Ali et al. 2012) can safely be used for a conservative value of these two parameters.

Where,

$$f'_{mc} = 0.55 \left(f_b \right)^{0.7} \left(f_m \right)^{0.3} \tag{5.3}$$

$$c = 0.0337 \left(f_m \right)^{0.6} \tag{5.4}$$

Here, V_M = shear strength of URM wall; L, H, b = length, height and thickness of the masonry wall; f'_{mc} = compressive strength of masonry prism; A_g = sectional area of wall = $(L \times b)$; α_1 = factor for boundary condition (0.5 for cantilever wall and 1.0 for fixed-fixed wall); τ_{sld} = average bed-joint sliding shear stress of URM wall; c = cohesion between mortar and brick; σ_n = vertical compression on masonry wall; ϕ = frictional angle at sliding surface (Approx. 20°, Hansen 1999) ; f_b, f_m = uniaxial compressive strength of brick and mortar respectively.

Considering the ongoing discussion, the following conclusions can be made:

1) Masonry with an aspect ratio (L/H) nearly 1.5 and with a low vertical pressure (0.25 MPa) can have either shear sliding or toe crushing type of failure.

2) Shear sliding offer more resistance than toe crushing and the existing FEMA 356 provisions can fairly predict the test results.

3) More tests are necessary to observe diagonal tension failure in masonry with the same aspect ratio but with higher vertical stresses.

Table 5.3. *Summary of Test Results for Masonry Walls*

FRP Types	Wall ID	Peak Load (kN)	Def. at peak load (mm)	FRP area A_f,(mm^2)	FRP axial stiffness E_fA_f, (MN)
--	RWS1	48	8.7	--	--
	RWS2	30	5.4		
PET-FRP	PSD1	114	8.9	81	810
	PSD2	101	24.7		
	PSG1	129	10.0	353	3530
	PSG2	88	9.7		
	PSF	168	6.5	1467	14670
CFRP	CSD1	95	2.9	11	2610
	CSD2	94	4.4		
	CSG1	134	2.5	47	11420
	CSG2	99	7.0		
	CSF	107	2.7	194	47430
Nylon-FRP	NSD	103	15.5	225	744
Jute-FRP	JTSF	104	21.4	2274	3640
Cotton-FRP	CTSF	133	15.7	2264	4075

Note: A_f = sectional area of FRP, E_f = Elastic modulus of FRP

5.4.2 Analysis of Strengthened Masonry

Experimental results summarized in Table 5.3 illustrates that the in-plane shear capacity of the tested walls was significantly enhanced by the proposed strengthening technique but the ductility behavior was not essentially the same. Fig.5.15 to Fig.5.18 depicts the crack patterns and failure modes for all the retrofitted walls. It is interesting to see that the mode of failure in masonry when they are strengthened with diagonal FRP, is diagonal tension and they are quite similar to each other (except for the case of CSD1, where there might be high possibility that the anchorage at the bottom of the diagonal tension strip was somehow loosen that prompted a flexural tension

cracking). Bonding FRP material onto the surface of the walls in diagonal fashion made it stronger against flexural cracking due to the tied-action of the FRP tension diagonals and triggered a diagonal cracking along the compression diagonal. Accumulated compression stresses at the toe region of the wall eventually caused a toe crushing and to some extent and ruptured the CFRP tension diagonal as for the case of wall CSD2. Though there is not much difference in shear strength among these five walls, significant difference can be noticed in deformation capacity. Table 5.3 shows that the FRP stiffness in CFRP diagonal is three times more than that of PET-FRP and Nylon-FRP diagonal, but the mean deformation at peak load is only one-fifth of PET-FRP or Nylon-FRP strengthened wall. This is due to the fact that PET and Nylon possesses a higher fracturing strain (more than six and ten times respectively) than CFRP (see Table 5.2). It is worth noting here that high stiffness not necessarily offers high shear strength, rather the reverse is very likely. Another interesting thing here is that the stain in FRP remains quite low before the inception of any potential cracking in masonry. Once there is a crack, the internal stress is redistributed and shifts its position from masonry to FRP, thus increase the strain in FRP, especially in tension diagonal strips as illustrated in Fig. 5.25. During that time, debonding phenomenon was also observed in FRP that resulted a fluctuation in distribution of internal strain in FRP. It is also important to mention here that even at the time of masonry failure when the lateral load reaches its peak; the effective strain remains quite low and amounting to only some fraction of the ultimate fracturing strain of FRP. Based on this principal, most of the analytical models assume a low value of effective strain in FRP while calculating the shear contribution by FRP (CNR DT 200 R1/2013, ACI440). These phenomena hold true for CFRP, PET and Nylon-FRP as well. Therefore, many authors (Stratford et al. 2004, Marcari et al. 2007) argued that it is impossible to accurately predict the FRP contribution to shear strength as they prove by their experimental test that the contribution of the FRP to the shear strength of masonry wall is far less than its ultimate tensile strength. So, it can be concluded that,

1) The mode of failure in masonry may change from shear sliding to masonry diagonal cracking when they are externally strengthened by FRP diagonal strips.

2) FRP with high elastic modulus and low fracturing strain such as CFRP offer less ductility and possibly less in-plane shear strength, which is not a good option for masonry strengthening.

3) PET-FRP and Nylon-FRP show good ductile behavior at both pre-peak and post-peak regimes and significantly enhances masonry shear capacity.

4) FRP debonding is a common phenomenon for CFRP, PET and Nylon-FRP, but the rupture of PET or Nylon sheet is very unlikely where as occasional rupture of the CFRP cannot be ruled out.

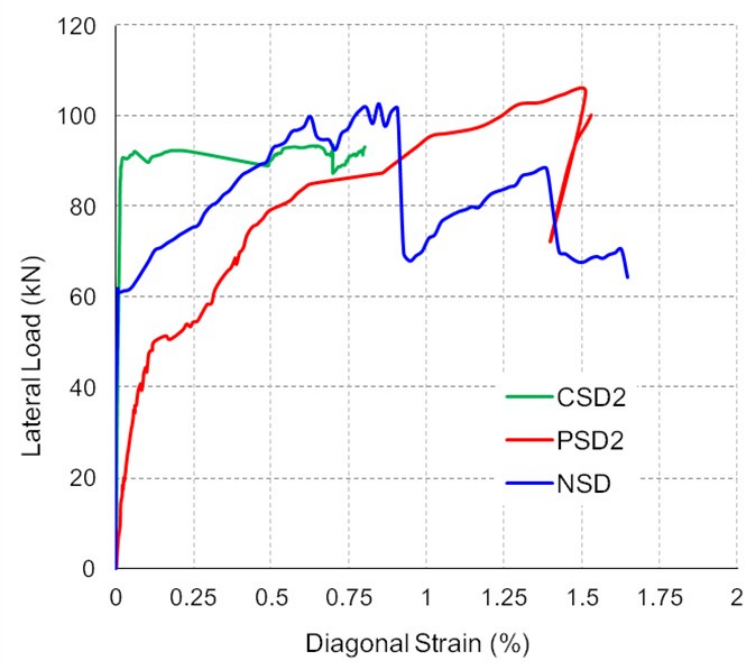

Fig. 5.25. *Load–axial strain responses in diagonal FRP strips of CFRP, PET-FRP and Nylon-FRP strengthened walls at point 2 on Fig. 5.14(a)*

In the case of FRP grid system, mixed mode of failure can be seen in Fig. 5.16 for both CFRP and PET-FRP reinforced walls, and their load-deformation responses are quite similar to each other (Fig. 5.23). This is due to the fact that beyond certain limit of FRP amount, the failure mode of masonry wall commutes from diagonal tension to predominantly flexural cracking irrespective of the type of FRP. Numerical modeling and analysis of masonry is the best tool to evaluate this threshold value. The horizontal strips of FRP played a crucial role here that restricted the wall from failing in a diagonal tension mode. These horizontal strips made the walls stronger in shear than in flexure. Though the vertical strips contributed in flexural strength to some extent, eventually it could not out strength the shear capacity, and caused the wall to fail in flexure. It is also interesting to make a comparison between Fig. 5.21 and Fig. 5.23 that once masonry walls are strengthened with CFRP in gird fashion, its brittleness in diagonal configuration changed into a ductile one. High FRP stiffness (11420 MN) did not change the overall stiffness of the masonry wall substantially, rather it helped the wall to deform as a composite system in such a way that can be compared as elastic-perfectly plastic deformation. But of course the deformability of high stiff CFRP will be less than that of PET as PET has higher deformation rate than CFRP. Another important point here to note that by increasing the amount and stiffness of FRP material on the surface of the wall does not necessarily increase the shear strength of the strengthened wall. Because it was point out earlier that a suitable material that has a moderate strength with a good deformability will be coherent with the fragile nature of

masonry. One interesting observation that could be made here is that, in absence of vertical strips the wall would have been experienced in shear sliding along the planes that are not offset by the horizontal strips (Alcaino and Santa-Maria 2008). So it can be concluded that:

Higher amount of FRP material bonded on the external surface of the masonry wall does not serve the purpose of strengthening; rather it will only increase the cost of the strengthening work and in some instance increases the stiffness of the masonry.

Although the PET-FRP in grid system does not compromise with the overall ductility of the masonry, it is not an effective system of strengthening as it does not help much to enhance the masonry in-plane shear strength as compare to the diagonal system. Same is true for the CFRP gird system as well.

FRP with high stiffness may change the masonry mode of failure from diagonal tension cracking into a flexural cracking.

As for the case of fully wrapped walls, ductility is hugely compromised for either of the FRP material i.e CFRP or PET. Although Fig. 5.24 does not depict the real deformation picture as it was stated earlier that these walls underwent some rotation at their bottom and a premature failure at the grip was noticed. Even then, the deformability of these walls can be foreseen from these load-deformation plots. So, it can be said that though PET-FRP wall can resist more lateral load than its counterpart CFRP, either of them is not a good option for masonry strengthening as long as they are used in a fully wrapped manner Wall retrofitted by bio-FRP such as Jute-FRP and Cotton-FRP behave in a ductile manner than their counterpart CFRP wall. PET-FRP wall can resist more lateral load than any of them, where as the lateral shear resistance by Cotton-FRP wall is more than Jute-FRP wall.

One interesting point that came out from the analysis of these experimental results is that the contribution of FRP in masonry shear strength, irrespective of their types and arrangements, is only become manifest after a certain time which is somewhat like 60% of the peak strength and that can be attributed to the service loading condition. Only after that some potential cracks show up in the masonry and the FRP start to take part in contributing to shear. That is why, there is no significant difference in the initial stiffness of the unreinforced masonry as well as masonry with FRP [Fig. 5.21, Fig.5.23. and Fig. 5.24] and that is why the initial strain in FRP is also very small (Fig. 5.25). So it can be concluded that FRP strengthening of the masonry can have only marginal effect on the shear strength at the service load condition but contribute a lot at some accidental overloading such as earthquake.

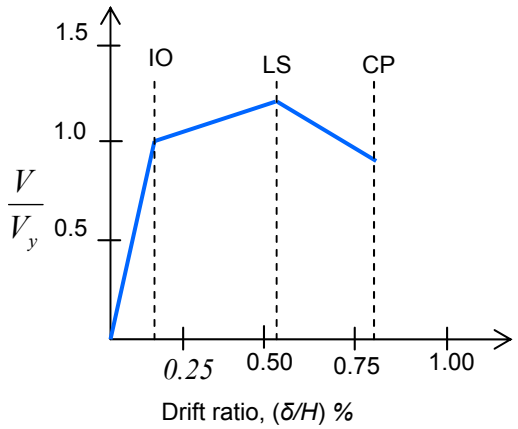

Fig. 5.26. *Performance indices*

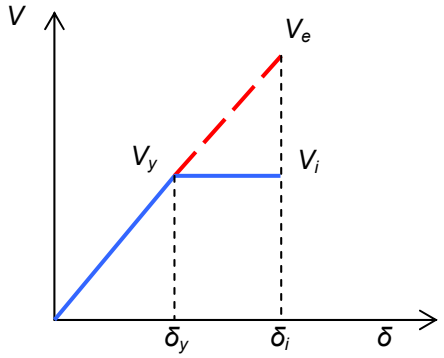

Fig. 5.27. *Equal displacement rule for linear elastic analysis*

5.5 Analysis of Masonry Performance

Inelastic analysis of a structure becomes increasingly important with the emergence of performance-based engineering (PBE) as a technique for seismic evaluation and design (ATC 1996; SEAOC 1995; Terán-Gilmore et al. 2008, Magenes and Calvi 1997). PBE uses the prediction of performance to forecast decisions regarding safety and risk. For this purpose, PBE characterizes performance primarily in terms of expected damage to structural and nonstructural components. Today's standard and model codes for seismic design of structures and structural components have shifted from the earlier arbitrary concept of "moderate damage", "severe damage", and "some damage" to the more accurately predictable performance based design (PBD) approach. In this approach the buildings and their components are designed with the objective of desired performance level (PL) for each seismic earthquake level, and with possible seismic hazards based on some acceptance criteria (FEMA 440, Abrams 2001). In this procedure, seismic damage is observed following earthquakes (expected damage is predicted for future earthquakes), and categorized on the basis of some engineering judgment. Finally, appropriate rehabilitation (strengthening/retrofitting) is suggested.

5.5.1 Performance of URM

FEMA 356 provides a set of guidelines for URM walls that restricts the damage to three basic levels of performance. These are shown on the normalized force-deflection curve on Fig. 5.26. Drifts of approximately 0.1% are known to result in minor extents of cracking with very limited structural damage and very low life threatening injury, which correspond to the immediate occupancy (**IO**) performance limit state. Although some minor structural repairs may be appropriate, these would generally not be required prior to re-occupancy. Peak lateral strength is associated with a drift equal to about 0.6% which includes damage to structural components but

retains a margin against onset of partial or total collapse in compliance with the acceptance criteria specified in AC125. This is assumed to correspond with the life-safety (**LS**) limit state. A loss of strength is permitted before reaching the collapse-prevention (**CP**) state at about 0.8% drift. The CP limit state for URM buildings is related to the distress state in which the building is on the verge of partial or total collapse. Substantial damage to the structure has occurred, potentially including significant degradation in the stiffness and strength of the lateral-force resisting system, when the lateral resistance of a building drops by 20% i.e., $V_{CP} = 0.8V_y$. Here, V_{CP} is the base shear in the building at the collapse prevention limit state, and the V_y is the effective yield strength of the building determined from the capacity curve.

For seismic rehabilitation, simple nonlinear analysis is performed, based on a linear static approach, where lateral displacements are approximated in terms of member forces based on the equal displacement rule (i.e. elastic and inelastic displacements are the same for structures beyond yield strength shown in Fig. 5.27). With this assumption, as noted in Eq. (5.5), elastic forces, V_e, will be equal to the inelastic strength, V_i, times the ductility factor, m, which is defined as the inelastic deflection at a given limit state, δ_i divided by the yield deflection, δ_y (Eq. 5.6). FEMA 356 provides a set of ductility factors, m for different limit states and for two different failure modes (rocking and shear sliding) of masonry. Table 5.4 provides the m-factors and drift ratios recommended by FEMA 356, along with the estimated performance of the shear walls in this study.

$$mV_i \geq V_e \tag{5.5}$$

$$\text{Here, } m = \frac{\delta_i}{\delta_y} \tag{5.6}$$

The nonlinear force-displacement curve (also known as pushover capacity curve) of the component of the structure shall be replaced with an idealized relationship to calculate the effective lateral stiffness, K_e, and effective yield strength, V_y, of the building. Tri-linear idealization of the lateral force displacement curves of a URM wall as well as of a FRP strengthened walls are shown in Fig. 5.28(a) and Fig.5.28(b), respectively. In this study, the target displacement δ_t, which is intended to represent the maximum displacement likely to be experienced during the design earthquake, has been simply assumed equal to δ_u, the deformation corresponding to ultimate shear strength. The detailed idealization technique and more accurate calculation of δ_t can be found in FEMA 440 (FEMA 2000) and ATC 40 (ATC 1996). From the idealized curve, the effective lateral stiffness, K_e, shall be taken as the secant stiffness calculated at a base shear force equal to 60% of the effective yield strength V_y of the structure. In the case of the unavailability of a

Table 5.4. *Performance of Experimental Shear Walls for Different Limit States*

Wall Type	References	Wall ID	Performance indeces	Performance Level			Elastic Stiffness K_e (N/mm)	Post-yield Stiffness factor, α_1	Softening Stiffness factor, α_2
				IO	LS	CP			
URM	FEMA 356		m-factor	1.0	6.0	8.0	--	--	--
			% Drift, *(δ/H)*	0.1	0.6	0.8			
	This study	RWS1	m-factor	1.0	13	25	61,000	0.02	0.05
			% Drift, *(δ/H)*	0.1	1.0	2.0			
		RWS2	m-factor	1.0	14	23	62,000	0.02	0.07
			% Drift, *(δ/H)*	0.1	0.6	1.1			
	Bosiljkov et al. (2004)	BNL4	m-factor	1.0	6.0	11.0	51,000	0.02	0.08
			% Drift, *(δ/H)*	0.1	0.8	1.5			
		BNL6	m-factor	1.0	18	32	33,000	0.01	0.03
			% Drift, *(δ/H)*	0.1	2.3	4.1			
	Magenes et al. (2008)	CL05	m-factor	1.0	2.0	4.0	114,000	0.04	0.22
			% Drift, *(δ/H)*	0.1	0.3	0.5			
		CL07	m-factor	1.0	2.0	3.0	20,000	0.01	0.32
			% Drift, *(δ/H)*	0.1	0.2	0.4			
	Modena et al. (2005)	15_5	m-factor	1.0	5.0	9.0	36,000	0.01	0.09
			% Drift, *(δ/H)*	0.3	1.4	2.6			
	Da Porto et al. (2009)	15_7	m-factor	1.0	6.0	11.0	54,000	0.01	0.07
			% Drift, *(δ/H)*	0.2	1.6	2.8			
	Fehling et al. (2007)	N1	m-factor	1.0	1.2	2.3	73,000	0.09	0.23
			% Drift, *(δ/H)*	0.1	0.1	0.2			
	Frumento et al. (2009)	18_3	m-factor	1.0	3.5	6.0	251,000	0.05	0.12
			% Drift, *(δ/H)*	0.1	0.2	0.4			
Reinforced with Diagonal FRP	This study	PSD1	m-factor	1.0	3.6	8.0	63,000	0.03	0.08
			% Drift, *(δ/H)*	0.3	1.1	2.3			
		PSD2	m-factor	1.0	13	20	70,000	0.01	0.05
			% Drift, *(δ/H)*	0.1	1.2	1.8			
		CSD1	m-factor	1.0	5.7	11	153,000	0.05	0.12
			% Drift, *(δ/H)*	0.1	0.3	0.7			
		CSD2	m-factor	1.0	3.7	8.0	149,000	0.09	0.15
			% Drift, *(δ/H)*	0.1	0.2	0.5			
Reinforced with Gird FRP	This study	PSG1	m-factor	1.0	5.0	12	83,000	0.10	0.19
			% Drift, *(δ/H)*	0.1	0.5	1.1			
		PSG2	m-factor	1.0	6.0	21	99,000	0.13	0.15
			% Drift, *(δ/H)*	0.1	0.4	1.4			
		CSG1	m-factor	1.0	6.0	18	810,000	0.05	0.06
			% Drift, *(δ/H)*	0.1	0.2	0.3			
		CSG2	m-factor	1.0	6.0	16.0	744,000	0.08	0.09
			% Drift, *(δ/H)*	0.1	0.2	0.3			

pushover curve, a reasonable estimation of in-plane shear stiffness of URM is suggested here, by Eq. (5.7), provided all the parameters related to masonry are readily available (Al-Chaar 2002).

$$K_e = \frac{1.2\sigma_n}{\frac{H^3}{3E_m I_g} + \frac{H}{A_g G_m}} \tag{5.7}$$

Here, I_g = Moment of inertia of the uncracked section of masonry; E_m = Masonry elastic modulus; G_m = Masonry shear modulus.

5.5.2 Performance of Strengthened Masonry

FEMA 356 and FEMA 440 guidelines do provide methods for estimating the strength and deformation capacity of existing URM walls and piers; however, they do not provide such information for components rehabilitated by FRPs. This is largely because such research data is limited. Only some strengthening techniques, design guidelines, and anchorage systems can be found elsewhere in the Model Code or Pre-standards like ACI 530, JSCE 2001, Euro Code 6, CNR DT 200 and ACI 440. From this experimental study, some of the parameters that were mentioned in the foregoing section regarding URM, are discussed here. Ductility factors, and collapse prevention are also addressed.

5.5.3 Damage Evolution and Ductility Capacity

From Table 5.4, it is evident that many of the URM shear walls have poor performance in Life Safety (LS) and Collapse Prevention (CP) limit states. Once the masonry walls are strengthened by FRP strips, their performance get better. Masonry wall strengthened by diagonal PET-FRP behaves in a more ductile manner than the rest of the strengthening walls. It also shows a very good post peak collapse prevention behavior as the drift ratio is over 1.5 with a drift ratio more than the FEMA recommended value of 0.8 for URM. It is interesting to note that, when the shear walls are strengthened with the PET-FRP grid system, their stiffness increased and made the seismic ductility demand for CP much higher. On the other hand walls strengthened by CFRP show low percent drift ratio with a low ductility factor. As mentioned earlier, to be harmonized with masonry, a strengthening material needs to be identified that offers a moderate stiffness with a good ductile behavior. CFRP offers a higher stiffness with a low ductility performance, though having good enhancement of shear strength over PET-FRP. So, masonry externally reinforced with CFRP will not be a good alternative over PET-FRP.

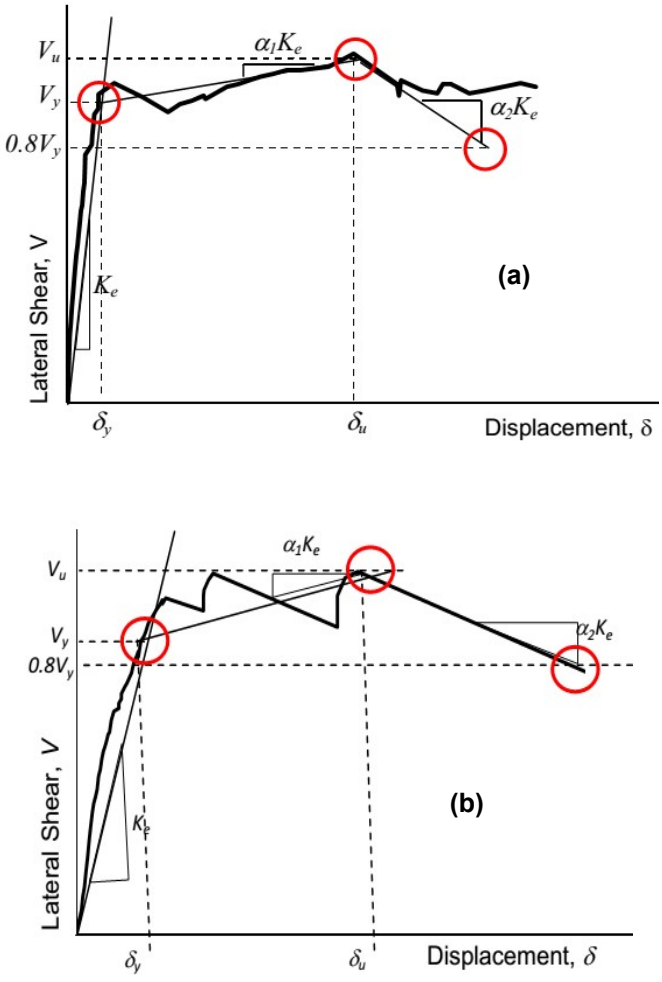

Fig. 5.28. *Idealized force-displacement curve for (a) RWS1 and (b) CSD1 panels*

5.6 Concluding Remarks

The in-plane shear behavior of fifteen masonry walls have been studied having been strengthened by three types of synthetic fibers, namely CFRP, PET-FRP and Nylon-FRP, and two types of natural fibers, namely Jute-FRP and Cotton-FRP sheets in three different configurations with similar boundary conditions under monotonic lateral loading in a quasi-static test facility. Vertical loads were applied at two points prior to lateral loading. Load-deformation characteristics were observed for each wall and subsequent damages were evaluated. Some of the performance criteria set by FEMA 356 are assessed. Based on the foregoing results and observations, the following remarks can be outlined:

1) Two unreinforced reference walls failed in shear sliding and toe crushing preceded by a flexural cracking, which is largely seen as common failure mode of the URM wall with aspect ratio between 1 and 1.5 having a moderate pre-compression vertical load. For FRP strengthened masonry walls, the failure mode changed to predominantly a diagonal tension

and toe crushing preceded by a flexural cracking where debonding was the most common phenomenon for the failure of FRP. In two occasions only the rupturing of CFRP were observed.

2) This study demonstrates the ability of all of the FRPs such as CFRP, PET-FRP, Nylon-FRP, Jute-FRP and Cotton-FRP sheets to enhance the shear resistance to a great extent; more than twice the capacity of the URM wall in the case of diagonal bracing and about three times in the case of fully FRP wrapping. Among the fives, PET-FRP and Nylon-FRP have a better ductility performance than CFRP, as they show pronounced ductile behavior in pre-peak regime and softening behavior in post-peak regime. Ductility is a must needed criterion rather than strength for a structure to absorb substantial seismic energy and ensure structural integrity and margin of safety against collapse. Though the CFRP increases the shear capacity of a masonry wall, it substantially reduces the ductility of the wall, which may eventually cause an explosive type of masonry failure. On the other hand, Jute-FRP and Cotton-FRP also enhanced the shear capacity of masonry wall to almost thrice of that of URM walls, and they also show better ductile behavior than CFRP.

3) The in-plane shear strengths observed in this experimental study are almost equal to each other for the cases where the amount of FRP was greater than a certain limit. This information will assist to some extent to develop an analytical model for FRP strengthened wall based on effective strain in FRP.

4) The elastic stiffness of unreinforced masonry walls was largely modified by the use of FRP, externally bonded over the surface of the walls but it was observed that stiffness value beyond some specific range does not increase the in-plane shear strength of masonry and it will only increase the cost of strengthening works.

5) Diagonal bracing with PET-FRP or Nylon-FRP sheet can be the best option, where not only capacity enhanced but, at the same time, the wall is made quite ductile, substituting a catastrophic mode of failure by a ductile one.

6) Another interesting point that is manifest from this experimental study is that the FRP strengthening of the masonry can have only marginal effect on the structural performance at the service load condition but contribute a lot at some accidental overloading such as earthquake, where the seismic demand is high.

7) As masonry is quite fragile against lateral movement with a low lateral stiffness, diagonal bracing with PET-FRP sheet can be one of the options if the cost of the material is not compromised. If seeking for a low-cost strengthening material, Nylon-FRP, Jute-FRP and Cotton-FRP could be one of the variable alternatives, where not only capacity is enhanced

but, at the same time, the wall is made quite ductile, reversing a catastrophic mode of failure to a ductile one. Moreover, unlike synthetic FRP such as CFRP, PET-FRP and Nylon-FRP, Jute and Cotton are bio-degradable materials, that do not pose any threat to the ambient environment.

8) Finally it has been shown that PET-FRP has a better seismic performance than CFRP especially at Life-Safely (LS) and Collapse Prevention (CP) state of the wall.

However, further study is needed for the advancement of knowledge on FRP in general and on PET in particular concerning some of the unresolved issues that could not be addressed in this paper such as brick-FRP interface behaviour, optimum percent of FRP for masonry, delayed debonding and issue related to anchorage system of FRP with masonry. A concerted effort and a harmonized approach are necessary to make externally bonded FRPs as a lucrative solution for many historically valued masonry structures for retrofitting and rehabilitation purposes. Though the present work is not very exhaustive, it can be one step forward in achieving this goal.

References

ACI 440. (2008). "Guide for the design and construction of externally bonded FRP systems for strengthening concrete structures." *American Concrete Institute*, Farmington Hills, MI 48331 U.S.A.

ACI 530. (2002). "Building code requirements for masonry structures" *ACI 530/ASCE 5/TMS 402.*

ATC 40 (1996). "Seismic evaluation and retrofit of concrete buildings." *Applied Technology Council*, Vol-1.

ASTM D 1777., Standard test method for thickness of textile materials. ASTM international 2015.

ASTM D 2905., Practice for Statements on Number of Specimens for Textiles. ASTM international 2002.

ASTM C 1557, Standard test method for tensile strength and Young's modulus of fibers. ASTM international 2014.

Ali, Q., Badrashi, Y. I., Ahmad, N., Alam, B., Rehman, S., and Banori, F. A. S.(2012) " Experimental investigation on the characterization of solid clay brick masonry for lateral shear strength evaluation." *Int. J. of earth sciences and engr*. 5(4), 782 -791.

Abrams, D. P. (2001). "Performance based engineering concepts for unreinforced masonry building structures." *Journal of Progress in Structural Engineering and Materials*, Wiley Interscience, 3(1), 48–56.

Altin, S., Anil,O., Kara, M. E., and Kaya, M. (2007). "An experimental study on strengthening of masonry infilled RC frames using diagonal CFRP strips" *Elsevier J. of Composites. Part B: Engineering.*1-14.

Al-Chaar, G. (2002). " Evaluating strength and stiffness of unreinforced masonry infill structures." *ERDC/CERL TR-02-1 report*, Engineer Research and Development Center, US Army Corps. of Engineers.

Alcaino, P. and Santa-Maria, H. (2008), "Experimental Response of Externally Retrofitted Masonry Walls Subjected to Shear Loading" *J. Compos. Constr.*, 12(5), 489– 498.

Akın, E., Özcebe, G., Canbay, E. and Binici, B. (2014). "A Numerical Study on CFRP Strengthening of Reinforced Concrete Frames with Masonry Infill Walls", *J. of Compos. Constr.,* 18(2), 04013034.

Anggawidjaja. D., Ueda. T., Dai. J., and Nakai. H. (2006). "Deformation capacity of RC piers wrapped by new fiber-reinforced polymer with large fracture strain." *Elsevier J. of Cement and Conrete*. Compos. 28(2006), 914-927.

Benedetti, A. and Steli, E. (2006). "Analytical models for shear–displacement curves of unreinforced and FRP reinforced masonry panels." *Elsevier J. of Const. and Bldg. Mat.*1-11.

Bosiljkov, V., Page, A. W., Bokan-Bosiljkov, V. and Zˇ arnic´, R. (2003). "Performance based studies of in-plane loaded unreinforced masonry walls." *Masonry International 2003*; 16(2):39–50.

Bosiljkov, V., Tomazevic, M., and Lutman, M. (2004). "Optimization of shape of masonry units and technology of construction for earthquake resistant masonry buildings: research report-part one and two." *ZAG Ljubljana*, Slovenia.

Bosiljkov, V., Page, A. W., Bokan-Bosiljkov, V., and Zˇarnic´, R. (2008). "Review paper, progress in structural engineering and material: structural masonry evaluation of the seismic performance of brick masonry walls." *Struct. Control Health Monit.* 17,100–118.

Burgoyne, C. and Balafas, I. (2007). "Why is FRP not a financial success?", *FRPRCS-8,* University of Patras, Patras, Greece, pp.1-10.

Beckwith, S. W., Natural fiber reinforcement materials, low cost technology for composites applications, *Technical Report, Comp. Fabrication,* pp. 12-16, 2003.

CNR-DT200. (2013). "Guide for the Design and Construction of Externally Bonded FRP Systems for Strengthening Existing Structures." *CNR-DT 200 R1,* Italian National Research Council, Italy.

Da Porto, F., Grendene, M., and Modena, C. (2009). "Estimation of load reduction factors for clay masonry walls." *Earthq. Eng. Struct. Dyn.* 38:1155–1174.

Dizhur, D., Griffith, M. C., and Ingham, J. M. (2013). "In-plane shear improvement of unreinforced masonry wall panels using NSM CFRP strips." *J. Compos. Constr.*, 17(6), 04013010.

Eurocode 6 (2005). "Design of masonry structures - Part 1-1: General rules for reinforced and unreinforced masonry structures". *EN 1996 -1 -1: 2005, CEN, Brussels.*

Ehsani, M. R., Saadatmanesh, H., and Al-Saidy, A. (1997). "Shear behavior of URM retrofitted with FRP overlays." *J. Compos. Constr.*, 1(1), 17– 25.

ElGawady, M. A., Lestuzzi, P., and Badoux, M. (2005). " Performance of masonry walls under in-plane seismic loading." *TMS Journal, 23(1),*85-104.

ElGawady, M. A., Lestuzzi, P., and Badoux, M. (2007). "Static cyclic response of masonry walls retrofitted with fiber-reinforced polymers" *J. Compos. Constr.*, 11(1), 50– 61.

FEMA 274. (1997). "NEHRP commentary on the guidelines for the seismic rehabilitation of buildings" *for building seismic safety council by ATC 33*, Washington, D.C.

FEMA 356. (2000). "Prestandard and commentary for the seismic rehabilitation of buildings." *Federal emergency management agency*, Washington, D.C.

FEMA 440. (2005). "Improvement of nonlinear static seismic analysis procedures." *Federal emergency management agency*, Washington, D.C.

Fehling, E., Stuerz, J., and Emami, A. (2007). "Tests results on the behaviour of masonry under static (monotonic and cyclic) in plane lateral loads" *Tech. report of the col. res. pro. ESECMaSE*, eliverable D7.1a. Germany.

Frumento, S., Magenes, G., Morandi, P., and Calvi, G. M. (2009). "Interpretation of experimental shear tests on clay brick masonry walls and evaluation of q-factors for seismic design." *IUSS Press*, Pavia.

Foraboschi, P. (2009). "Coupling effect between masonry spandrels and piers." *Mat. and Str.* 42, 279-300.

Foraboschi, P., and Vanin, A. (2013). "New methods for bonding FRP strips onto masonry structures: Experimental results and analytical evaluations." *Comp.: Mech., Comp., Appli. An Int. J.*, 4(1), 1-23.

Foraboschi, P. (2015). "Analytical model to predict the lifetime of concrete members externally reinforced with FRP." *Theoretical and Applied Fracture Mechanics*, 75(1), 137-145.

Hamid, A., EI-Dakhakhni, W. W., Hakam, Z., and Elgaaly, M. (2005). "Behaviour of composite unreinforced masonry-fiber-reinforced polymer wall assemblages under in-plane loading." *J. Compos. Constr.*, 9(1), 73–83.

Hansen, K. F. (1999). "Bending and shear test with masonry." SBI bulletin 123, Danish Building research Institute, Hørsholm, Denmark.

JSCE (2001). "Recommendation for Upgrading of Concrete Structures with use of Continuous Fiber Sheets." *Concrete Engineering Series 41*, Japan Society of Civil Engineers, Tokyo, Japan.

Magenes, G., and Calvi, M. (1997). "In-plane seismic response of brick masonry walls." *Earthquake Engineering and Structural Dynamics*, 26, 1091-1112.

Magenes, G., Morandi, P., and Penna, A. (2008). "Tests results on the behaviour of masonry under static cyclic in plane lateral loads." *Tech. report of the coll. res. pro. ESECMaSE*, Uni. of Pavia, Italy.

Marcari, G., Manfredi G., Prota A. and Pecce, M. (2007). "In-plane shear performance of masonry panels strengthened with FRP." *Elsevier J. of Comp.* Part B 38, 887–901.

Modena, C., Da Porto, F., and Garbin, F. (2005). "Ricerca sperimentale sul comportamento di sistemi per muratura portante in zona sesmica: *draft 2005/01*." University of Padua, Italy.

Maeda Kosen Co. Ltd. Japan. (2005). "Fiber Frontier System" (http://www.maedakosen.jp/) (May 10, 2013).

Nippon Steel & Sumikin Materials Co. Ltd. Japan. (1997). "Construction Materials: FORCA Towsheet" (http://www.nck.nsmat.co.jp/english.html) (April 6, 2013).

NGCC. (2008) "Sustainable FRPs – naturally derived resins and fibres" NGCC Technical Sheet 08, *Network group for composites in construction*.

Rahman, A. and Ueda, T. (2014). "Experimental investigation and numerical modeling of peak shear stress of brick masonry mortar joint under compression." *J. Mat. C. Eng.*, 26(9), 04014061,1-13.

Salmanpour, A. H., Mojsilovic, N., and Schwartz, J. (2013). “Deformation capacity of unreinforced masonry walls subjected to in-plane loading: a state-of-the-art review.”*Int. J. of Adv. Struc. Eng. Springer* 5(22), 1-12.

SEAOC (1995). “Performance Based Seismic Engineering.” Report prepared by *Structural Engineers Association of California*.

Stratford, T., Pascale, G., Manfroni, O., and Bonfiglioli, B. (2004). “Shear strengthening masonry panels with sheet glass-fiber reinforced polymer”. *J. Compos. Constr.*, 8(5), 434– 443.

Shrestha, J., Ueda, T., and Zhang, D. (2014). “Durability of FRP concrete bonds and its constituent properties under the influence of moisture conditions.” *J. Mat. C. Eng.*, 0899-1561/A4014009(14).

TNO. (2004). “Shear test on masonry panels; literature survey and proposal for experiments. *TNO Building and Construction Research*. 2600 AA Delft.

Terán-Gilmore, A., Oscar Zuñiga-Cuevas, Z., and Ruiz-García, J. (2008) “Model for the nonlinear analysis of confined masonry buildings” *The 14th World Conf. on Earthquake Engineering*, Beijing, China.

Tomaževič, M., and Gams, M. (2009). “Shear resistance of unreinforced masonry walls.” *Ingineria Sismica*, 26: 3, 5-18.

Wang, Q., Chai, Z., Huang, Y., Yang, Y. and Zhang, Y. (2006) “Seismic shear capacity of brick masonry wall reinforced by GFRP.” *Asian Journal Of Civil Engg. (Building And Housing)*, 7(6), 563-580.

Zhuge, Y. (2010). “FRP-retrofitted URM walls under in-plane shear: review and assessment of available models” *J. Compos. Constr.*, 14(6), 743– 753.

Chapter 6

Analytical Modeling of Masonry Wall

6.1 Modeling Background

Since the early 1990s, numerous research studies and engineering projects have been dedicated to FRP retrofitted RC structures (Nanni 1993; Khalifa et al. 1998; Rizkalla et al. 2003; El-Sokkary and Galal 2013) but there have been fewer researches on masonry structures. Among them, research on shear strength of FRP retrofitted masonry walls has been limited (Stratford et al. 2004, Ehsani et al. 1997; Tumialan et al. 2001; Valluzzi et al. 2002; ElGawady et al. 2007). Those researches have focused on assessment of strength and ductility characteristics of masonry walls strengthened by FRP. It is necessary, however, to complement the experimental work with analytical models and design guidelines for professionals to use FRPs in real applications.

6.2 Existing Analytical Models

It has been stated earlier that the behavior of URM is rather complex due to its non-homogeneous composite nature, and various modes of failure that make the failure behavior difficult to predict, and cannot be calculated by a single equation.

Attempts have been made by numerous researchers to develop models for accurate estimation of shear strength of URM walls. Some of the models and their pertinent equations have also been incorporated in some national pre-standard and model codes. Among them, the most widely accepted equations are those proposed in FEMA 356 (2000). Four separate equations for calculating the shear strengths of URM walls, corresponding to the four primary failure modes, are presented in Sec 6.3.

For masonry retrofitted with externally bonded FRP, not so many conclusive models have been developed so far (Triantafillou and Antonopoulos 2000; Tumialan et. al. 2003). Only some formulation can be seen in the design code and pre-standard and they are very much conservative and cannot be applied for all types of FRPs. Table 6.1 gives some of the existing equations proposed by some researchers and some are available in some model codes and pre-standards. Moreover, the strength of wall retrofitted by FRP will be affected by many factors. Some of them are: strength; orientation; anchorage length; modulus of elasticity; and strain distribution of FRP. Not all equations and models deal with all of these papremeters.

Table 6.1 *Overview of Existing Models for Prediction of Shear Strength*

References	Pertinent Equations	Definition of Parameters
Prota et al. (2008) for Diagonal FRP	$V_T = V_M + V_{FRP} = V_M + n\varepsilon_f E_f A_f \cos\theta$	V_M = masonry contribution; V_{FRP} = FRP contribution; $V_T = V_M + V_{FRP}$ = total shear capacity; n = number of FRP ply; E_f = modulus of FRP; w_f = width of the FRP strips; t_f = thickness of the FRP strips; θ = inclination of FRP strips with the wall principal axis; A_f = $w_f \times t_f$ = area of single FRP strip (for U wraps, multiplied by 2); ε_f =fracture strain of FRP; ε_{eff} = effective strain in FRP; s = c/c spacing of FRP strips; γ_f = partial safety factor for FRP in tension (1.15, 1.2, and 1.25 for CFRP, AFRP and GFRP respectively); ρ_f = FRP reinforcement ratio = A_f/A_g
Alcaino and Santa-Maria (2008) for Diagonal FRP	$V_T = V_M + E_f \varepsilon_f A_f \cos\theta$	
Triantafillou and Antonopoulos (2000) for FRP grid system	$V_T = V_M + V_{FRP} = V_M + 0.9\frac{\varepsilon_{eff} E_f L A_f}{\gamma_f s}$ For FRP debonding: $\varepsilon_{eff} = 0.65\left[\frac{(f'_{mc})^{2/3}}{E_f \rho_f}\right]^{0.56} \times 10^{-3}$ [E_f in GPa] For FRP rupture: $\varepsilon_{eff} = 0.17\left[\frac{(f'_{mc})^{2/3}}{E_f \rho_f}\right]^{0.3} \times \varepsilon_f$ [E_f in GPa]	
CNR DT200 (2013) for FRP grid system	$V_T = V_M + V_{FRP} = V_M + \frac{1}{\gamma_{rd}} \cdot \frac{0.6 L A_f E_f \varepsilon_f}{s}$ For FRP debonding use ε_{eff} instead of ε_f in above. $\varepsilon_{eff} = \sqrt{\frac{2F_{fk}}{E_f t_f}}$ and $F_{fk} = c_1\sqrt{f'_{mc} \cdot f_{dtu}}$	f_{dtu} = direct tensile strength of masonry normal to bed joint ($0.1\hat{f}_{mc}$); F_{fk} = specific fracture energy at debonding; c_1 = experimental factor (0.015); f_f = fracture strength of FRP; f_{eff} = effective stress in FRP $= 0.004E_f \le 0.75 f_f$.
ACI 440 (2008) for FRP grid system	$V_T = V_M + \frac{n A_f \varepsilon_{eff} E_f (\sin\theta + \cos\theta) L}{s}$ $\varepsilon_{eff} = 0.41\sqrt{\frac{f'_{mc}}{n E_f t_f}} \le 0.45\varepsilon_f$	
AC 125 (2010) for fully wrapped wall	$V_T = V_M + V_{FRP} = V_M + 2nt_f f_{eff} L \sin^2\theta$	

Note: In this table and elsewhere in this thesis, the units are: force in kN; Stress in MPa, Distance in mm; angle in Deg.

In the following section, a detailed analytical model has been proposed to predict the shear strength of masonry wall strengthened with various types of FRPs.

6.3 Proposed Analytical Model

Until now, very limited number of design models have been developed and adopted in standards for masonry wall retrofitted with externally bonded FRP (ACI 440, CNR DT200 2013, JSCE 2001, Triantafillou et. al 2000). All of them have the common terminology and based on the assumption that the shear strength of masonry wall is sum of the contribution from uncracked masonry wall and contribution from FRP. Thus, the total shear force is given by,

$$V_T = V_M + V_{FRP} \tag{6.1}$$

The first term, V_M, may be calculated according to provisions in FEMA 356 (2000), which gives the following four different equations to calculate the shear strength of URM for four modes of failure (Fig. 5.1), they are:

1) Shear strength for rocking:

$$V_M = V_{rock} = 0.9\alpha_1 \sigma_n A_g \left(\frac{L}{H}\right) \tag{6.2}$$

2) Shear strength for toe crushing:

$$V_M = V_{tc} = \alpha_1 \sigma_n A_g \left(\frac{L}{H}\right)\left(1 - \frac{\sigma_n}{0.7 f'_{mc}}\right) \tag{6.3}$$

3) Shear strength for bed-joint sliding:

$$V_M = V_{sld} = A_g \tau_{sld} = A_g \left(c + \sigma_n \tan\phi\right) \tag{6.4}$$

4) Shear strength for diagonal tension cracking:

$$V_M = V_{dt} = f_{dt} A_g \left(\frac{L}{H}\right)\sqrt{1 + \frac{\sigma_n}{f_{dt}}} \tag{6.5}$$

Some of the parameters used in these equations depend on test results. In absence of candid test results for masonry compressive strength, cohesion and masonry diagonal tension strength, Eq. (6.6) (CEN 2005), Eq. (6.7) (Ali etl.al. 2012), and Eq. (6.8) (Ali etl.al. 2012), can safely be used for a conservative value of these three parameters.

Where,

$$f'_{mc} = 0.55\left(f_b\right)^{0.7}\left(f_m\right)^{0.3} \tag{6.6}$$

$$c = 0.0337\left(f_m\right)^{0.6} \tag{6.7}$$

$$f_{dt} = 0.075\left(f'_{mc}\right)^{0.375} \tag{6.8}$$

Here, V_M = shear strength of URM wall; *L, H, b* = length, height and thickness of the masonry wall respectively; f'_{mc} = compressive strength of masonry prism; A_g = sectional area of wall = *(L* $\times$ *b);* α_1 = factor for boundary condition (0.5 for cantilever wall and 1.0 for fixed-fixed wall); τ_{sld}

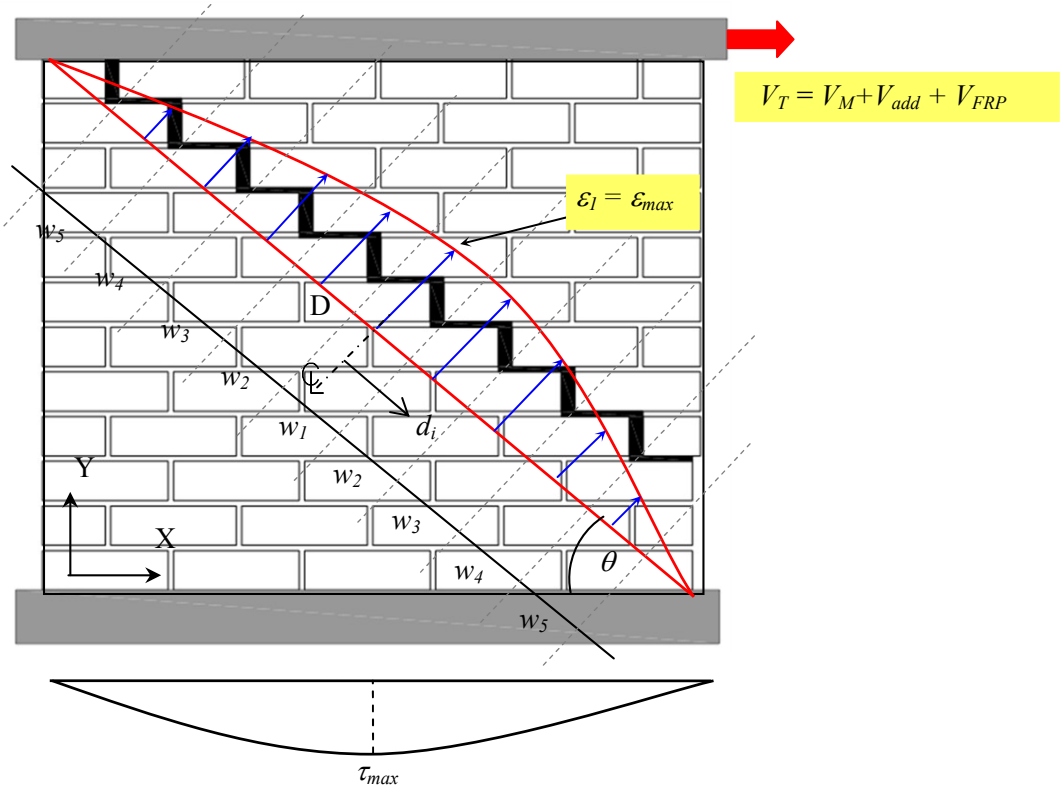

Fig. 6.1. *Effective strain based model*

= average bed-joint sliding shear stress of URM wall; c = cohesion between mortar and brick; σ_n = vertical compression on masonry wall; ϕ = frictional angle at sliding surface; f_{dt} = masonry diagonal tensile strength. f_b, f_m = uniaxial compressive strength of brick and mortar respectively.

So, the major differences between available models are attributed to FRP contribution, V_{FRP} and how the mechanism of this contribution has been clarified. The strength of V_{FRP} will be affected by but not limited to the strength of FRP, the orientation of FRP, the anchorage length of FRP, the modulus of elasticity of FRP, and more importantly, the strain distribution in FRP. Therefore, many authors (Stratford et. al. 2004 and Alcaino and Santa-Maria 2008) argued that it is impossible to accurately predict the FRP contribution to shear strength. It would be ideal if FRP reaches its tensile strength at failure. However, most experimental data showed that the contribution of the FRP to the shear strength of masonry wall is far less than its ultimate tensile strength due to premature debonding.

In this section, an attempt is made to propose a simplified analytical model based on effective strain, which can predict the FRP contribution in masonry wall fully wrapped and diagonally braced with any type of FRP, with fair accuracy.

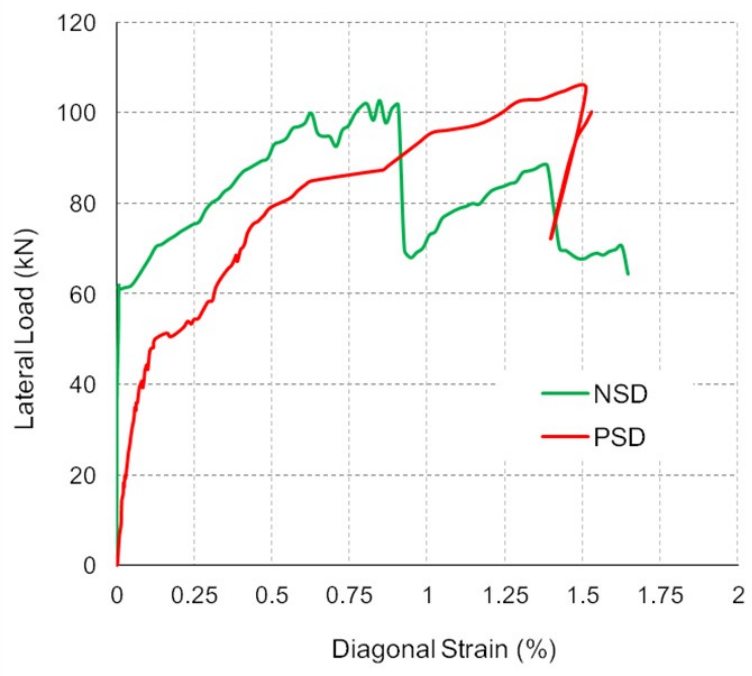

Fig. 6.2. *Load-FRP strain response of diagonally reinforced walls (NSD and PSD)*

6.3.1 Effective Strain Based Model

The proposed model is based on the assumption that the effective tensile strain in FRP varies parabolically along the principal compression diagonal having maximum strain at the center in a manner similar to the distribution of internal shear stress along the length of the wall as shown in Fig. 6.1. The length of compression diagonal D (Eq. 6.9) is subdivided into a finite number of strips, m of equal width, w_i, which can be taken conveniently as the diagonal length of a half brick ($l/2$) plus its surrounding mortar thickness, t_m (Eq. 6.10).

$$D = \sqrt{H^2 + L^2} \tag{6.9}$$

$$w_i = \sqrt{\left(h + t_m\right)^2 + \left(\tfrac{1}{2} l + t_m\right)^2} \tag{6.10}$$

So, the number of strips is, $m = \dfrac{D}{w_i}$

It is further assumed that before formation of any potential diagonal cracking in brick masonry, the effective strain in FRP is quite low, as shown in Fig. 6.2. The diagonal tension crack, once formed, spreads either immediately or at only higher load, traversing along the compression diagonal of the wall in a stepped fashion through mortar between bricks. Crack may go through the bricks also, depending on the relative strength of brick and mortar. Once a crack is formed, no tension force perpendicular to the crack can be transmitted across it. However, FRP wrap, more specifically the vertical wrap (or the vertical component of the bi-directional sheet), whose

chief contribution is in flexure, adds some stiffness to the wall and as a result it retards the formation of diagonal tension crack and restrict the crack opening. As long as the crack is narrow, it can still transmit some shear forces in its own plane through friction of the surface roughness. This sizable contribution to shear force has to be incorporated with an addition term V_{add} (Eq. 6.11) in Eq. (6.2) to Eq. (6.5), depending on the governing failure mode of FRP retrofitted wall that limits the shear strength. Eq. (6.11) gives an imperial relationship among the parameters used in this equation.

$$V_{add} = K\frac{\rho_f E_f L}{H} \tag{6.11}$$

Where, $\rho_f = \frac{nt_f}{b}$ = FRP area fraction in horizontal direction, n = number of FRP ply, t_f = FRP thickness, E_f = FRP elastic modulus. The empirical constant K in this equation was found to be 25 in SI unit. More test results for different aspect ratios of the wall and for different FRP ratios are needed for a better correlation of this constant K.

So, Eq. (6.1) which gives the total shear strength of FRP retrofitted masonry walls, takes the final shape as,

$$V_T = V_M + V_{add} + V_{FRP} \tag{6.12}$$

It is worth mentioning here that the proposed model can also predict the shear strength for other modes of failure as well.

The effective strain for each strip can be calculated as,

$$\varepsilon_i = \varepsilon_1\left[1-\left(\frac{2d_i}{D}\right)^2\right] \tag{6.13}$$

Where, $i = 1, 2, 3 \ldots\ldots\ldots m$ (m = number of strips)

In the above Eq. (6.13), the diagonal distance d, from the center of the wall, can be calculated by Eq. (6.14),

$$d_{i-1} = (i-1)w_i \quad \le \frac{D}{2} \tag{6.14}$$

In this Eq. (6.13), ε_1 is the maximum effective strain, ε_{max}, which can be calculated by the following Eq. (6.15), originally proposed by ACI 440 (2008).

$$\varepsilon_1 = \varepsilon_{eff} = 0.41\sqrt{\frac{f'_{mc}}{nE_f t_f}} \le 0.9\varepsilon_{fu} \tag{6.15}$$

It was observed that the peak strain in Nylon-FRP, PET-FRP and CFRP for diagonally braced walls were 1.38, 1.51 and 0.69 percent respectively (Fig. 5.25) where as the calculated maximum effective strain by Eq. (6.15) for these three FRPs were 1.28, 1.22 and 0.68 percent respectively.

The calculated strains are quite close and below the experimental strains. So, the use of Eq. (6.15), proposed by ACI for mainly concrete structures are quite reasonable to use for masonry as well.

The horizontal component of effective diagonal tensile strain found from Eq. (6.13) and Eq. (6.15) can be calculated as Eq. (6.16) by the rule of strain transformation (Mohr's circle), where the effect of orthogonal strain along compression diagonal on this horizontal component (ε_{xi}) is insignificant and can be neglected for simplicity. Thus,

$$\varepsilon_{xi} = \varepsilon_i \cos^2\theta \tag{6.16}$$

where, θ = angle between diagonal and base of the wall.

From Fig. 6.1, it is evident that the lateral shear contributed by the FRP is equal to the summation of all horizontal components of the diagonal tension developed in all of the diagonal strips. Thus,

$$V_{FRP} = nE_f t_f w_i \sin\theta\left[\varepsilon_{x1} + 2\left(\varepsilon_{x2} + .. + \varepsilon_{xi}\right)\right] \tag{6.17}$$

The above Eq. (6.17) can be used for all types of FRP having fiber in horizontal direction.

If the FRP is applied in a grid system [Fig. 5.9(c)], the Eq. (6.14) to calculate the diagonal distance of the grid from the center of the wall can be changed into Eq. (6.18) and Eq. (6.17) can be modified as Eq. (6.19),

$$d_{i-1} = \frac{(i-1)\mathrm{S}}{\sin(\theta)} \quad \le \frac{D}{2} \tag{6.18}$$

$$V_{FRP} = nE_f t_f w_{if} \sin\theta\left[\varepsilon_{x1} + 2\left(\varepsilon_{x2} + .. + \varepsilon_{xi}\right)\right] \tag{6.19}$$

Where, S is the c/c spacing to the FRP horizontal strips and w_{if} is the width of the each FRP strips.

If the FRP fiber is oriented along the diagonal of the wall as for the case of wall strengthening with the diagonal bracings, the above Eq. (6.20) can be simplified as,

$$V_{FRP} = nt_f E_f w_1 \varepsilon_{\max} \cos\theta \tag{6.20}$$

6.3.2 Model Implementation and Validation

In this proposed model, the FRP contribution to lateral shear comes from the internal strains as explained in the model. The proposed model is best suited for the cases when the bonded FRP undergoes substantial debonding. Proposed effective strain based model will not be fitted well, when the FRP shows extensive fracture and damage. Table 6.2 gives a comparison between analytical prediction and experimental results of masonry shear strength for different FRP

configurations. The information on in-plane tests on masonry wall retrofitted by fully wrapped FRPs are very limited and the uses of bio-FRPs for masonry strengthening are yet to begin.

Table 6.2 *Verification of proposed model for FRP strengthened walls*

Retrofitting Type	Ref.	Wall ID	*L/H*	FRP Type	V_T Exp. (*kN*)	$V_M + V_{add}$ Predic-ted (*kN*)	V_{FRP} Predict-ed (*kN*)	V_T Predict-ed (*kN*)	Calculated effective strain, ε_{max}, (%)	Observed failure mode*	Ratio of test to model predic-tion
Reinforced with Diagonal FRP	Santa-Maria et al. (2006)	CA-FX-01	1.0	Carbon	259	103	140	243	0.56	DT-DB	1.07
		CA-FX-03			230	95	93	188		DT-DB	1.22
	This Study	CSD	1.5	Carbon	95	93	49	142	0.68	DT-FR	0.67
		PSD		PET	114	76	27	103	1.22	DT-DB	1.10
		NSD		Nylon	103	74	28	102	1.28	DT-DB	1.01
	Wang et. al. (2006)	GW4	2.0	Glass	254	225	20	245	0.46	TC-DB	1.04
		GW5			265	222	23	245		SLD-DB	1.08
		GW6			222	217	30	247		TC-DB	0.90
		GW7			242	217	31	248		TC-DB	0.98
		GW8			228	223	23	244		SLD-DB	0.93
	Marcari et al.(2007)	C1	0.9	Carbon	189	167	33	200	0.16	DT-DB	0.94
		C2			227	176	94	270	0.11	DT-DB	0.84
		G1		Glass	156	160	14	174	0.36	DT-FR	0.89
		G2			180	161	41	202	0.26	DT-DB	0.89
	Chuang et. al. (2004)	W2	1.0	Carbon	30	18	11	29	0.73	F-DB	1.03
		W3			42	18	18	36	0.57	F-DB	1.16
	Stratford et. al. (2004)	Clay3	1.2	Glass	190	84	118	202	1.11	DT-DB	0.94
		Concrete1			130	78	87	165	0.81	DT-DB	0.80
Reinforced with fully wrapped FRP	El-Gawady et. al. (2007)	S2-GF-ST	2.2	Glass	51	48	29	77	1.03	TC-FR	0.66
		M2-GF-ST			70	48	29	77	1.03	TC-FR	0.91
		M2-2GF-ST			95	53	42	95	0.73	TC-FR	1.00
		M2-AF-S		Aramid	160	77	70	147	0.44	TC-DB	1.09
	This Study	CSF	1.5	Carbo	107	85	145	230	0.68	--	0.47
		PSF		PET	168	74	81	155	1.22	--	1.09
		JTSF		Jute	104	70	41	111	2.41	--	0.94
		CTSF		Cotton	131	70	42	112	2.53	--	1.17

* DT-DB (or FR) = Diagonal tension in wall and debonding (or fracture) in FRP; SLD- DB (FR) = Sliding in wall and debonding (or fracture) in FRP; F-DB (FR) = Flexural cracking in wall and debonding (or fracture) in FRP. TC- DB (FR) = Toe crushing in wall and debonding (or fracture) in FRP.

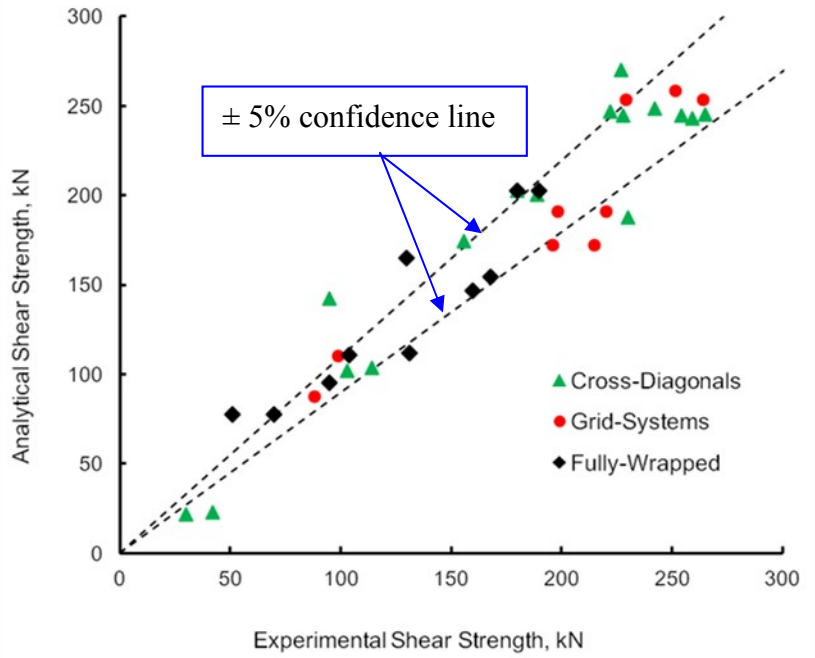

Fig. 6.3. *Comparison between experimental results and analytical prediction presented in Table 6.2.*

The presented data in Table 6.2 depict that the proposed model can estimate the shear strength of FRP retrofitted masonry walls with reasonable accuracy where the average of the ratios of prediction to test results is 0.97 and the coefficient of variation is about 0.18. Fig. 6.3 depicts the comparison between experimental and analytical results presented in Table 6.2. Only a few cases the prediction is poor, especially when the wall is reinforced with CFRP sheets. In the case of fully wrapped wall with CFRP sheet (CSF), the predicted shear strength was more than twice of the experimental observed value. This was due to the fact that the test panel did not reach its ultimate strength and failed prematurely in anchorage slip at grip of the wall bottom. Moreover, the model predicted higher effective strain than that was in experiment. Although anchorage slip was observed for other cases (PSF, JTSF, CTSF) also, but that happened at a later stage of the experiment when the wall reached at a constant state of load-deformation relationship as can be seen in Fig. 5.24. So, this proposed model can be implemented to almost all of the masonry walls that are reinforced with conventional FRPs and bio-FRPs having moderate to high fracturing strain.

In this proposed model, the failure mode of FRP retrofitted masonry can qualitatively be predicted from the aspect ratio of the walls. Having an aspect ratio less than one, the wall would presumably fail in flexural rocking followed by a toe crushing. On the other hand, wall with an aspect ratio above one, can have an expected mode of failure similar to diagonal cracking. In both of the cases, debonding of FRP would take place rather than rupture.

6.4 Concluding Remarks

Proposed analytical model based on effective strain in FRPs, can fairly predict the shear strength of masonry wall retrofitted with different FRPs. The model shows a reasonable prediction of shear strength for masonry walls failed in debonding rather than fracturing in FRPs. For CFRP strengthened wall, the model prediction is rather poor due to the estimation of higher strain value for CFRP. On the contrary, Jute and Cotton both have high fracturing strain and their effective strains are also high in transferring shear. The present work is not conclusive and more test results on masonry retrofitted with bio-FRPs are necessary to validate the model for different strengthening scheme and for different anchorage system.

Reference

AC 125. (2010). "Acceptance criteria for concrete and reinforced and unreinforced masonry strengthening using eternally bonded fiber-reinforced polymer (FRP) composite systems." *ICC Evaluation Service.*

Alcaino, P. and Santa-Maria, H. (2008). "Experimental response of externally retrofitted masonry walls subjected to shear loading." *J. Compos. Constr.*, 12(5), pp.489– 498.

Ali, Q., Badrashi, Y. I., Ahmad, N., Alam, B., Rehman, S. and Banori, F. A. S. (2012). "Experimental investigation on the characterization of solid clay brick masonry for lateral shear strength evaluation" *Int. J. of earth sciences and engr*., 5(4), pp.782 -791.

ACI 440.(2008). "Guide for the design and construction of externally bonded FRP systems for strengthening concrete structures" *American Concrete Institute*, Farmington Hills, MI 48331 U.S.A.

CEN (European Committee for Standardization) (2005). "Design of masonry structures - Part 1-1: General rules for reinforced and unreinforced masonry structures" *EN 1996 -1 -1: 2005, Brussels*, Belgium.

Chuang, S. and Zhuge, Y. (2004) "Seismic retrofitting of unreinforced masonry walls by FRP strips and cable system" *Proc., 18th Australian. Conf. on the Mechanics. of Str. and Mat.*, pp.49–54.

CNR-DT200. (2013). "Guide for the design and construction of externally bonded FRP systems for strengthening existing structures" *CNR-DT 200 R1,* Italian National Research Council, Italy.

ElGawady, M. A., Lestuzzi, P., and Badoux, M. (2007). "Static cyclic response of masonry walls retrofitted with fiber-reinforced polymers" *J. Compos. Constr.*, 11(1), 50– 61.

ElGawady, M. A., Lestuzzi, P. and Badoux, M. (2007). "Static cyclic response of masonry walls retrofitted with fiber-reinforced polymers" *J. Compos. Constr.*, 11(1), pp.50– 61.

El-Sokkary, H. and Galal, K. (2013). "Seismic behavior of FRP-strengthened RC shear walls" *J. Compos. Constr.* Online Version.

Ehsani, M. R., Saadatmanesh, H. and Al-Saidy, A. (1997). "Shear behavior of URM retrofitted with FRP overlays" *J. Compos. Constr.*, 1(1), pp.17– 25.

FEMA 356 (2000). "Prestandard and commentary for the seismic rehabilitation of buildings" *Federal emergency management agency*, Washington, D.C.

JSCE. (2001). "Recommendation for upgrading of concrete structures with use of continuous fiber sheets" Concrete Engineering Series 41, *Japan Society of Civil Engineers,* Tokyo, Japan.

Khalifa, A., Gold, W. J., Nanni, A., and Aziz, A. (1998). "Contribution of externally bonded FRP to shear capacity of RC flexural members" *J. Compos. Constr.*, 2(4), 195– 202.

Marcari, G., Manfredi G., Prota A. and Pecce, M. (2007). "In-plane shear performance of masonry panels strengthened with FRP" *Elsevier J. of Comp.* Part B 38(7), pp.887–901.

Nanni, A. (1993). "Flexural behavior and design of RC members using FRP reinforcement." *J. Struct. Eng.*, 119(11), 3344– 3359.

Prota, A., Manfredi, G. and Nardone, F. (2008). "Assessment of design formulas for in-plane FRP strengthening of masonry walls." *J. Compos. Constr.*, 12(6), 643– 649.

Rizkalla, S., Hassan, T., and Hassan, N. (2003)"Design recommendations for the use of FRP for reinforcement and strengthening of concrete structures". *Prog. Struct Engng Mater. 5, 16-28.*

Stratford, T., Pascale, G., Manfroni, O. and Bonfiglioli, B. (2004). "Shear strengthening masonry panels with sheet glass-fiber reinforced polymer". *J. Compos. Constr.*, 8(5), pp.434– 443.

Santa Maria, H., Alcaino, P. and Luders, C. (2006). "Experimental response of masonry walls externally reinforced with carbon fiber fabrics", *Proc. of the 8th U.S. Conf. on Earth. Eng.,* CA, USA, p-1402.

Triantafillou, T. C. and Antonopoulos, C. (2000). "Design of concrete flexural members strengthened in shear with FRP" *J. Compos. Constr.*, 4, pp.198–205.

Tumialan, G., Huang, P.-C., Nanni, A., and Silva, P. (2001). "Strengthening of masonry walls by FRP structural repointing." *Proc., 5th Int. Conf. on Fibre Rein. Plastics for Rein. Concrete Struc.*, Thomas Telford, Cambridge, U.K., 1033–1042.

Triantafillou, T. C., and Antonopoulos, C. (2000). "Design of concrete flexural members strengthened in shear with FRP." *J. Compos. Constr.*, 4, 198–205.

Tumialan, G., Huang, P.-C., Nanni, A., and Silva, P. (2001). "Strengthening of masonry walls by FRP structural repointing." *Proc., 5th Int. Conf. on Fibre Rein. Plastics for Rein. Concrete Struc.*, Thomas Telford, Cambridge, U.K., 1033–1042.

Valluzzi, M. R., Tinazzi, D. and Modena, C. (2002). "Shear behavior of masonry panels strengthened by FRP laminates" *J. of Cont. and Bldg. Mat.*, Elsevier, 16 (2002) 409–416.

Wang, Q., Chai, Z., Huang, Y., Yang, Y. and Zhang, Y.(2006). "Seismic shear capacity of brick masonry wall reinforced by GFRP" *Asian J. of Civil Engineering (Building And Housing)*, 7(6), pp.563-580.

Chapter 7

Conclusions and Recommendations

7.1 Conclusions

Based on the entire experimental as well as analytical results and observations, the following remarks were outlined:

1) This experimental study demonstrates the ability of all of the FRPs such as CFRP, PET-FRP, Nylon-FRP, Jute-FRP and Cotton-FRP sheets to enhance the shear resistance to a great extent; more than twice the capacity of the URM wall in the case of diagonal bracing and about three times in the case of gird configuration and walls fully wrapped with FRPs. Among the synthetic FRPs, PET-FRP and Nylon-FRP have a better ductility performance than CFRP, as they show pronounced ductile behavior in pre-peak regime and softening behavior in post-peak regime. Ductility is a must needed criterion rather than strength for a structure to absorb substantial seismic energy and ensure structural integrity and margin of safety against collapse. Though the CFRP increases the shear capacity of a masonry wall, it substantially reduces the ductility of the wall, which may eventually cause an explosive type of masonry failure. On the other hand, Jute-FRP and Cotton-FRP also enhanced the shear capacity of masonry wall to almost thrice of that of URM wall and they also showed better ductile behavior than CFRP.
2) The elastic stiffness of URM wall was largely modified by the use of FRPs, externally bonded over the surface of the walls but it was observed that stiffness value beyond some specific range does not increase the in-plane shear strength of masonry and it will only increase the cost of strengthening works.
3) As masonry is quite fragile against lateral movement with a low lateral stiffness, diagonal bracing with PET-FRP sheet can be one of the options, if the cost of the material is not compromised. If seeking for a low-cost strengthening material, Nylon-FRP, Jute-FRP and Cotton-FRP could be one of the variable alternatives, where not only capacity is enhanced but, at the same time, the wall is made quite ductile, reversing a catastrophic mode of failure to a ductile one. Moreover, unlike synthetic FRP such as CFRP, PET-FRP and Nylon-FRP, Jute and Cotton are bio-degradable materials, and they do not pose any threat to the ambient

environment. For low cost strengthening work, Jute, Cotton or Nylon can be good alternatives to PET and Carbon.

4) Another interesting point that is manifest from this experimental study is that the FRP strengthening of the masonry can have only marginal effect on the structural performance at the service load condition but contribute a lot at some accidental overloading such as earthquake, where the seismic demand is high.
5) The in-plane shear strengths observed in this experimental study are almost equal to each other for the cases where the amount of FRP was greater than a certain limit. This information has assisted to some extent to develop an analytical model for FRP strengthened wall based on effective strain in FRP.
6) The proposed model equations have uniqueness in their simplicity and can predict the peak shear stress as well as the initial stiffness and the softening behavior of the interface quite well for the experimental results examined in this study. The necessary information for the proposed model is only the Young's modulus of brick and mortar, the mortar thickness and the normal compressive stress acting on the interface. Any reasonable value for c and ϕ will produce good numerical approximation.

7.2 Recommendations

Considering the whole experimental, analytical and numerical studies carried out in this research work, some further developments that can be suggested are the following:

1) In all strengthening work, cost of the material and installation is prime concern of both engineers and builders. The cross-diagonal bracing with PET-FRP requires least materials and minimum installation works, and whose material cost is less than CFRP. On the contrary, diagonal bracing with Nylon-FRP also showed good shear resistance and better ductility behavior than CFRP and PET-FRP and having lower cost than these two. Wall fully covered by CFRP or PET-FRP is not a suitable option for external strengthening due to the use of higher amount of materials that makes the wall much stiffer against lateral deformation, but they are quite good when Jute or Cotton sheet are used. However, structures will rarely be economic unless sensible decisions are made using whole-life costing and taking into account all the costs of repair and strengthening.
2) Although in this experimental study the walls strengthened with FRPs were designed in such a way that they will not fail in the anchorage of the FRPs, it remains a crucial task in the practical field of application and should be dealt with sufficient care. Insufficient development length and inappropriate anchorage technique may lead to a premature

anchorage failure of the wall. And in some instance that might be detrimental for the safety of the structure. Since, existing building codes and provisions mostly dealt with RC and Steel structures, future research can also be done for the search of appropriate anchorage techniques for masonry structures.

3) Proposed analytical model based on effective strain in FRPs, can fairly predict the shear strength of masonry wall retrofitted with different FRPs. The model shows a reasonable prediction of shear strength for masonry walls failed in debonding rather than fracturing in FRPs. For CFRP strengthened wall the model prediction is rather poor due to the estimation of higher strain value for CFRP. On the contrary, Jute and Cotton both have high fracturing strain and their effective strains are also high in transferring shear. The present work is not exhaustive and more test results on masonry retrofitted with bio-FRPs are necessary to validate the model for different strengthening scheme and for different anchorage types.

4) Bio-FRP composites made from natural fiber are renewable, cheap, completely or partially recyclable, and biodegradable. A lot of research needed to be done on bio-FRP, ranging from bond stress-slip model to resin-fiber interaction. A harmonized effort is necessary to bring the bio-FRPs in the vast strengthening market as lucrative retrofitting materials.

5) Research work, analytical modeling, model codes and provisions for RC structures strengthened by conventional FRPs such as CFRP and GFRP have gone a long way in the last two decades, whereas, it is still far away from standard design practice and performance based seismic assessment of masonry structures. A concerted effort and a harmonized approach are therefore necessary for masonry to meet that target. With the use of well-tested materials with reasonable cost, expert installation crews, and proper design guidelines, externally bonded FRPs made from natural fiber can be a unique solution to many masonry structures for retrofitting and rehabilitation purposes in the third world countries. Experimental results and recommendations proposed in this study can be one step forward in achieving this goal.

6) However, further study is needed for the advancement of knowledge on FRP in general and on PET in particular concerning some of the unresolved issues that could not be addressed in this paper such as brick-FRP interface behaviour, optimum percent of FRP for masonry, delayed debonding and issue related to anchorage system of FRP with masonry. A concerted effort and a harmonized approach are necessary to make externally bonded FRPs as a lucrative solution for many historically valued masonry structures for retrofitting and rehabilitation purposes. Though the present work is not very exhaustive, it can be one step forward in achieving this goal.

7) A comprehensive numerical strategy is needed to verify those proposed numerical models for full scale walls. General purpose commercial Finite Element program such as ANSYS, DIANA or MATLAB can be the best option for this numerical work. Sufficient care should be taken at the time of implementing these proposed models into the user-defined subroutine of this FEA software, so that the units and parameters are consistent with the program input and output.

THE END

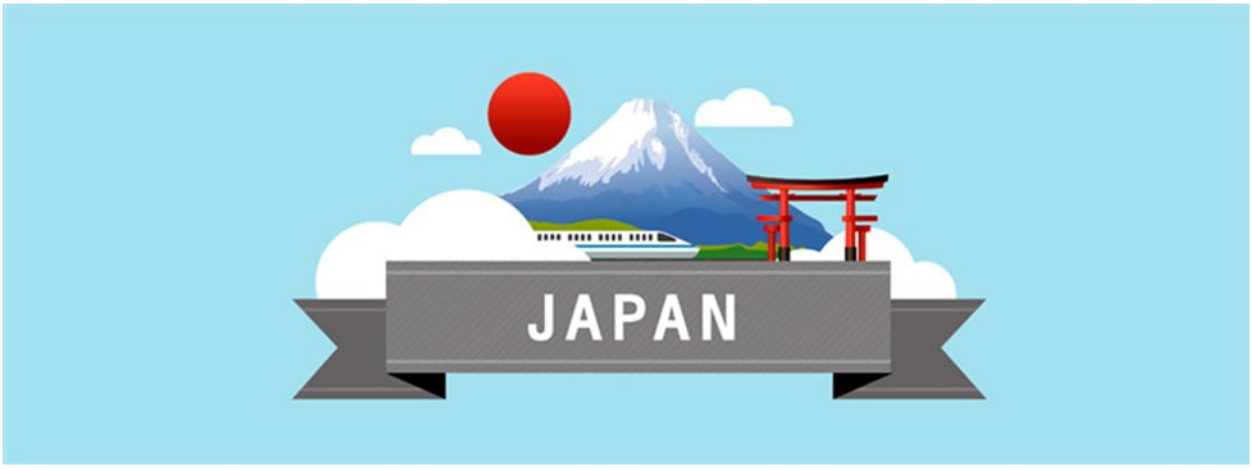
JAPAN